UNIVERSITÀ
DEGLI STUDI
DI PADOVA

Sede Amministrativa: Università degli Studi di Padova

Centro di Ateneo di Studi e Attività Spaziali CISAS "Giuseppe Colombo"

CORSO DI DOTTORATO DI RICERCA IN: SCIENZE TECNOLOGIE E MISURE SPAZIALI

INDIRIZZO: MISURE MECCANICHE PER L'INGEGNERIA E LO SPAZIO

CICLO XXXIV

METHODS OF ANALYSIS FOR STEREO OBSERVATION OF PLANETARY SURFACES AND LIBRATIONS

Coordinatore: Ch.mo Prof. Francesco Picano

Supervisore: Ch.ma Dott.ssa Cristina Re

Co-Supervisore: Ch.mo Prof. Stefano Debei

Dottorando: Nicolò Borin

Table of contents

List of figures

List of tables

List of acronyms

AME - Absolute Measurement Error

APE - Absolute Performance Error

ASI - Italian Space Agency

ASP - Ames Stereo Pipeline

BELA - BepiColombo Laser Altimeter

BRDF - Bidirectional Reflectance Distribution Function

CaSSIS - Colour and Stereo Imaging System

CNES - French Space Agency

CMOS - Complementary Metal Oxide Semiconductor

CPM - Chemical Propulsion Module

DEM - Digital Elevation Model

DN - Digital Number

DoF - Degrees of Freedom

DPU - Digital Processing Unit

DTM - Digital Terrain Model

ESA - European Space Agency

FOV - Field of View

FPA - Focal Plane Assembly

GSD - Ground Sample Distance

HRIC - High-spatial Resolution Imaging Channel

HRSC - High Resolution Stereo Camera

IFE - Instrument Front End

INAF - Istituto Nazionale Astrofisica

ISIS - Integrated System for Imagers and Spectrometers

JAXA - Japanese Aerospace eXploration Agency

LRO - Lunar Reconnaissance Orbiter

LROC - Lunar Reconnaissance Orbiter Camera

LSM - Least Square Matching

MCS - Mercury Composite Spacecraft

ME - Main Electronics

MESSENGER - Mercury Surface, Space Environment, Geochemistry and Ranging

MEX - Mars EXpress

MORE - Mercury Orbiter Radio-Science Experiment

MMO - Mercury Magnetospheric Orbiter

MPO - Mercury Planetary Orbiter

MRO - Mars Reconnaissance Orbiter

MTF - Modulation Transfer Function

MTM - Mercury Transfer Module

NAIF - Navigation and Ancillary Information Facility

NASA - National Aeronautics and Space Administration

PDS - Planetary Data System

POG - Pixel On Ground

PU - Power Unit

QE - Quantum Efficiency

RANSAC - RANdom SAmple Consensus

RMS - Root Mean Square

S/C - Spacecraft

SELENE - Selenological and Engineering Explorer

SEPM - Solar Electric Propulsion Module

SIFT - Scale-Invariant Feature Transform

SIMBIO-SYS - Spectrometer and Imagers for MPO Bepicolombo Integrated Observatory – SYStem

SNR - Signal Noise Ratio

SPICE - Spacecraft Planet Instrument C-matrix Event

STC - Stereo Imaging System

SURF - Speeded Up Robust Features

TA - True Anomaly

TGO - Trace Gras Orbiter

UDSC - Usuda Deep Space Center

USGS – United States Geological Survey

VIHI - Visual and Infrared Hyperspectral Imager

Abstract

BepiColombo is ESA/JAXA mission composed by two spacecrafts, MPO and MMO, with the goal to explore the planet Mercury.

Among the different scientific products, the mission will provide in particular Digital Terrain Models of the surface of the planet by means of the Stereo imaging Channel (STC) of the SIMBIO-SYS (Spectrometer and Imaging for MPO BepiColombo Integrated Observatory SYStem) imaging package onboard MPO.

The work presented in the thesis is focused on SIMBIO-SYS and can be divided in two main topics: analyzing and optimizing the acquisition planning of the instrument and creating Digital Terrain Models of the surface of the planet from stereo pairs.

In order to evaluate the mission planning for SIMBIO-SYS, different acquisition scenarios are simulated using real mission parameters calculated with customized MATLAB routines exploiting the SPICE kernels.

The DTMs are obtained from synthetic images of planetary surfaces: a complete workflow from the rendering of the stereo pairs up to the reconstruction of tridimensional models is presented and different simulations are executed changing the acquisition conditions, simulating different acquisition scenarios.

Two different typologies of DTMs are presented. The first category are high resolution DTMs created from the High spatial Resolution Imaging Channel (HRIC) of SIMBIO-SYS: being the camera rigidly integrated with the spacecraft, this latter must be tilted to acquire stereo pairs necessary for the 3D reconstruction.

The second category are created with a novel approach for the creation of stereo pairs, considering images of HRIC and STC together: this method proves to be more accurate in the reconstruction of Digital Terrain Models in comparison to the normal method with only STC images, and results particularly suited for the exploration of the polar regions of the planet.

The Digital Terrain Models obtained are evaluated and an analysis of the best acquisition conditions is performed, helping to improve the image acquisition strategy of SIMBIO-SYS.

In addition, a strategy for the creation of a mosaic from different images acquired with the high resolution channel of SIMBIO-SYS is explained, giving the possibility to obtain tridimensional products of extended targets.

Finally, some insights about the use of high resolution Digital Terrain Models for the study of planetary surfaces are given, focusing in particular on the libration experiment.

Introduction

Space exploration is a subject that always fascinated generations of humans since the ancient times, but it was in the middle of the previous century that the technology reached a level capable to send probes in space and to other planets.

In the year 1957 the URSS's satellite Sputnik, the first man-made object to orbit around the Earth, was launched. It was the beginning of the space race era, particularly encouraged during the Cold War between URSS and USA. Several scientific missions followed, orbiting around the Earth, landing on the Moon, exploring the Solar System and finally landing on other planets and celestial bodies. Along with the American NASA and the Russian Roscosmos, other space agencies were created over the years, in which the most important are the European ESA, the Japanese JAXA, and the new Chinese and Indian agencies.

The interest in space exploration increased and several probes were sent to other planets, equipped for either landing or orbiting. Major interest was reserved to terrestrial planets, like Venus and Mars especially, while Mercury was posed in second place for years.

Mercury, the inner planet of our Solar System, presents some unique characteristics: it is the smallest planet, it orbits around the Sun with a particular 3:2 spin-orbit resonance, it has a peculiar configuration of the nucleus and presents the most extreme temperature difference between the hot and cold face of the surface. Due to its position, the planet results difficult to explore both from Earth, as it is visible only for a short time, and from orbit, as the extreme temperature of the surface and the proximity with the Sun pose difficulties in the control of a probe.

After the American missions MARINER-10 launched in 1974 and MESSENGER launched in 2004, ESA and JAXA started a collaboration for the development of the BepiColombo mission in 2020. This challenging mission was launched in October 2018 and it is composed by two spacecrafts, MPO (Mercury Planetary Orbiter) and MMO (Mercury Magnetospheric Orbiter), with different tasks for the exploration of Mercury. MPO is designed specifically for the examination of the Hermean surface and stores several instruments aimed to this objective. In particular, the SIMBIO-SYS (Spectrometer and Imagers for MPO Bepicolombo Integrated Observatory – SYStem) suite is designed to collect images of the Planet surface. The instrument is composed by three channels: HRIC (High-spatial Resolution Imaging Channel), STC (Stereo Imaging System), and VIHI (Visual and Infrared Hyperspectral Imager). The different channels

work together in order to provide high resolution images of the most interesting areas, a global tridimensional mapping of the surface and a mineralogical map of its composition.

The tridimensional reconstruction of planetary surfaces plays an important role in the space exploration, as it facilitates the analysis of the morphological characteristics of the terrain and provides useful information for the mission itself, facilitating the planning and the eventual landing of a probe.

The 3D model of a surface, called DTM (Digital Terrain Model), is usually created by a stereo camera, specifically designed to acquire images from different perspective allowing the triangulation of every point of the target. This strategy proved to be successful in different missions, as for example in the Mars Express and MRO (Mars Reconnaissance Orbiter) on Mars and in the LRO (Lunar Reconnaissance Orbiter) on the Moon and many others.

The work presented in this thesis covers principally two different topics: simulating the tridimensional reconstruction of the surface of Mercury and presenting a planning strategy for SIMBIO-SYS images acquisition.

The first part of the thesis is focused on a general description of the mission BepiColombo and the instrument SIMBIO-SYS, giving the context for the research conducted. Moreover, some insights on photogrammetry and stereo vision are given. These concepts are useful to understand the procedure to produce DTMs, summarized in the following steps: 1) un-distortion of the images, 2) rectification, 3) finding correspondences, 4) triangulation.

Stereo couples of rendered images of planetary surfaces are simulated by means of a ray tracing software and lately processed in order to obtain a DTM of the target. Several simulations are conducted changing different operative parameters, as the illumination conditions and the stereo angle, providing useful information for the mission planning. An innovative strategy to create high resolution DTMs using HRIC images is presented. While the channel STC is specifically designed to obtain stereo pairs and DTMs, HRIC can be used as well with some adjustments for the same purpose: as the camera is rigidly integrated in the spacecraft, this latter must be rotated in order to obtain stereo pairs. These off nadir maneuvers must be carefully planned as some instruments can be damaged if hit directly by the Sun. On the other hand, this strategy permits undoubtedly to obtain higher quality 3D as the resolution of HRIC is around 10 times better than the one of STC. Moreover, stereo couples obtained with combined HRIC and STC images are simulated and processed for the creation of DTMs: this new acquisition strategy, feasible because of the possibility to integrate data obtained with the different channels of SIMBIO-SYS, proves to be more effective for the DTM reconstruction than the normal strategy with STC images.

An acquisition strategy with SIMBIO-SYS is presented, covering different aspects as the change of on-ground resolution and the possibility to perform a mosaic with multiple images. Concerning this topic, a MATLAB code for mosaicking different HRIC images has been written.

In addition, in the last chapter some applications of high resolution DTMs are presented, as the possibility to use them for the study of librations and to correlate the data with other instruments, along with an error budget analysis on the pointing on ground of SIMBIO-SYS.

The overall research presented in this thesis can efficiently support the planning of the BepiColombo mission, helping the different scientific working teams.

Chapter 1: BepiColombo Mission

The first chapter gives a general overview of the planet Mercury and of the BepiColombo mission.
Mercury is the inner and smaller planet of the Solar System and presents some unique characteristics worth to be investigated. Due to technical difficulties related to the position close to the Sun, just two missions were sent to Mercury in the past years. The mission BepiColombo, a joint venture between ESA and JAXA, aims to fill the gaps in the knowledge of the planet.
The mission is composed by two spacecraft, specifically equipped to fulfil the task of studying the surface and the particle environment of Mercury.
All general information about the mission, as objectives and phases, are described in details.

1.1 Context of the mission

The spacecraft Luna-2 was the first human-made object to move from the Earth to another celestial body: the Moon, in the year 1959. Since then, the interest in space exploration increased and several missions succeeded one next to the other to send probes to explore different objectives, like planets, comets and asteroids.
One of the main objective of the planetary research is focused in acquiring information that can lead to a better knowledge of the origin of the Solar System.
Among the planets, Mercury represents an interesting and unique target for several reasons.
It is the closest planet to the Sun and its temperature reaches 700 K in the face oriented to the star. The atmosphere in almost totally absent and this causes thermal variations of more than 500 K between the diurnal and nocturnal faces. Mercury presents the highest density of all the planets. The inner part seems formed by a solid iron core immersed in a liquid iron core and this explains the presence of the weak magnetic field that interacts with the solar wind.
The orbit of Mercury around the Sun is highly eccentric and tilted (this characteristic is unique in comparison to the orbits of the other planets) and the rotational state of the planet is a 3:2 spin-orbit resonance: it means that the planet rotates 3 times around its axis every 2 revolution around the Sun.

All these aspects make Mercury unique and its study can lead to answer several questions about the origin of the Solar System.

Unfortunately, Mercury results difficult to study both from Earth and orbit. From the Earth it is visible just for two hours every day preceding the sunrise and following the sunset and with a maximum elongation from the Sun of 28°, with the radiation coming from the star always as a background that can damage the telescopes. A spacecraft orbiting around the planet has to face extreme thermal and attitude challenges due to the proximity to the Sun. In fact, the solar flux is 10 times higher than the one at Earth's distance and the surface of the planet is the hottest of the Solar System. Moreover, the high gravitational forces exerted by the Sun disturbs the attitude control of the spacecraft.

The first mission to Mercury was Mariner 10 in 1974 which performed 3 flybys of the planet and provided images of around 45% of the surface.

Thirty years later, in 2004, NASA sent a second mission, MESSENGER (MErcury Surface, Space ENvironment, GEochemistry and Ranging) [1], to perform measurements of the composition and geometry of the surface along with analyses of the atmosphere and magnetosphere. The spacecraft reached Mercury in 2011 and sent images of the previously unexplored hemisphere.

Meanwhile, ESA started to plan a dedicated mission to Mercury as well. Initially proposed in 1993, the BepiColombo mission [2] finally reached an agreement in 1996. The mission is a joint venture between ESA and JAXA with the goal of deeply explore Mercury. The scientific payload is hosted in two spacecraft, the Mercury Planetary Orbiter (MPO) and the Mercury Magnetospheric Orbiter (MMO). The mission was then fully approved on 6th November 2003 and successfully launched on 20th October 2018. BepiColombo will arrive on Mercury in 2025 and will orbit the planet for one year, with a possible extend of another year.

1.2 Mercury

Several characteristics make Mercury singular and unique in the Solar System: it is the smallest and closest planet to the Sun (0.3 AU at Perihelion) and it is one of the four terrestrial planets among with Venus, Earth and Mars. Furthermore, Mercury presents some peculiar characteristics in comparison to the other terrestrial planets.

The temperatures and their variations are the highest of all the planets (100 K in the night side and 700 K in the day side). The density is the highest (5.4 g/cm^3) suggesting a high Fe/Si ratio

probably due to a different evolutionary scenario with respect to the other terrestrial planets. In fact, the lighter materials normally present in the other planets were attracted by the Sun during the process of the creation of Mercury, leaving only the heavier materials to form the planet.
A theory also suggests that Mercury formed in a different position respect to the actual one, and moved later near the Sun.
From MESSENGER data it has been discovered that the core of Mercury is partially liquid. This discover is quite puzzling, because scientists used to think that the core must have solidified due to the small size of the planet. On the other hand, the existence of a liquid core explains the presence of a weak magnetic field (300 nT) that, from the data retrieved so far, seems to be shifted from the centre of the planet. In conclusion, different questions are still opened about the magnetic field of the planet.
The planet cooled quickly due to its small size causing compression in the surface and originating thrusts faults. The surface presents some particular features called hollows, similar to vents, probably caused by the evaporation of material from inside the planet. Hollows are defined as shallow, flat-floored irregular depressions notable for their relatively high reflectance and characteristic color [3]. Hollows are a morphologic structure detected uniquely on Mercury so far and their investigation is one the main objective of the mission.
The atmosphere, almost absent, is probably originated by the interaction of the solar wind with the surface of the planet. The lack of a thick atmosphere (that distributes the heat around the planet) and the slow rotation are the causes of the extreme thermal variation registered on the surface. Furthermore, without an atmosphere to protect the planet, the heavy bombardment that took place during the formation of the planet left still visible big craters all around the surface.
The vicinity with the Sun creates a particularly strong solar wind and particles flux that interact with the planetary surface producing a specific exosphere which characteristics change along the eccentric orbit of Mercury [4].
MESSENGER also discovered signs of the presence of ice water inside the craters in the poles. The presence of ice could be quite surprising in a planet where the surface temperature reaches 450°C, but can be explained by the fact the rotation axis of Mercury is almost perpendicular to the orbital plane, such that the rays of the Sun never reach the interior of the polar craters, forming some permanent shadowed regions. Thus, the temperature remains low and allows the presence of ice water.

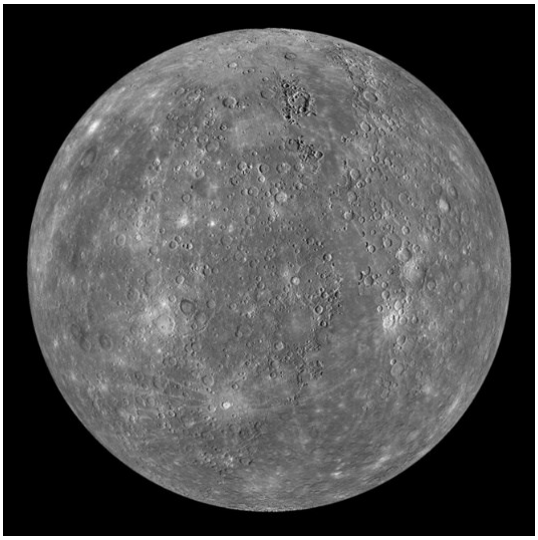

Fig 1 Mercury in true colour by MESSENGER

Tab 1 shows the principal physical properties of Mercury.

Mercury physical properties	
Mass [10^{24} kg]	0.3302
Volume [10^{10} km^3]	6.083
Mean density [kg/cm^3]	5427
Mean radius [km]	2439.7
Albedo	0.119
Surface temperature range [K]	100 – 688
Black body temperature [K]	442.5
Gravity [m/s^2]	3.701
Escape velocity [km/s]	4.435
Gravity constant GM [10^5 km^3/s^2]	0.02203
Dipole field strength [nTR_h^3]	330
Solar irradiance at Perihelion [W/m^2]	14490
Solar irradiance at Aphelion [W/m^2]	6290
Moment of inertia [C/MR^2]	0.33
J_2	60 10^{-5}

Tab 1 Main physical properties of Mercury

The solar ties influence the rotational state of Mercury, that results in a peculiar and unique 3:2 spin-orbit resonance, meaning that the planet performs 3 rotations every 2 revolutions. The spin velocity is 1.5 times the orbital velocity, resulting in a slow rotation period of 58,68 days and a revolution around the Sun in 87,96 days.
More details about the resonance cycle of the planet can be found in the following figure.

Mercury 3:2 spin-orbit resonance cycle

The red-line represents a fixed position on the Mercury surface.
In this case this is 90 degrees West (ref. : Vivaldi crater)

The figure on the right starts with an Aphelion season #0.
The periherm (day side) will be at 270 degrees West.
(ref. : Rembrandt crater)
(90 degrees West is on the night side in this Aphelion)

The figure shows dots for every 90 degrees rotation (2, 3, etc.).

At Perihelion (position 4) Mercury has rotated 270 degrees.
The periherm (night side) will be at 0 degrees. (ref. : Hemingway crater)
The apoherm (day side) will be a 180 degrees (ref. : Zola crater)

At Aphelion season #1 (position 7) Mercury has rotated 540 degrees.
The periherm (day side) will be a 90 degrees (above red line)

This means exactly the other side of the planet is visible with respect to the first aphelion season

From this figure the following conclusions follow:
- at Aphelion the longitudes 270 and 90 degrees will be visible
- at Perihelion the longitudes 0 and 180 will be visible.
- illumination conditions will be very similar for every 2nd aphelion or perihelion period
- after 2 Mercury years conditions start repeating itself
- theoretically Global Mapping full coverage can be achieved after 2 aphelion seasons, which is half of the nominal mission

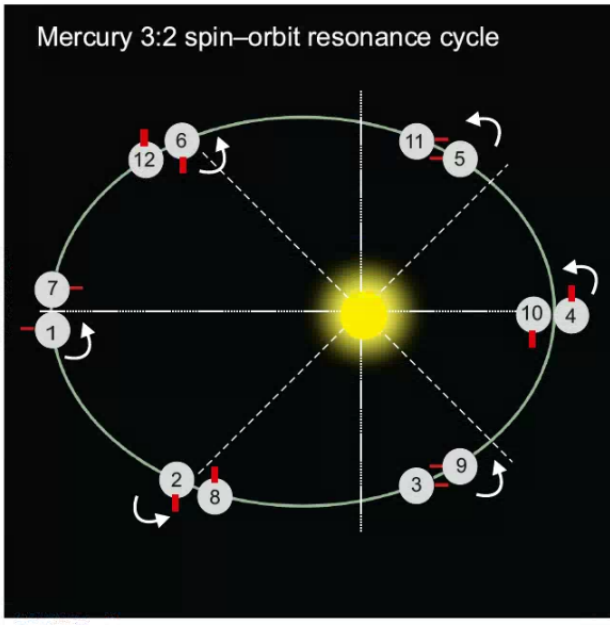

Fig 2 Mercury 3:2 spin-orbit resonance

The orbit of Mercury has the highest eccentricity and the smallest obliquity (axial tilt respect to the orbital plane) of all the planet of the Solar System.
The orbital parameters of the planet are described in the following table.

Orbital parameters of Mercury	
Semi major axis [10^6 km]	57.909
Semi minor axis [10^5 km]	56.672
Perihelion [10^6 km]	46.001
Aphelion [10^6 km]	69.817
Eccentricity	0.20563
Inclination [°]	7.005
Orbital sidereal period [yr]	0.2408467
Sideral rotation period [days]	58.646 ±0.0005
Length of Mercurian day [days]	175.94
Synodic period [days]	115.88
Mean orbital speed [km/s]	47.87
Maximum orbital speed [km/s]	58.98
Minimum orbital speed [km/s]	38.86
Obliquity to orbit [°]	0.01
Maximum angle from Earth – Sun line [°]	28
Maximum Earth – Mercury distance [10^6 km]	221.6
Minimum Earth – Mercury distance [10^6 km]	77.3

Tab 2 Principal orbital parameters of Mercury

1.3 BepiColombo Mission

The BepiColombo mission [5] [6] takes the name from the mathematician Giuseppe Colombo (1920-1984), who was the first to explain the correlation between the rotation period and the revolution period of Mercury and suggested how to perform the flybys of the planet during the Mariner 10 mission.

BepiColombo is the first European mission to Mercury, it was selected as a candidate during the Horizons 2000 scientific program in the 1996. Later, in July 2000, Japan was involved in the project and finally in October 2000 the Science Programme Committee (SPC) approved BepiColombo as the ESA's 5th Cornerstone mission.

Since then, BepiColombo is a partnership between ESA and JAXA, where each agency is focused on accomplishing different objectives.

The mission presents extreme and peculiar challenges in term of thermal and attitude control in comparison to other missions to other planets due to the close position of Mercury respect to the Sun.

1.3.1 Scientific objectives

The principal scientific objectives of BepiColombo can be summarized as the following:

- Study the origin and evolution of a planet close to its parent star.
- Evaluate Mercury's figure, interior structure, and composition.
- Evaluate the characteristics and origin of its internal magnetic field.
- Investigating the geological evolution of the planet: cratering, tectonics, polar deposits and volcanism.
- Determine the structure, composition, origin and dynamics of Mercury's exosphere.
- Determine the structure and dynamics of Mercury's magnetosphere.
- Perform a test of Einstein's Theory of General Relativity.

1.3.2 System architecture

The instruments that will study Mercury are hosted in two different spacecraft, the Mercury Planetary Orbiter (MPO) led by ESA and the Mercury Magnetospheric Orbiter (MMO) led by JAXA. Each spacecraft has different tasks, in particular:

- MPO is dedicated to remote sensing and radio science
- MMO is dedicated to the study of the magnetic field and particle science

The two spacecraft are carried to Mercury by an additional module, the Mercury Transfer Module (MTM), composed by two different modules, the Solar Electric Propulsion Module (SEPM) and the Chemical Propulsion Module (CPM). MPO, MMO and MTM are launched all together and the total spacecraft is called Mercury Composite Spacecraft (MCS). The launch took place on the 20th October 2018 from the Guiana Space Center in Kourou (French Guiana) with an Ariane 5 rocket. The cruise from Earth to Mercury will take approximately 7 years and the interplanetary trajectory will perform 9 different planetary flybys around Earth, Venus and Mercury itself. During the cruise, the propulsion is accomplished by the SEPM, while the CPM

will be activated to insert the spacecraft into the final orbit around Mercury. Finally, the MTM will be jettisoned and MPO and MMO will reach their operative orbits.
The task of controlling the spacecraft is divided between ESA and JAXA. ESA is responsible for the control of the launch and the operations with MCS and MPO. The ground segment is divided in two elements: the Mission Control Centre at ESOC in Germany and the Science Ground Segment at ESAC is Spain. JAXA is responsible for the control of MMO, provided from the Sagamihara Space Operation Centre in Japan.

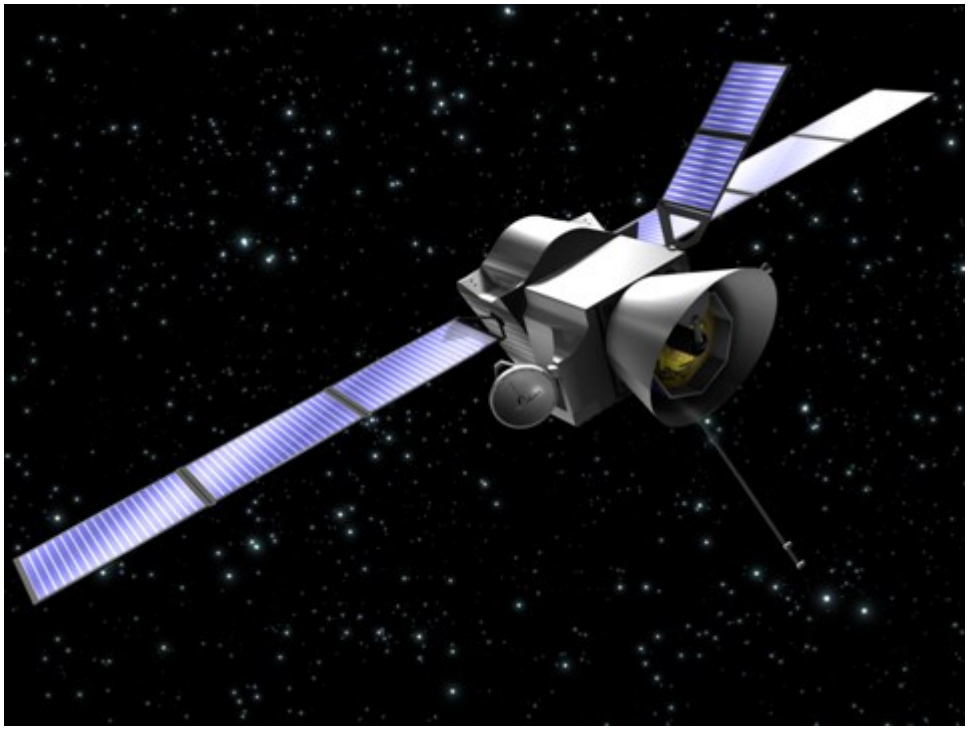

Fig 3 Representation of the Mercury Composite Spacecraft MCS

1.3.2.1 MPO

The Mercury Planetary Orbiter (MPO) is the spacecraft designed by ESA dedicated to remote sensing and radio science.
MPO is a three-axis stabilized and nadir pointing spacecraft that follows a polar and elliptic orbit with Periherm and Apoherm respectively at 480 km and 1500 km altitudes. Different phases are identified in dependence on the altitude of the spacecraft. When Mercury is at Perihelion (True Anomaly = 0°), MPO flights above the illuminated part of the surface of the planet with the highest altitude of its orbit.

The choice of this orbit derives from the high temperature of the surface of Mercury, that can damage the instruments distorting some of their components due to thermal deformations and can deteriorate the solar panels. To limit the temperature of the panels, their inclination has been modulated as function of the Mercury's True Anomaly. In order to maintain the solar panels always pointed to the Sun and the radiator always to the space, MPO has to perform a rotation of 180° around its Z axis when the true anomaly is equal to 0° and 180°. With this mission configuration, the spacecraft is close to the planet when the planet is far from the Sun and consequently the surface temperature is lower, and vice versa.

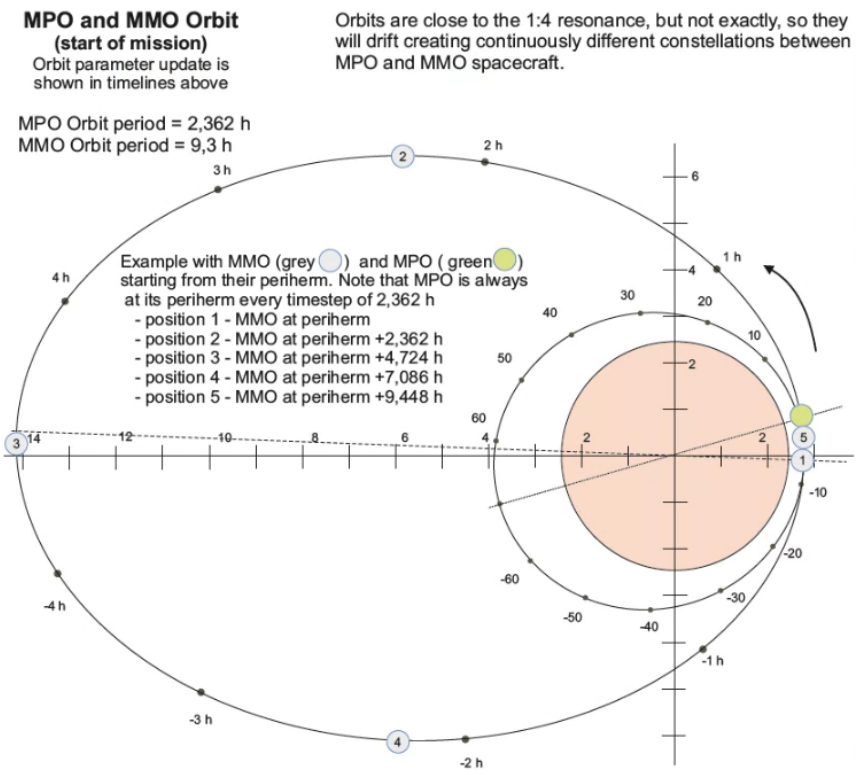

Fig 4 MPO and MMO orbit respect to Mercury

The spacecraft is equipped with four thrusters for the manoeuvre of insertion into the final orbit; four reaction wheels plus four thrusters for the attitude control; star trackers and star sensors for the attitude determination; a radiator to disperse the heat; a solar array and batteries (during the eclipses) for the power supply.

In addition, the payload is composed by the following instruments:

- BELA - BepiColombo Laser Altimeter
- ISA - Italian Spring Accelerometer

- MERMAG - MPO-Magnetometer (MERMAG includes the magnetometer on the MMO)
- MERTIS - Mercury Radiometer and Thermal Infrared Spectrometer
- MGNS - Mercury Gamma-Ray and Neutron Spectrometer
- MIXS - Mercury Imaging X-Ray Spectrometer
- MORE - Mercury Orbiter Radio-Science Experiment
- PHEBUS - Probing of Herman Exosphere by Ultraviolet Spectroscopy
- SERENA - Search for Exospheric Refilling and Emitter Natural Abundances
- SIMBIO-SYS - Spectrometer and Imagers for MPO BepiColombo Integrated Observatory System
- SIXS - Solar Intensity X-Ray and Particles Spectrometer

Instruments are mostly devoted to the study of the surface, the interior structure and the magnetometry of the planet.

Four instruments (ISA, MORE, SERENA, SIMBIO-SYS) are supervised by the Italian Space Agency (ASI), with a collaboration with NASA for MORE and SERENA and with CNES for SIMBIO-SYS.

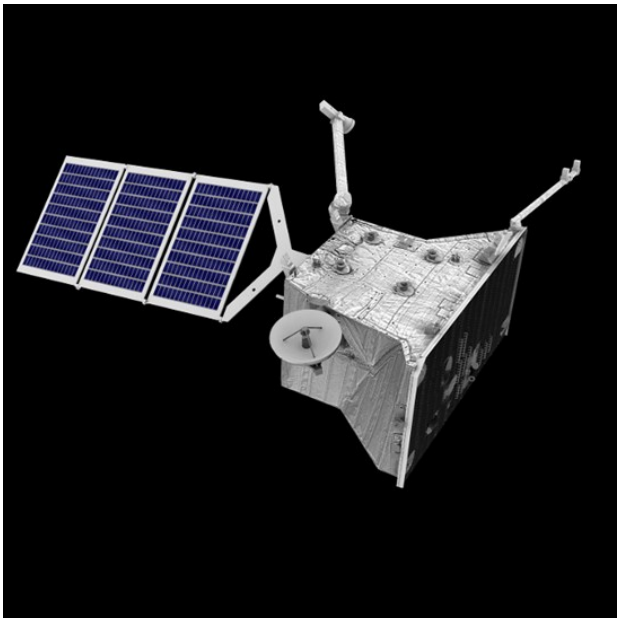

Fig 5 The Mercury Planetary Orbiter MPO

	MPO	MMO
Stabilization	3-axis stabilized	15-rpm spin-stabilized
Orientation	Nadir pointing	Spin axis at 90° to Sun
Orbit	Polar orbit, period 2.3 h 400 x 1500 km	Polar orbit, period of 9.3 h 400 x 11800 km
Spacecraft mass	1150 kg	275 kg
Payload mass	80 kg	45 kg
Payload power	100-150 W	90 W
TM band	X/Ka-band	X-band
Data volume downlink	1550 Gbits/yr	160 Gbits/yr
Equivalent average data rate	50 kbits/s	5 kbits/s
Antenna	High-temperature resistant, 1m X/Ka-band high-gain steerable antenna	0.8 m X-band phased array high-gain antenna
Operational life	>1 year	>1 year

Tab 3 MPO and MMO characteristics

1.3.2.2 MMO

The Mercury Magnetospheric Orbiter (MMO) is the spacecraft designed by JAXA dedicated to the study of the magnetic field and the particle environment.

MMO is a spin-axis stabilized spacecraft (the spin axis will be nearly perpendicular to Mercury's equator) with a spin period of 4s. The orbit is highly elliptical with the Periherm and Apoherm respectively at 590 km to 11639 km.

The spacecraft is equipped with star sensors and a star scanner, a propulsion system with cold gas and a passive nutation dumper.

The scientific instruments are the following:

- MDM - Mercury Dust Monitor
- MGF - Magnetometer
- MPPE - Mercury Plasma Particle Experiment
- MSASI - Mercury Sodium Atmospheric Spectral Imager
- PWI - Plasma Wave Investigation

Instruments are mostly devoted to the study of the magnetic field, waves and particle environment.

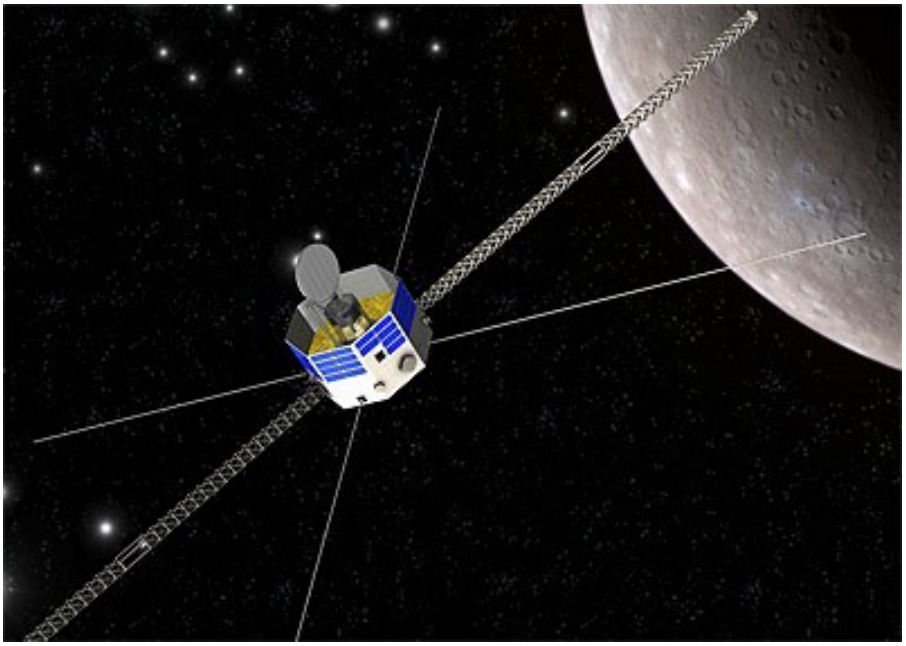

Fig 6 The Mercury Magnetospheric Orbiter MMO

1.3.3 Mission phases

Every space mission can be divided in two different phases: the non-operative phase and the operative phase.
The non-operative phase normally includes the launch, the commissioning phase and the flight.
The operative phase is the period of time in which the mission effectively accomplishes the scientific objectives it was planned for.
Fig 7 shows the different operations of BepiColombo during all the mission's lifetime.

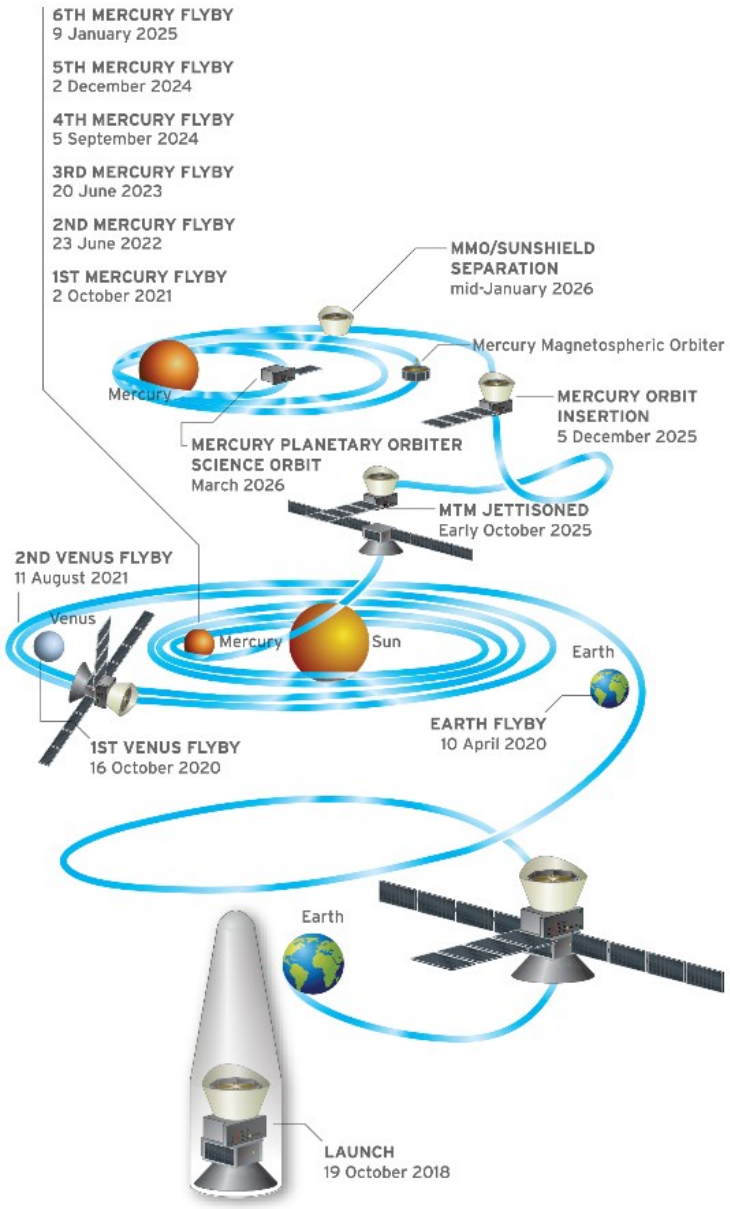

Fig 7 Summary of the different phases of BepiColombo mission

1.3.3.1 Non-operative phases

The non-operative phase includes the following operations:

- Launch and Early Orbit Phase (LEOP): starts with the pre-launch operations and ends four days after the launch. While in space, the MCS is separated from the launcher and some preliminary operations are performed, like the deployment of the solar arrays and the communication with the antennas.

- Near Earth Commissioning Phase (NECP): it lasts three months during which the commissioning is performed. It is performed the deployment of the medium- and high-gain antennas, the checkouts of some instruments and of the solar-electric propulsion system.
- Interplanetary Cruise Phase: the spacecraft leaves the Earth and after a flight of 7 years and nine flybys reaches the orbit of Mercury. Periodical checkouts of the instruments are planned during this phase.
- Mercury Approach Phase: this phase starts two months before the first Mercury orbit insertion maneuver and includes the orbital insertion of the spacecraft and lately the maneuvers for the separation and insertion of MPO and MMO in their specific orbits.

1.3.3.2 Operative phase

MPO and MMO reach the respective orbits and after the commissioning phase the acquisition of data can start. The following table summarizes the orbital parameters of the orbits of the two probes.

Orbital parameter	**MPO**	**MMO**
Periherm [km]	480	590
Apoherm [km]	1500	11639
Inclination i [°]	90	90
Right ascension of ascending node [°]	68	68
Ascending node [°]	0	0
Argument of Periherm ω [°]	Variable	Variable

Tab 4 Orbital characteristics of MPO and MMO

In order to keep the radiator away for the Sun, the MPO has to perform a rotation of 180° every half revolution around Mercury. As the spacecraft is nadir-pointing, the pointing of the instruments towards the surface does not change.
During the mission the MPO argument of Periherm ω and altitude of Periherm hp will continuously change due to the variation of the value of the Mercury gravity field (J2).

The nominal duration of the operative mission is scheduled to be one year, but it has a planned extension of another year.

1.4 Communication

ESA is in charge of the control of the launch, of MCS during the cruise and of MPO during the operative phase. MPO communication are provided uplink via X-band (4 kbits/s) and downlink via X/Ka-band (30-675 kbits/s) with a downlink data of more than 1550 Gb during the nominal mission life.
The spacecraft is controlled by the Mission Control Centre at ESOC (Germany) via the Ground Station in Cebreros (Spain).
JAXA will control MMO by the Sagamihara Space Operations Center via the Usuda Deep Space Center (UDSC) antenna in Nagano (Japan).

Chapter 2: SIMBIO-SYS

The second chapter is focused on the SIMBIO-SYS camera on board MPO. The camera is a package containing three channels STC, HRIC and VIHI. The different channels are designed to cover specifically different tasks: global stereo coverage for the tridimensional reconstruction of the surface, high resolution imaging of selected regions and global spectroscopic analysis.
Every channel is described and the acquisition strategy and scientific objectives are presented.
Main scope of the thesis is to investigate the procedure to produce Digital Terrain Models of planetary surfaces from cameras onboard satellites. SIMBIO-SYS is the perfect instrument for this purpose: the stereo channel is specifically designed for this intention, but the high resolution channel can be used as well if the spacecraft rotates and acquires some off-pointing configurations. Moreover, the possibility to integrate the data of the three channels of SIMBIO-SYS increases the scientific outcome of the mission, allowing new acquisition scenarios and data analysis.

2.1 Overall description

The SIMBIO-SYS suite (The Spectrometer and Imagers for MPO Bepicolombo Integrated Observatory – SYStem) [7] is an integrated package of three instruments: the Stereo Imaging System (STC) [8], the High spatial Resolution Imaging Channel (HRIC) [9] and the Visual and Infrared Hyperspectral Imager (VIHI) [10].
The instrument has been funded by two space agencies, ASI and CNES, while Leonardo SpA in Florence (Italy) has been selected as the prime contractor.
SIMBIO-SYS aims to imaging and investigating the surface of Mercury in order to find information about the evolution of the planet and its geology. In the end it will provide a global mapping of the surface of the planet in stereo mode and high resolution images of the most interesting sites along with a spectral analysis of its composition.
The three channels are described in detail in the following:

- **STC – Stereo imaging Channel:** The STC channel will map the surface in stereo mode at 60 m/pixel resolution with panchromatic and colored filters. Working in stereo mode, STC will create a Digital Terrain Model of the entire surface of the planet. The objective is to topographically characterize the surface and to measure important geophysical parameters as tectonic features, craters and volcanos. In addition, STC will also provide the context for the HRIC in terms of identifying the most interesting targets. The FOV of the STC is 5.38º in the cross-track (CT) direction and 4.8° in the along-track (AT) direction. The detector is composed by four colored filters with wavelengths of 420, 550, 750 and 920 nm and two panchromatic filters centered at 700 nm. The angle between the panchromatic filters and instrument boresight is 21.375°.

- **HRIC – High spatial Resolution Imaging Channel**: HRIC will be able to provide images at ground pixel sizes of 6 m/pixel from an altitude of 480 km, in order to take high spatial resolution images of selected regions from more than 20% of the surface. The main objective of HRIC is the characterization of the most interesting targets with high resolution using a target oriented acquisition strategy. Its FOV is 1.47º, with a panchromatic filter with spectral range of 400–900 nm and three band-pass filters centered at 550, 750 and 880 nm.

- **VIHI – Visible Infrared Hyperspectral Imager Channel:** VIHI will map the planet in the visible and infra-red in order to provide a global mineralogical composition of the surface. The main objectives are to produce a global mineralogical map at spatial resolution better than 120 m, to identify mineralogical species and to correlate surface composition and surface features. VIHI has a FOV of 3.7º and the spectral range is 400-2000 nm and spectral sampling of 6,25 nm.

The three instruments are packaged in one integrated suite in order to reduce the mass, optimize the structural and thermal requirements, guarantee the alignment stability of all the channels and to share the same power supplies and main electronics. The possibility to work with the different channels together is one of the strength of SIMBIO-SYS.

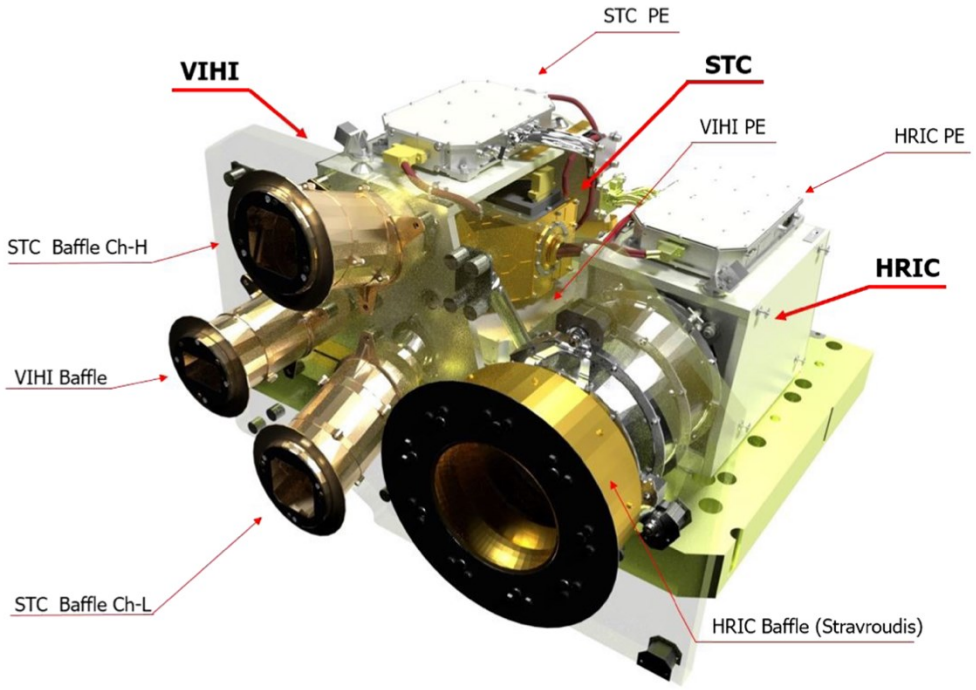

Fig 8 The SIMBIO-SYS suite with the three channels STC, HRIC and VIHI

2.2 Scientific goals

Here are listed the scientific goals of SIMBIO-SYS:

- Global Mapping of the planet in stereo mode in the firsts six months of the nominal mission at spatial scale < 120 m.
- Color mapping at least 10% of the surface with 4 broad band filters with a range of 410-930 nm.
- Mapping at least 20% of the surface with high resolution imaging (6 m/px) with a panchromatic filter and 3 different broad band filters with range of 200-900 nm.
- Global mineralogical mapping of the surface for correlating composition and features to a scale better than 500 m.
- Identify the different mineralogical spices with an accuracy of 10%.
- Provide spectral images of selected areas with a range of 400-2000 nm with a spectral resolution down to 200 m.
- Generation of DTMs at different resolution. High resolution DTMs can be used to investigate the libration phenomenon and some specific geologic targets.

2.3 Thermal and mechanical interfaces

SIMBIO-SYS is a suite containing three different channels that shares a common Main Electronics (ME) and a power supply.

The figure below represents the architecture of the hardware.

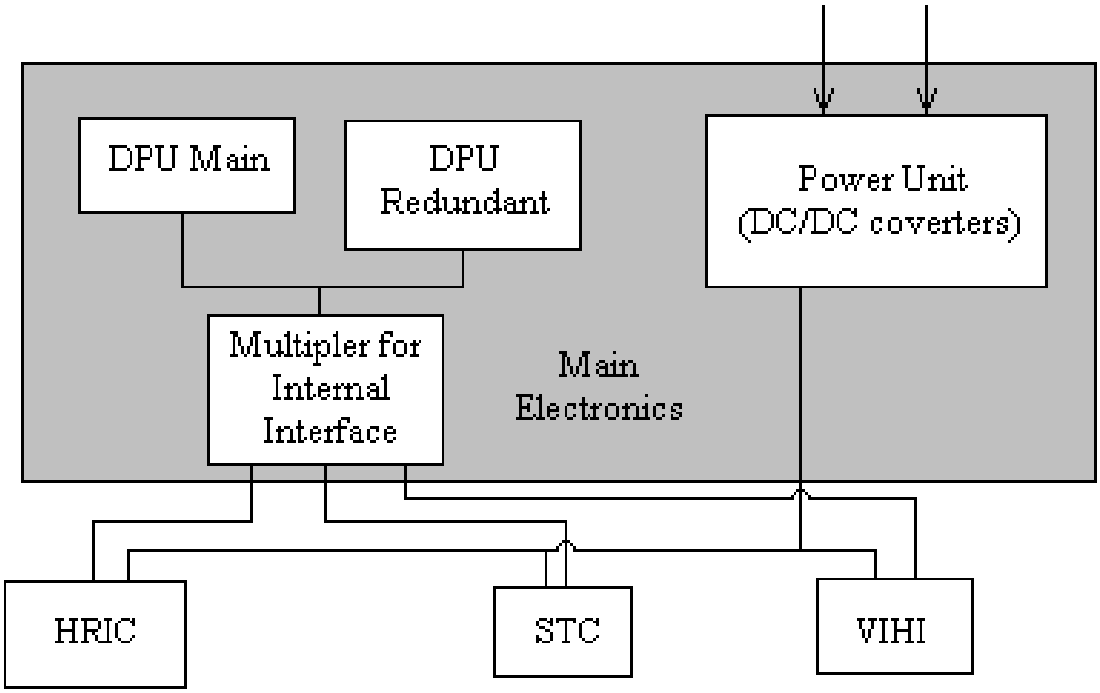

Fig 9 Hardware architecture of SIMBIO-SYS

The three channels HRIC, STC and VIHI form the Instrument Front End (IFE), connected to the ME. The ME has two different functions: data processing like management, compression and instrument control performed by the Digital Processing Unit (DPU) and power supply performed by Power Unit (PU).

A scheme for the ME is shown in Fig 10.

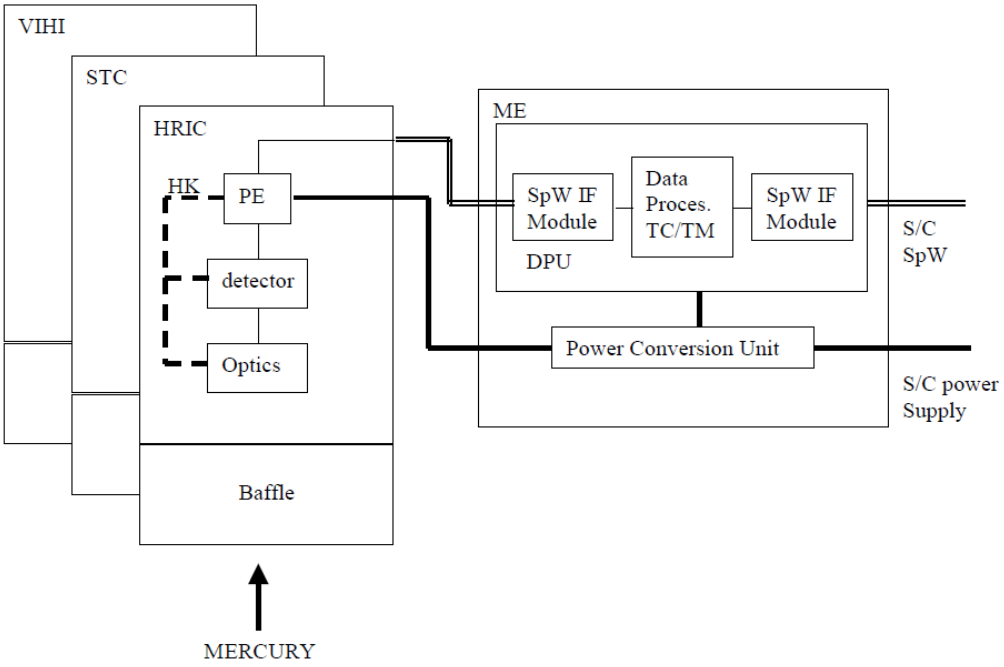

Fig 10 Main Electronic (ME) of SIMBIO-SYS

The working temperature is different for the different channels: the detector of HRIC and STC works in a temperature of 0°, while the detector of VIHI works below 0°, at 223 K. For this reason, an active thermal control is required, capable of removing heat from sensible parts. Thermal strips transfer the heat from the hot side of the detector to the heat pipe positioned in the cold side. All the SIMBIO-SYS suite is thermally decoupled from the rest of the spacecraft, so the thermal flux exchange is negligible.

Saving space and mass is one of the main driver for every space mission. Thus, every channel is designed to obtain a good balance between mass and performance, resulting in an overall compact and light instrument. Mass budget details and dimensions are listed in the following table.

SIMBIO-SYS component	
Total mass [kg]	14.751
Channels mass [kg]	8.747
Baffles mass [kg]	1.252
Electronics mass [kg]	3.568
MLI [kg]	0.267
Internal harness [kg]	0.917
Dimension [mm^3]	470 × 490 × 325

Tab 5 Mass budget and dimension of SIMBIO-SYS

2.3.1 Baffles

The baffle is the conical extremity of the camera designed to protect the optics from the incoming radiation of the external environment. This passive thermal control system limits the stray-light radiation and shields the detector, ameliorating its performances and duration.
The working principle of a baffle is shown in the following image.

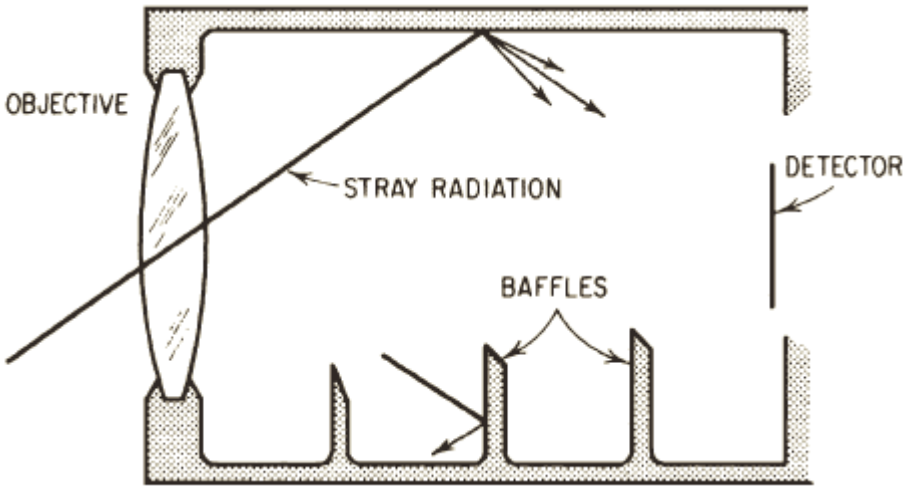

Fig 11 Baffle working principle

Every optical channel of SIMBIO-SYS is protected by a baffle. HRIC baffle is designed with a Stavroudis configuration, formed by reflective hyperbolas and parabolas surfaces capable of

rejecting the incident light. STC and VIHI baffles present a similar configuration, with internal black vanes.

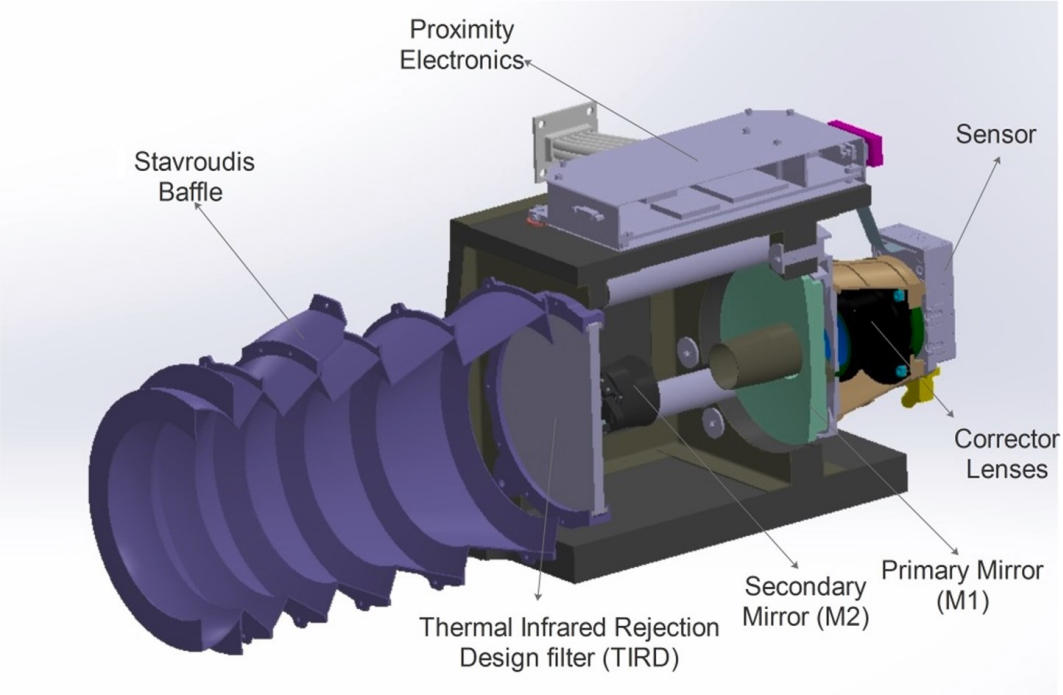

Fig 12 HRIC baffles

2.4 HRIC

HRIC is the High Resolution Channel of SIMBIO-SYS. It will be able to provide images at 6 m/pixel resolution at Periherm in panchromatic filter and in three band-pass filters centred at 550, 750 and 880 nm. The configuration of the mirrors is a catadioptric Ritchey-Chretien telescope, satisfying the desired performances but also the stringent dimensional and low mass requirements.

2.4.1 Optical design

The optical structure is a Ritchey-Chretien configuration with a ratio between the secondary mirror diameter and the primary mirror diameter equal to 0.3. The field of view of the camera is a global 1.47° with 2.5’’/pixel. The detector equipped is a hybrid SiPIN array with 2048 × 2048 pixel of 10 µm size.

The channel has a focal length of 800 mm with a focal ratio of *f*/9.4 in order to be diffraction limited at 400 nm.

The overall design balances performances and compactness, one of the most challenging constrains of the instrument.

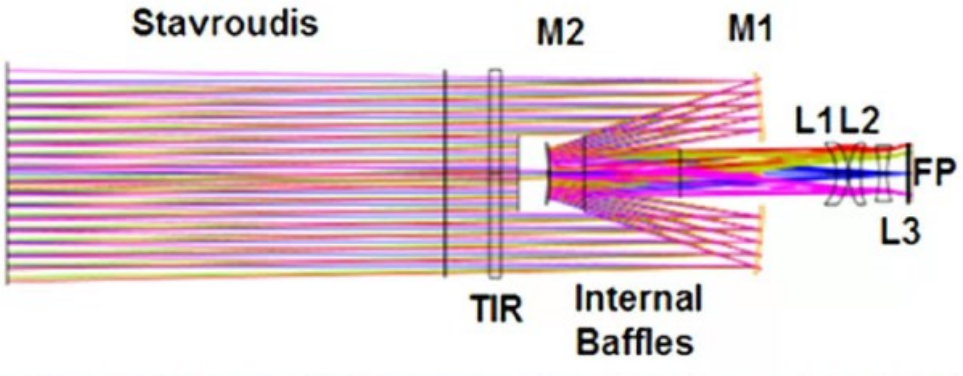

Fig 13 HRIC optical design

Parameter	**Unit**	**Value**
Aperture	mm	Diameter 85
Focal length	mm	800
Focal number		9.4
λ for diffraction limit	nm	400
Field of view	°	1.47
Central obstruction	%	10
Pixel IFOV	μrad	12.5
Spectral range	nm	400 – 900
Filter bandwidth	nm	40/50
Spectral channels	nm	Panchromatic 650; 550, 700, 880
Mirror material		Aluminium
Diffraction EE in one pixel	%	68
MTF at Nyquist frequency	%	30 – 33
Rms spot diameter	μm	1.6
Field curvature	nm	0.03
Distortion	%	0.05

Tab 6 HRIC optical parameters

2.4.2 Sensor

The sensor is a 2048 × 2048 pixels SiPIN Complementary Metal Oxide Semiconductor (CMOS) with a pixel size of 10 µm. The sensor is capable of converting the incident light in electric charge that is measured inside the photodiodes of the circuit of the CMOS.

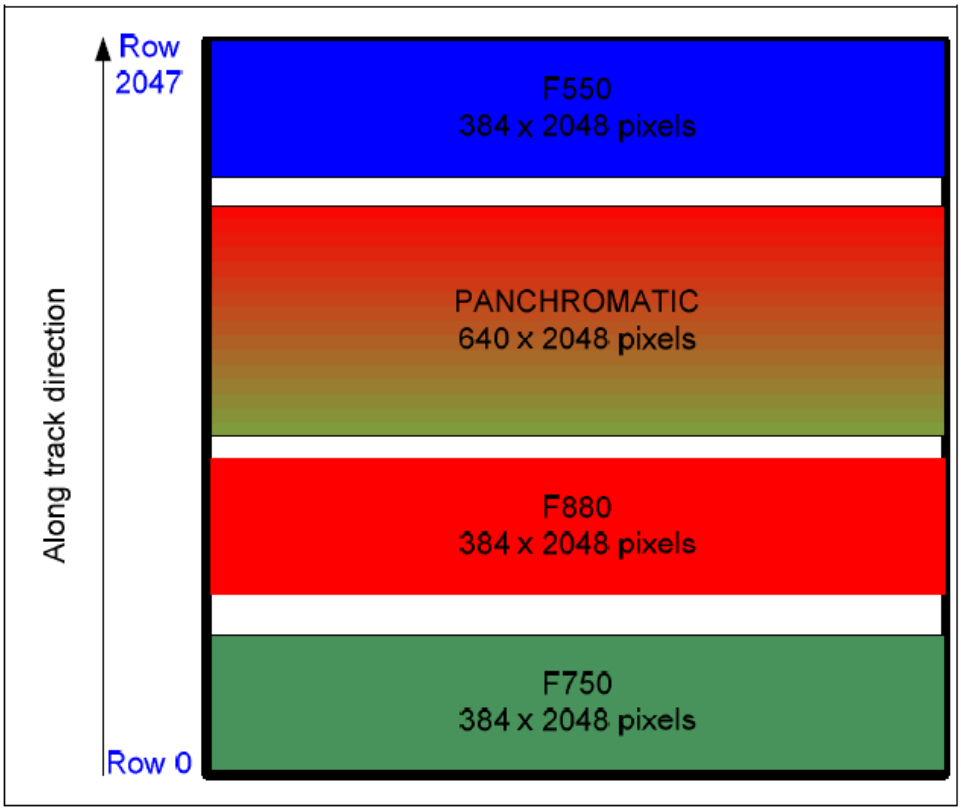

Fig 14 HRIC filters. In particular: panchromatic (FPAN) and three coloured filters F550, F880, F750

The following table shows the characteristic of the sensor.

Parameter	**Unit**	**Value**
Sensor type		Si-PiN-Hybrid
Format		2048 × 2048
Pixel size	µm	10 x 10
Spectral range	nm	400 – 1000
QE x FF	%	>42 for 400 to 800 nm >24 for 800 to 900 nm >10 for 900 to 950 nm
MTF	%	>50 at Nyquist frequency
Read noise at 20°C	e^-	<100
Dark signal at 20°C	e^-/s	<10000
DSNU	%	<5 (rms)
Full well capacity	ke^-	120
PRNU	%	<2 (rms)
Exposure time	ms	4
Read out	MPS	<5
Spurious charge	e-/s	<100
Non operating temperature	°C	-40 to 60
Operating temperature	°C	-5 to 20
Linearity	%	<±1
Power dissipation	W	<0.1
FPN	mV	<15
Defects		<0.5%
Radiation-total dose		70 krads(Si)
Radiation-SEE	$MeV/mg/cm^2$	SEL threshold >70 SEU threshold >70
CVF	µV/e-	14
Photon flux	ph/pxl/s	-high flux case: 8 10^8 to 2 10^9 photons -low flux case: 10^6 to 10^7 photons

Tab 7 HRIC and STC sensor parameters

2.4.3 Observation strategy

The main objectives of HRIC are the following:

- Provide high resolution images of the surface of the planet, nominally 6 m/pixel.
- Map in high resolution at least 20% of the planet.
- Provide high resolution images in panchromatic and three broad-band filters at 550, 750, 880 nm.

HRIC will work in two modes, high resolution and low resolution mode. High resolution mode is achieved at Periherm when Mercury is in the Aphelion, while low resolution mode is achieved at Apoherm when Mercury is in the Perihelion. The acquisition strategy is target oriented and the targets are selected for their scientific importance, with their size and position that vary on the surface. Therefore, the final data volume depends on the targets' choice.
Due to the small FOV, images acquired in one orbit are not always contiguous with images acquired in the following one. For this reason, the longitudinal coverage of a target must be completed with other passages after one entire rotation of the planet or by tilting the spacecraft, but this latter operation must be carefully planned as it affects the nominal S/C attitude. In the along-track direction the acquisition is simpler as it is just necessary to operate with a push-frame approach choosing a specific repetition time.

2.4.4 Performances

The performances of the camera are dependent to the position and observation time of the selected target.
On-ground pixel size is influenced by the altitude of the spacecraft while orbiting. The MPO orbit is polar and elliptic, so its altitude varies with the Latitude. The following plot shows the altitude of the spacecraft in dependence of the Latitude.

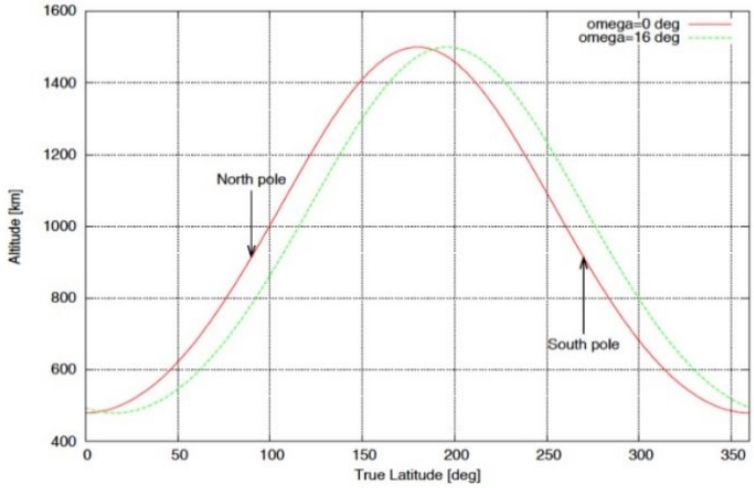

Fig 15 Altitude of the MPO as function of the true Latitude. In green the Periherm is at 16° N (beginning of the mission), in the Periherm is at 0° (six months after the beginning of the mission)

Also the signal to noise ratio (S/N) depends on the Latitude. Fig 16 shows the variation of the S/N varying the albedo and the position of Mercury around the Sun. On the left, the broad band filter at 550 nm is taken into account; on the right the panchromatic filter is taken into account.

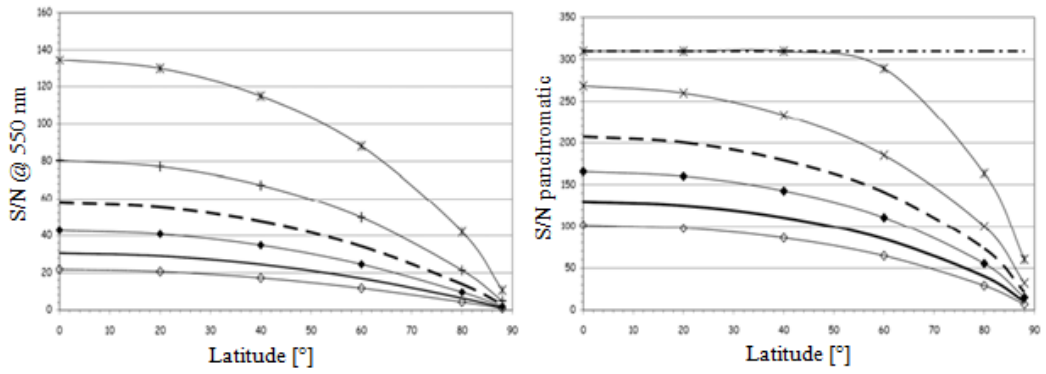

(a) (b)

Fig 16 Signal-to-noise ratio with 550/40 nm (a) and panchromatic filter (b). Blank rhombi: albedo A = 0.08, Aphelion; black rhombi: albedo A = 0.08, Perihelion; crosses: albedo A = 0.45, Aphelion; stars: albedo A = 0.45, Perihelion; continuous line: A = 0.12, Aphelion; dotted line: A = 0.45, Perihelion; horizontal line: saturation level

As explained in the previous paragraph, SIMBIO-SYS operates in two modes: high resolution mode and low resolution mode. The limits of the phases are identified by the position of Mercury around the Sun, described by the True Anomaly. For HRIC, the High Resolution Phase is identified within 110° and 250° of TA, while the Low Resolution Phase within 290-70° TA. The following table shows the dimension of the footprint on ground of the PAN of HRIC during the first Periherm of the mission.

Parameter	**Periherm**	**Poles**
S/C altitude [km]	480	966.7
Pixel on ground [m]	6.0	12.1
Swath CT [km]	12.3	24.8
Swath CT [°]	0.30	4.78
Swath AT [km]	3.8	7.7
Swath AT [°]	0.09	0.18

Tab 8 HRIC observation parameters for the PAN filter during the first Periherm of the mission

2.5 STC

STC is a wide angle camera composed by two sub-channels named High (H) and Low (L) oriented +20° and -20° with respect to the nadir, allowing to acquire images of the same area at close moments taking advantage of the along-track movement of the spacecraft. The design is innovative, as the two sub-channels share the same detector in order to minimize mass and power. STC has been conceived to obtain stereo pairs useful to reconstruct Digital Terrain Models (DTMs) of the surface of the planet with a vertical accuracy of 80 m. The camera has six filters: two panchromatic centred at 700 nm and 4 broad band filters at 420, 550, 750, 920 nm.

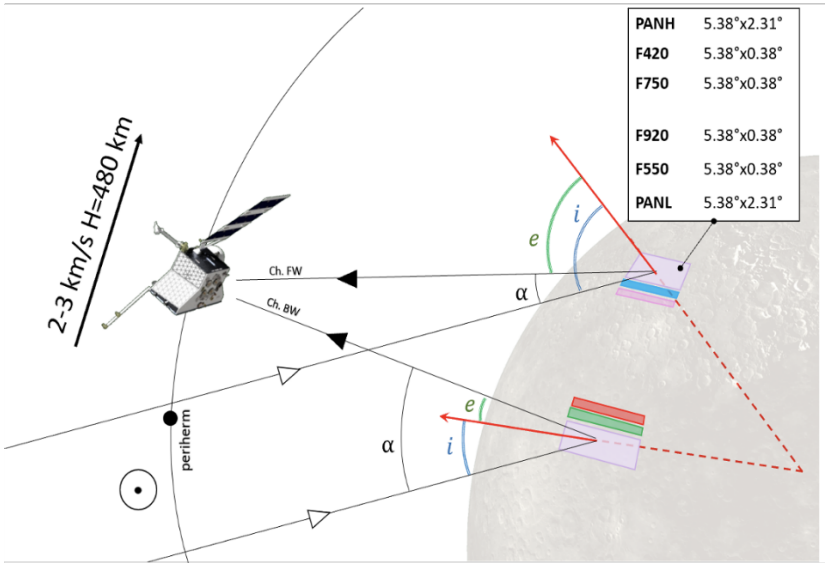

Fig 17 STC working concept with the projection on ground of the different filters and angles: e = emission angle, i = incidence angle, α = phase angle

2.5.1 Optical design

STC has a modified Schmidt optical design with two channels that share most of the optical elements. The classical Schmidt correcting plate is replaced by a correcting doublet, designed to correct the aberrations produced by the primary mirror. This solution saves space and mass, reducing the telescope length by a factor 2 respect to a normal configuration. The field of view of the camera is a rectangle of 5.3° × 4.8° for both channel, corresponding to 23''/pixel. At Periherm, where the altitude is the lower, the resolution on ground is around 60 m/pixel and the FOV covers an area of 40 × 19 km^2 with the panchromatic filter and an area of 40 × 3 km^2 with the coloured filters.

The focal length of the system is 95 mm with a focal ratio of *f*/6. The detector is a 10 µm pixel size SiPIN CMOS.

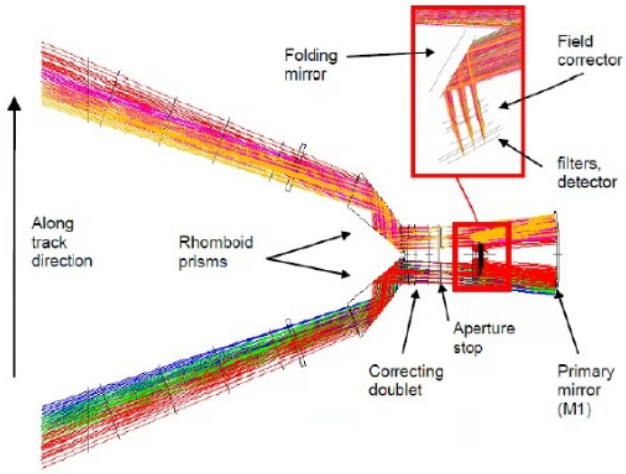

Fig 18 STC optical design

Parameter	**Unit**	**Value**
Aperture	mm	Diameter 24
Focal length	mm	90
Focal number		6
Field of view	°	5.3 × 4.5
Pupil size	mm	15
Central obstruction	%	0
Pixel IFOV	μrad	111
Spectral range	nm	410 – 930
Filer bandwidth	nm	20/200
Spectral channels	nm	Panchromatic (700); 420, 550, 750, 920
Mirror material		BK7
Mirror efficiency	%	>80
Mirror coating		Al + MgF2
Diffraction EE in one pixel	%	<70
MTF at Nyquist frequency	%	>60
Distortion	%	<1.6

Tab 9 STC optical parameters

2.5.2 Sensor

The sensor is the same type of the HRIC one, a 2048 × 2048 pixel SiPIN Complementary Metal Oxide Semiconductor (CMOS). The characteristics are summarized in the Tab 7.

The detector can be commanded only to acquire images with dimensions multiple of 64 pixels, with a minimum possible acquisition window of 64 × 128 pixels (H × W). An area of 64 × 128 pixels, called Window X, is reserved for calibration purposes measuring the amount of dark current. The following table show the characteristics of the different filters present on the sensor.

	Raw Definition		Dimension	Bsight Dir	FoV	Angle Definition (vs Nadir)		Angle Definition (vs +-20°)		Bsight (vs ±20°)
	Starting	End				Starting	End	Starting	End	
	[px]	[px]	[px]	[°]	[°]	[°]				[°]
F750	32	95	64	17.95	0.38	17.76	18.14	-2.24	-1.86	-2.05
GAP	96	239	144	18.585	0.87	18.15	19.02	-1.85	-0.98	-1.42
F420	240	303	64	19.22	0.38	19.03	19.41	-0.97	-0.59	-0.78
GAP	304	436	133	20.2975	0.81	19.89	20.70	-0.11	0.70	0.30
PANH	437	820	384	21.375	2.31	20.22	22.53	0.22	2.53	1.38
GAP	821	1226	406	-	-	-	-	-	-	
PANL	1227	1610	384	21.375	2.31	20.22	22.53	0.22	2.53	1.38
GAP	1611	1744	134	20.2975	0.81	19.89	20.70	-0.11	0.70	0.30
F550	1745	1808	64	19.22	0.38	19.03	19.41	-0.97	-0.59	-0.78
GAP	1809	1952	144	18.585	0.87	18.15	19.02	-1.85	-0.98	-1.42
F920	1953	2016	64	17.95	0.38	17.76	18.14	-2.24	-1.86	-2.05

Tab 10 Position and geometric characteristics of each filter present on the detector

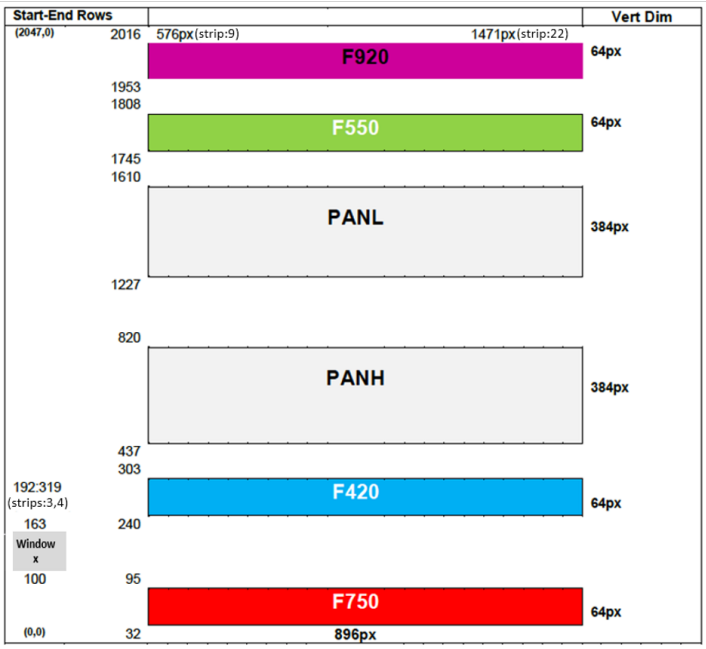

Fig 19 Position of the filters on the detector

2.5.3 Observation strategy

STC has to map the entire surface of the planet in stereo mode for the generation of a global DTM. The camera will work in two modes: Stereo Mapping and Colour Mapping.

The Stereo Mapping will cover the entire surface of the planet with the PAN filters and will be performed during the first six months of the mission, and eventually in the following six. The large FOV of STC permits to acquire images in two successive orbits that always overlap, facilitating the mosaicking. The global mapping is the starting point that will drive the selection of specific targets for HRIC which can provide more details for the most scientifically interesting areas.

The Colour Mapping will be performed in the second six months of the mission and will be target-oriented, investigating the most interesting targets with the broad-band filters.

The observation strategy of the instrument is very flexible, thanks to the possibility to work with one or both sub-channels, use different filters combinations and different compression ratios.

STC operates inside the range of 138°-222° TA for the High Resolution Phase and of 278°-82° for the Low Resolution Phase.

In order to facilitate the acquisition planning and decrease the data volume, a possibility might be to divide each orbit around Mercury in different segments (11 or 21). The segments are

function of the subnadiral latitude: in the two segments near the poles only one sub-channel will work (the one that is pointing towards the illuminated part of planetary surface), while in the other both the sub-channels will work simultaneously. The following image shows the orbit division in segments.

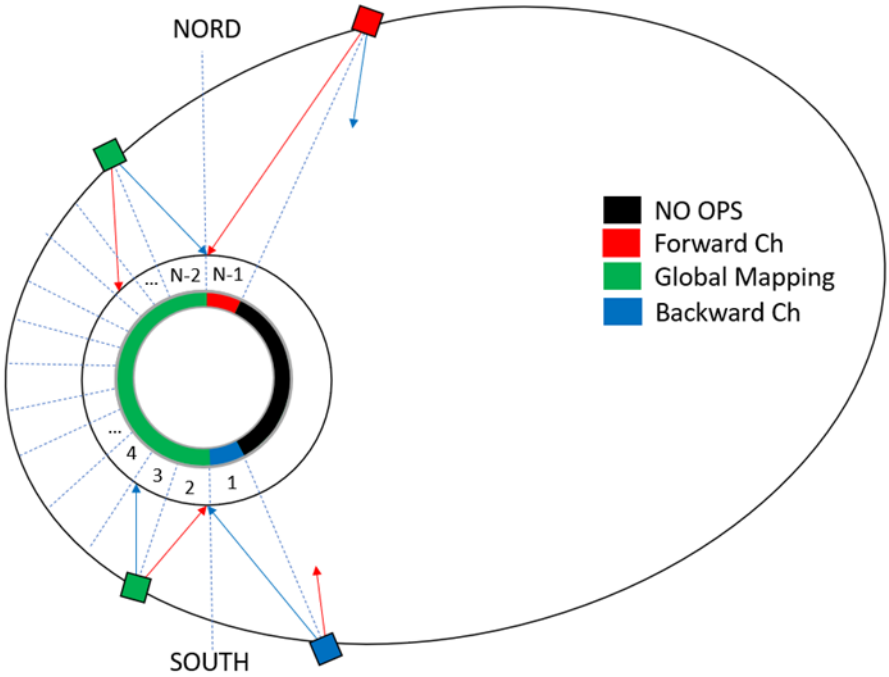

Fig 20 Segment orbit subdivision. In the red and blue area STC works with only one sub-channel, in the green with both.

The following table shows the footprint dimension on ground of the PAN filter of STC during the first Periherm of the mission.

Parameter	Periherm	Poles
S/C altitude [km]	480	966.7
Pixel on ground [m]	58	121.8
Swath CT [km]	48.3	100.96
Swath CT [°]	1.19	7.9
Swath AT [km]	23.3	52.5
Swath AT [°]	0.55	1.2

Tab 11 STC observation parameters in the PAN filter during the first Periherm of the mission

2.6 VIHI

The instrument is composed by a telescope in a modified Schmidt configuration and a grating spectrometer in Littrow configuration working in the range between 400-2000 nm. The main goals of the instrument are mapping the entire surface of the planet and providing a global mineralogical compositional map. The global map will be obtained with resolution better than 400 m, while 5-10% of the surface will be mapped in higher resolution of 100 m.

2.6.1 Optical design

The instrument is divided in two parts: a telescope and a spectrometer. The telescope is based on a modified Schmidt design and a diffraction-grating spectrometer with a Littrow configuration. The instrument has 160 mm focal length with a focal number of *f*/6.4 and a field of view of 3.7°. The image of the slit is diffracted by the grating over the spectral range (400-2000 nm) and the image itself is then built as the sum of subsequent acquisitions while the spacecraft is moving in the along-track direction. The FOV in the cross-track direction is large enough to overlap two acquisitions with two successive orbits, allowing to perform a global coverage in six months.

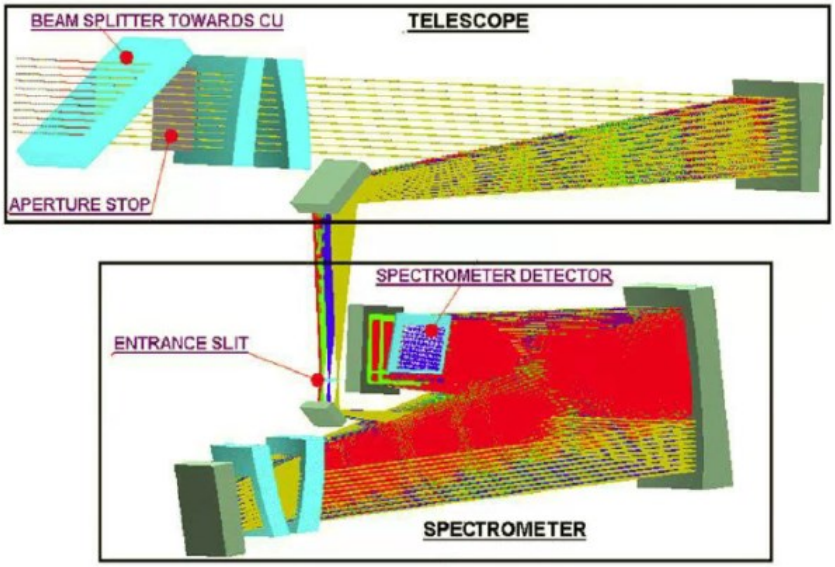

Fig 21 VIHI optical design

Parameter	**Unit**	**Value**
Aperture	mm	Diameter 25
Focal length	mm	160
Focal number		6.4
Field of view	μrad	64 × 0.25
Central obstruction	%	0
Pixel IFOV	μrad	250
Scale per pixel	m/pixel	120
Spectral range	nm	400 – 2000
Spectral channels		256
Spectral dispersion	nm/pixel	6.25

Tab 12 VIHI optical parameters

2.6.2 Sensor

The sensor is a 264 × 264 pixels array of SWIR HgCdTe photodiodes hybridized on a silicon ReadOut Integrated Circuit (ROIC). The dimension of each pixel is 40 µm.
The detector is cooled down to the operative temperature of 220 K by a two-stage thermoelectric cooler and the heat dispersion is achieved with cold fingers.
The main characteristics of the sensor are summarised in the following table.

Parameter	**Unit**	**Value**
Sensor type		Hybrid HgCdTe
Format		264 × 264
Pixel size	µm	40
Dark current	Me-/s	10
Wavelength range	µm	0.4 – 2.2
Peak quantum efficiency	%	> 50
Read noise	e-	<600
Full well capacity	e-	>2 10^6
Readout rate	Mpix/s	>4
Power dissipation	mW	<100
Operability	%	>96
Operating temperature	°C	<-50
Exposure time	ms	10

Tab 13 VIHI sensor data

2.6.3 Observation strategy

VIHI will obtain the global map in the first six months of the mission and the high resolution map of the most interesting regions in the following part of the mission with a target-oriented strategy. In the second part, the flexibility is the key in the acquisition process, with the possibility to change different measurement parameters in dependence on the selected target.

Chapter 3: Photogrammetry overview

Photogrammetry is defined as: *"the science and technology of obtaining reliable information about physical objects and the environment through the process of recording, measuring and interpreting photographic images and patterns of electromagnetic radiant imagery and other phenomena"*. For what concerns the work presented in this thesis, only the specific topic of the creation of Digital Terrain Models is explored.
At the beginning of the chapter, some concepts related with the camera equations are given; then, it is explained how to retrieve geometrical data from images with the use of matching algorithms and the triangulation of features. All these passages are necessary for the creation of Digital Terrain Models.

3.1 The projection matrix

Image formation is the procedure of mapping points of a scene from the 3D world to a 2D image plane. Thus, it is necessary to define a transformation to map from the three-dimensional space to the 2D space. This transformation is called perspective projection and can be described with a matrix called projection matrix.
Some preliminary knowledge about image formation are necessary to understand the significance of the projection matrix. The image formation process can be explained with the concept of a pinhole camera, a simplified camera model without lenses and with a tiny aperture. Light is assumed to pass through the aperture and it forms an inverted image on the other side. This effect is called "camera obscura".

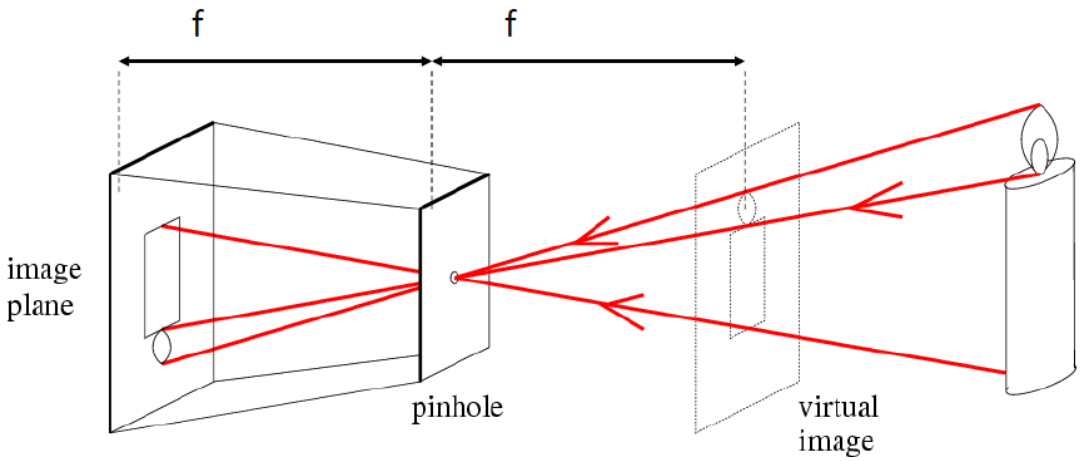

Fig 22 Schematic representation of a pinhole camera

Fig 22 shows an example of a pinhole camera. The focal length *f* measures the distance at which light converges or diverges in an optical system, that corresponds to the position where the image is formed on the image plane. The image is formed on the image plane positioned after the pinhole, while a virtual image is formed before it. The real object is positioned in the 3D world with the coordinates X, Y, Z. Assumed Z as the direction perpendicular to the image plane, the coordinates of the object in the image are expressed as:

$$x = f\frac{X}{Z} \tag{1}$$

$$y = f\frac{Y}{Z} \tag{2}$$

For pinhole cameras it is assumed that a unique projection center exists, so that the light rays between object and image points pass through a single point.

Image coordinates can be expressed in two types, Cartesian and Homogeneous. Homogeneous coordinates simplify the representation of lines in two dimensions, as they can be expressed with the same form of points. In this way, vertical lines can be represented without going to infinite. Moreover, elements expressed in homogeneous coordinates are invariant to multiplication by a scalar.

Cartesian: $p = (x, y)$

Homogenous: $\tilde{p} = (x, y, 1)$

It is possible to convert from Homogeneous to Cartesian systems with a simple transformation:

$$x = \frac{\tilde{x}}{z} \tag{3}$$

$$y = \frac{\tilde{y}}{z} \tag{4}$$

The pinhole equation can be expressed with a matrix written in Homogeneous coordinates as:

$$\begin{pmatrix} \tilde{x} \\ \tilde{y} \\ \tilde{z} \end{pmatrix} = \begin{bmatrix} f & 0 & 0 & 0 \\ 0 & f & 0 & 0 \\ 0 & 0 & 1 & 0 \end{bmatrix} \begin{pmatrix} X \\ Y \\ Z \\ 1 \end{pmatrix} \tag{5}$$

In order to deal with digital images, the concepts of the pinhole camera are slightly modified to obtain the central projection model. In this case, the image is formed in front of the camera, and the rays spread from the real object converge in the camera origin. The image is divided in cells called pixels expressed in the internal coordinates *u*, *v*. The dimensions of the image are converted from meters to the dimension of the pixels. In addition, there is a shift of the coordinates, as the origin of the image coordinates is positioned in the top left corner.

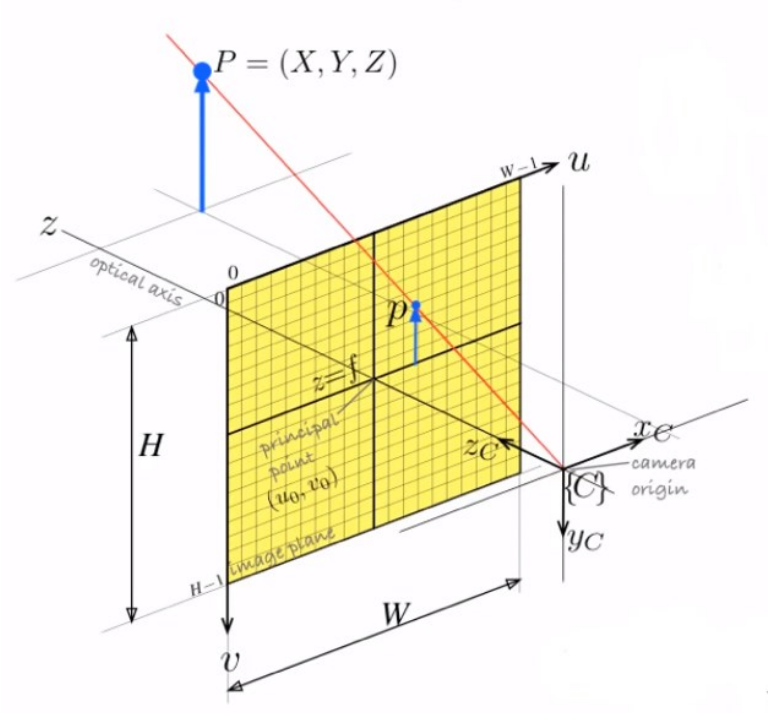

Fig 23 Central projection model: P is the object in the space, C is the position of the camera and the yellow plane is the image plane where the point P is mapped

The camera matrix M, shown below, can efficiently transform a point known in a generic coordinate system and map it to the image plane:

$$\begin{pmatrix} \tilde{x} \\ \tilde{y} \\ \tilde{w} \end{pmatrix} = \begin{bmatrix} f & s & u_0 \\ 0 & f & v_0 \\ 0 & 0 & 1 \end{bmatrix} \begin{bmatrix} r_{11} & r_{12} & r_{13} & t_x \\ r_{21} & r_{22} & r_{23} & t_y \\ r_{31} & r_{32} & r_{33} & t_z \end{bmatrix} \begin{pmatrix} X \\ Y \\ Z \\ 1 \end{pmatrix} \tag{6}$$

With:

f = dimension of the focal expressed in pixel, normally this value is equal in both the x and y direction

s = skew factor

u_0, v_0 = principal points

r = rotation parameters

t = translation parameters

Where the matrix can be decomposed in two different matrices:

$$K = \begin{bmatrix} f & s & u_0 \\ 0 & f & v_0 \\ 0 & 0 & 1 \end{bmatrix} \tag{7}$$

and

$$RT = \begin{bmatrix} r_{11} & r_{12} & r_{13} & t_x \\ r_{21} & r_{22} & r_{23} & t_y \\ r_{31} & r_{32} & r_{33} & t_z \end{bmatrix} \tag{8}$$

representing the intrinsic camera matrix (K) and extrinsic camera matrix (RT).
The matrix is called projection matrix of the camera, written in a compact form as:

$$P = KR[I| - t] \tag{9}$$

The intrinsic parameters (5 DoF) represent the internal parameters of the camera, such as pixel dimension and focal length, which is responsible for the zooming factor of the image. The extrinsic parameters (6 DoF) represent the position of the camera in the space with respect to the object, both with translation (where the camera is respect to the object) and rotation (how the camera is pointing the object).

In conclusion, image formation depends on different factors: position of the camera, orientation of the camera, focal length and pixel dimension.

If the points of the object lie on one plane the equation of the projection matrix can be simplified as:

$$\begin{pmatrix} \tilde{u} \\ \tilde{v} \\ \tilde{w} \end{pmatrix} = \begin{bmatrix} H_{11} & H_{12} & H_{13} & H_{14} \\ H_{21} & H_{22} & H_{23} & H_{24} \\ H_{31} & H_{32} & H_{33} & 1 \end{bmatrix} \begin{pmatrix} X \\ Y \\ 1 \end{pmatrix} \tag{10}$$

This new matrix with 8 parameters is called homography matrix and maps points from a plane to points of an image.

Homography is useful to obtain perspective rectification, the process to project different images in a common plane. The rectification of images is the first step for the triangulation of stereo pairs.

3.2 Epipolar geometry

The concept of central projection model described before is used to define the epipolar geometry. Epipolar geometry describes the geometry of stereo vision, with two cameras viewing a 3D scene from different perspectives.

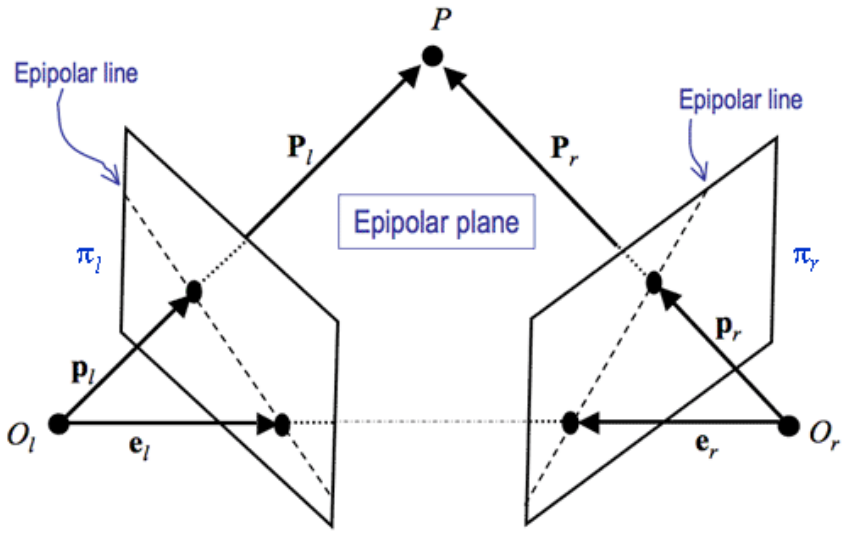

Fig 24 Epipolar geometry

Fig 24 shows two pinhole cameras with projection points O_l and O_r pointing the object P. The distance between O_l and O_r is called baseline and represents the distance between the two cameras that are acquiring the scene. P_l and P_r represent the projection of the point P on the two image planes π_1 and π_2. The plane formed by O_l, O_r and P is defined as epipolar plane, and it intersects the two image planes in two lines called epipolar lines, in this case P_l-E_l and P_r-E_r. The two points E_l and E_r are called epipoles.
Using the epipolar geometry, finding corresponding points in two images results easier. In fact, given a point in the first image, the corresponding point in the second image lies on its epipolar line. If the two images are rectified, meaning that the two image planes coincide, the epipolar lines lie horizontally and the search of corresponding points is done along horizontal lines, simplifying and speeding up the procedure of searching.

3.3 Image matching

Image matching is the process of bringing two images geometrically into agreement so that corresponding pixels in the two images correspond to the same physical region of the scene being imaged [11]. Given two images, often called left image and right image for simplicity, some corresponding points must firstly be searched and identified in both, and after that the desired transformation can be performed. From these points a disparity map is then calculated: the disparity map encodes the differences of the coordinates in pixels of the corresponding points of the two images and from this the triangulation process can take place.
The search between identical features in two images is achieved by image matching algorithms. Matching algorithms can be divided in two main categories, according with the technique used to find the correspondences:

1. Feature based matching algorithms (FBM): the features present in the images are extracted and analyzed using specific operators and a correspondence between the two images is found.
2. Area based matching algorithms (ABM): the correspondence is searched comparing the intensity values of the pixels of the two images (gray scale).

Feature based methods are normally more efficient than area based methods but they need clear recognizable points to perform properly, but unfortunately this characteristic is difficult to match in planetary surface images. So, for the study of planetary surfaces, the area based matching algorithms are the most used.

3.3.1 Feature based matching

The first step of the feature based matching algorithm is to search and extract features with the use of an interest operator based on the recognition of radiometric characteristics [12]. Once the features are identified, their information are stored in a descriptor operator, a vector of data that is invariant to geometric transformations as scale, translation and rotation. The second step is then finding the same features in the second image by comparing the information contained in the descriptors.

The use of epipolar geometry accelerates the matching process: in fact, if the two images are rectified, the corresponding points lie on the same line, so the search has to be performed in just one dimension, decreasing the computation load.

Two popular feature detectors are SIFT (Scale-Invariant Feature Transform) [13] and SURF (Speeded Up Robust Features) [14].

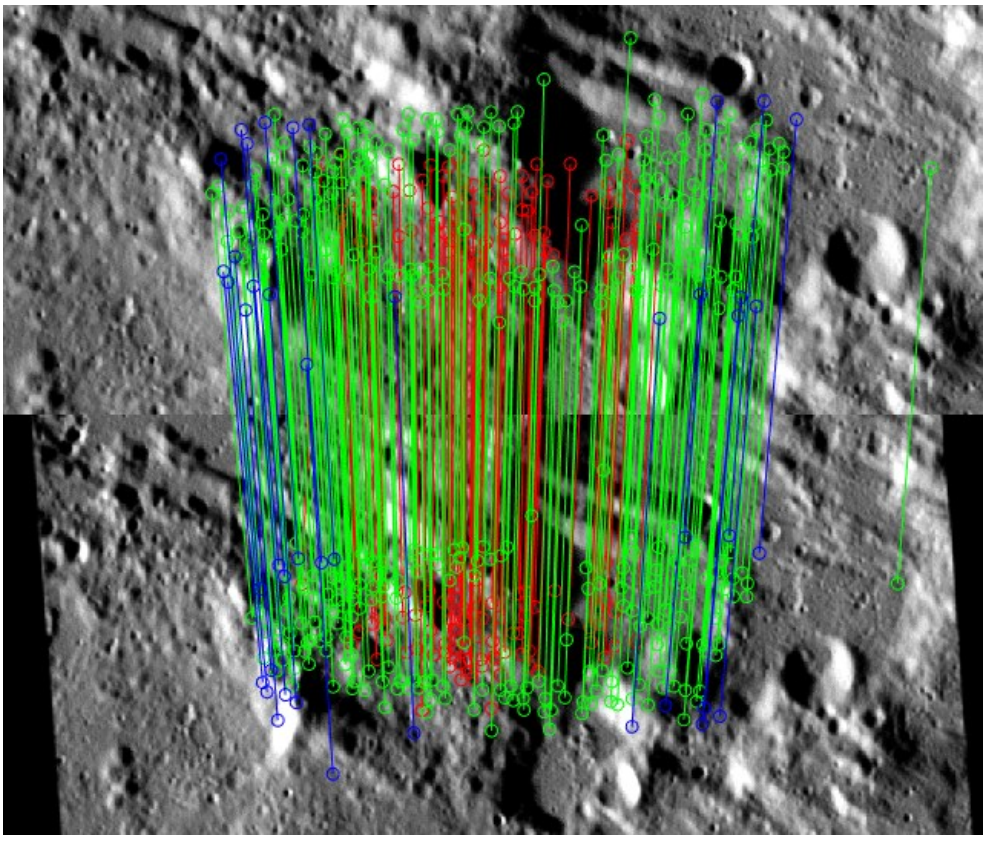

Fig 25 Example of Feature Based Matching. The screenshot is taken from the CaSSIS Reader, the software used in this thesis to match a stereo pair

3.3.2 Area based matching

Area based matching algorithms analyze the radiometric properties of two images in order to find correspondences. The gray values of the reference image, called master image, are compared to the gray values of the search image, called slave image. The two images are divided in smaller areas to facilitate the search: the master image is divided in windows of pixel called templates, the slave image in patches. The correspondence is found when template and patch are equal, or at least similar, because the inevitable changing in the acquisition conditions of the two images makes almost impossible to find a perfect equivalence between them.
There are different correlation methods that are used to compare the gray scale value. Some methods are simpler and faster, like for example the Normalized Cross Correlation (NCC) [15], that searches for comparisons in the gray scale taking into account only the eventual translation of the pixels; other methods, like for example the Least Square Matching (LSM) [16], take into account also the rotation and scale changes of the pixels, performing a resample of the images: LSM executes a geometric and radiometric transformation in the master and slave images in order to minimize the least-square sum of the pixel value differences. LSM algorithms are more precise but also more computationally demanding.

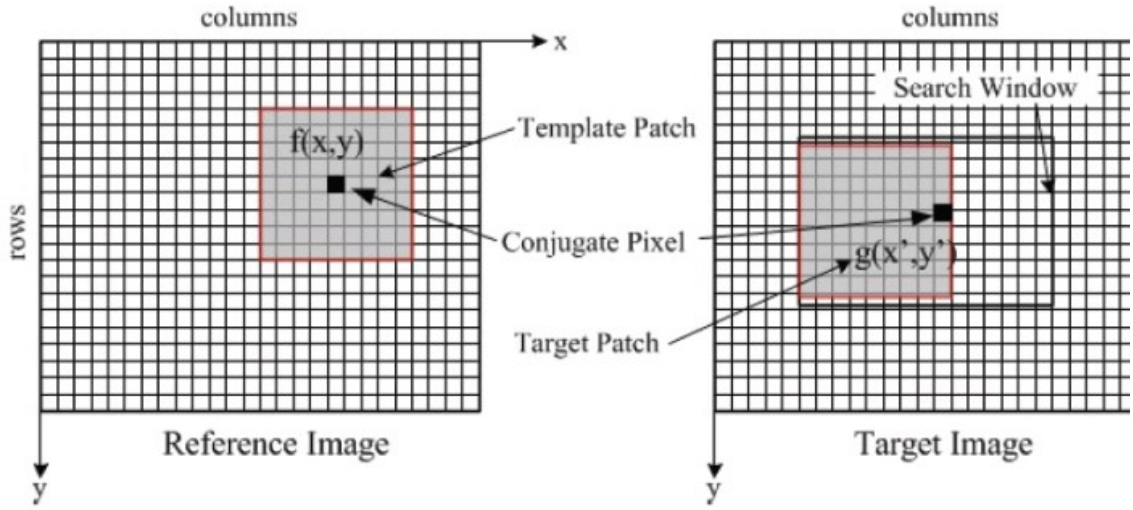

Fig 26 Example of Area Based Matching [17]

3.3.2.1 Least Squares Matching

Least square matching is a flexible technique that allows simultaneous radiometric and geometric corrections while matching different images. The technique was developed to respond to the increasing demand of processing aerial digital images, where geometrical and radiometric distortions pose limits to the use of cross-correlation methods. The novelty of the process lies on the automatic correction of system parameters during the least squares iterations. Given two images, called left and right, the two functions f(x,y) and g(x,y) can be defined as the conjugate regions of the images respectively.
A perfect correlation is ideally established if

$$f(x,y) = g(x,y) \tag{11}$$

but because of inevitable random noise present in the images an error vector e(x,y) is added as

$$f(x,y) - e(x,y) = g(x,y) \tag{12}$$

The goal of the procedure is to find the location of the function g(x,y) and this is achieved by minimizing a goal function that measures the distances between the gray levels in the left and right images. The location of g(x,y) is initially approximated in g^0(x,y) and the function is linearized as

$$\mathrm{f(x,y)} - \mathrm{e(x,y)} = g^0(\mathrm{x,y}) + \frac{g^0(x,y)}{\delta x}dx + \frac{g^0(x,y)}{\delta x}dy \tag{13}$$

The equation can be written in a matrix form with A the design matrix containing the transformation parameters, the vector difference *l* as f(x,y) – g^0(x,y) and simplifying e = e(x,y)

$$l - e = Ax \tag{14}$$

the solution vector is then

$$x = (A^T PA)^{-1}(A^T Pl) \tag{15}$$

after the solution vector is obtained, a second iteration for g^0(x,y) is performed using a new set of parameters of the matrix A. The process stops when the solution vector x reaches a certain limit.

The LSM is the core of the matching process used in the 3DPD [18] software developed at the INAF (National Institute of Astrophysics) of Padova for the tridimensional reconstruction of planetary surfaces. 3DPD was previously validated using images of Mars and it used for the research conducted in this thesis as well.

3.4 Triangulation

Triangulation is the process aimed at inferring depth in an image by calculating the distance of a point seen from two different perspectives and it is the final step for the creation of a DTM.
For the triangulation process it is necessary to know the intrinsic and extrinsic parameters of the camera, often summarized in the projection matrix.
The triangulation process makes use of a disparity map between the left and right images: the disparity is defined as the difference in image location of an object seen from different perspectives, and the disparity map takes into account the shift of every point in the images. The disparity is higher for points closer to the camera where the distance is shorter, so it is inversely proportional to depth.
In order to retrieve the 3D location of the points, a ray that spreads from the camera and intersects the object must be traced: having two (or more) cameras, the rays coming from the different perspectives intersect in one point that is the tridimensional position of the points of the target. In practice, because of every point of an image corresponds to a line in 3D, the goal is to intersect two lines belonging to a pair of corresponding points (the homologues image points).

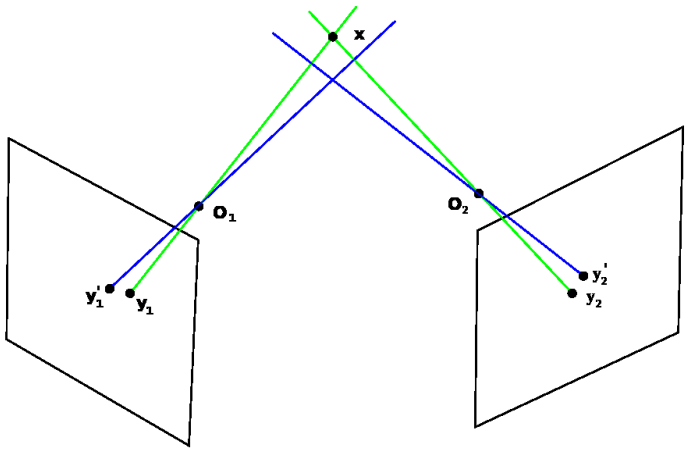

Fig 27 Triangulation problem: the real coordinates of the object are y_1 and y_2 (green lines), while y'_1 and y'_2 (blue lines) represent the coordinates affected by errors

The result is a point cloud which quality depends directly on the accuracy of the disparity map. The triangulation problem is theoretically simple, with a basic geometry that deals just with intersecting lines in the tridimensional space. However, the coordinates of the image points are normally affected by errors (lens distortions, detection errors in the corresponding points...) and the corresponding lines do not intersect in the 3D world.

Fig 27 clarifies this aspect, where the real X tridimensional position (calculated from y_1 and y_2) is shifted if affected by measurements errors in the position of the corresponding points (calculated from y'_1 and y'_2).

In order to correct the 3D position reconstructed, different algorithms can be applied, minimizing for example the distance between the position of the point retrieved and the correspondent expected position.

After the creation of the point cloud, it is necessary to express it in dependence of a coordinate system: for a planetary surface for example, the cloud must be transformed in geographic coordinates with a map projection.

3.5 DTM of planetary surfaces

A Digital Terrain Model (DTM) [19] is a mathematical representation of a ground surface in form of a regular grid where an elevation value is associated to every pixel. 3D models of planetary surfaces are useful for the metrical investigation of the celestial bodies. In fact,

information about the morphology and the altitude of the surface are useful for every aspect of a space mission, from planning to interpreting scientific data, but also to help rovers or astronauts in case of landing.

There are two methods to create DTMs: from laser altimeter data and from stereo images.

Laser data are obtained from the instrument positioned on the satellite pointing down to the surface: by the measure of the response time of the laser after hitting the surface it is possible to calculate its distance from the spacecraft. The data are very accurate along-track, providing a "continuous" profile of the surface; on the other hand, the data are very poor in the cross-track direction, as there may be a long displacement between swaths of different orbits. In addition, the spatial resolution on ground is low because it depends on the dimension of the spot of the laser on ground.

The second strategy uses stereo images, that are normally acquired by a stereo camera that moves in the space Alternatively, stereo images can also be produced by from a single camera that is tilted with respect to the normal to the surface. Stereo images permit to triangulate the position of every point because of the parallax effect caused by the different orientation in the acquisitions, allowing the creation of 3D models. The parallax effect is the apparent shift of an object when pointed from different perspectives. This strategy is more complex than the laser altimeter, but could undoubtedly provide more flexible and comprehensive results. In particular, the spatial resolution is equal in both the along and cross-track directions.

On ground images with different perspectives are normally obtained by means of stereo cameras. There are two different types of stereo cameras used in space missions in dependence of the detector there are using: push-broom and push-frame. In the push-broom cameras, the most common, the image is acquired one scan line of pixels at a time while the spacecraft is moving. In the push-frame cameras, all the pixels of the image are taken simultaneously and the entire image is associated to the same external parameters.

STC is a push-frame stereo camera formed by two optical channels inclined of 20° and -20° respect to nadir: while MPO is orbiting upon Mercury, the first channel takes one image of a portion of the surface positioned forward respect to the direction of motion and after some time the second channel, pointing backwards, takes a second image of the same portion of surface from a different perspective.

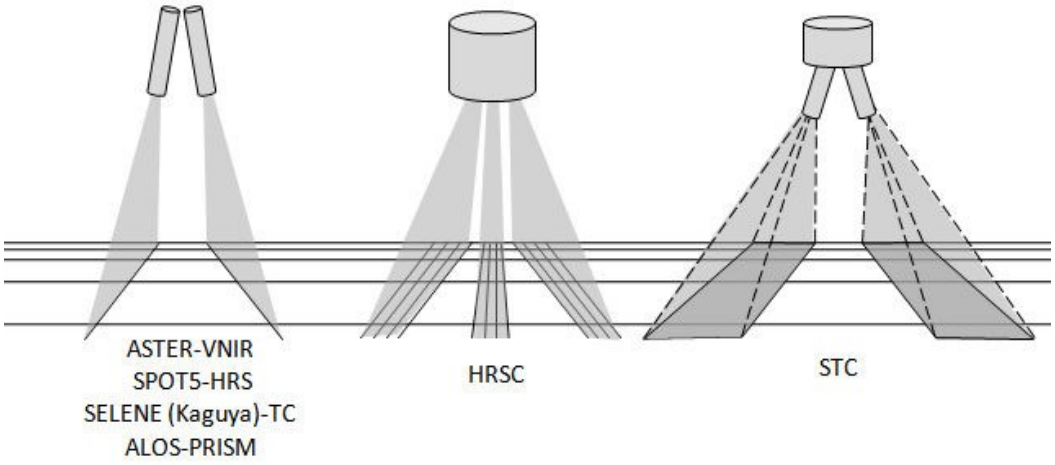

Fig 28 Examples of push broom (the first two) and push frame (STC) cameras

Creating a DTM is a long process that involves different steps and specific software. In the last decades the increasing demand of DTMs of planetary surfaces led to an increment of the automation in the process of DTM creation, but the intervention of an operator is still necessary in some crucial passages.

Here are briefly summarized the steps necessary to obtain a DTM from a stereo pair:

- Un-distortion: lens distortion must be removed from the images.
- Rectification: the two images must be rectified and row-aligned. This procedure facilitates the matching between the two images and increases the quality of the tridimensional product.
- Find correspondences: the same feature must be identified in both the left and right camera views. The relative distance of the features in the two images forms a disparity map. Both intrinsic and extrinsic parameters of the camera must be known to perform these calculations.
- Triangulation: a depth map is calculated from the disparity map. The depth map contains information of the tridimensional position of every feature and from it is possible to create the 3D object.

The photogrammetric process aimed to obtain tridimensional reconstruction of objects includes a wide range of application. DTMs are obtained from aerial images, mainly from satellites, but in the recent years the usage of airplanes or drones for this purpose increased rapidly. Other tridimensional products, as the 3D models of small objects for industrial and engineering applications, can be constructed using digital cameras and even smartphones. A large number

of commercial software was developed for this last sector [20] [21] but few of them are available for the creation of planetary surfaces.

ISIS [22], developed by the United States Geological Survey (USGS), is a commercial software specifically designed to deal with planetary images, modeling sensors and matching. This software unfortunately lacks the possibility to produce DTMs but generated “cube” files that can be processed by ASP [23] designed by the NASA AMES Research Centre, a software specifically designed for the DTMs creation. In this way, the two software can be used together to derive DTMs, with ASP taking advantage of the models created by ISIS but including also the possibility to perform the triangulation of stereo pairs.

Other commercial digital mapping companies developed their own photogrammetric software, such as for example Photomod developed by Racurs [24] and SOCET SET developed by BAE System [25]. SOCET SET in particular became one of the main choice for organizations specialized in cartography such as USGS and Arizona State University.

Other commercial and open-source software are available for the photogrammetric community but they lack of quality in practice.

Finally, research centers spread all over the world are used to develop their specific tool for planetary mapping and image processing, but these software are meant for internal use and are not available to the scientific communality. Two examples are Planetary3D [26] and 3DPD, with this latter used in particular for the work presented in this thesis.

Chapter 4: Image simulation and DTM creation

This chapter describes the entire workflow for the creation of DTMs, starting from the image rendering up to the triangulation of the features extracted from a stereo pair.
The inputs for the creation of a DTM are a stereo pair and the intrinsic and extrinsic parameters of the camera that acquired the two images. The necessary information about the position are retrieved with customized MATLAB routines.
The use of two specific software for the creation of DTMs is described: SurRender for synthetic image creation thanks to rendering procedure and 3DPD for the matching process and the final triangulation.
A customized MATLAB code for the mosaic of HRIC images is also presented, allowing to combine several images together.

4.1 SPICE kernels

SPICE kernels [27] are a collection of files containing ancillary and navigation information of every space mission. The data are developed by the NASA's Navigation and Ancillary Information Facility (NAIF) and are freely available to space agencies and scientists. The aim of the project is to support scientists and engineers in planning and interpreting scientific observations. NAIF also provides the archiving facility for NASA's Planetary Data System (PDS). The SPICE structure is composed by a software suite called SPICE Toolkit that contains specific applications to read the SPICE data files. It is also possible to code specific routines to perform calculations about geometry and other various kind of solar system events.
The codes are available in different programming languages as FORTRAN 77, ANSI C, IDL and MATLAB.
The work presented in this thesis was developed using customized MATLAB routines, designed to retrieve specific information for the mission. The information can be divided in two

categories: geometric calculations and geometric event finders. In the first category, a geometric parameter is calculated in a precise instant or interval of time: for example, it is possible to calculate a frame definition or transformation, an illumination condition or a pointing of an instrument. In the second category, an instant or interval of time in which a particular geometric event takes place is calculated. For example, it is possible to find the interval of time in which a target is visible, or a particular constraint is met.

The information retrieved by the SPICE data is the first step in the long procedure to obtain a DTM. In particular, from SPICE data is possible to retrieve: camera parameters (retrieved from the instrument kernel, ik), orientation and position of camera and planet (retrieved from the frame kernel, fk), illumination conditions (retrieved from the frame kernel, fk).

Apart from the importance in the creation of DTMs for what is concerning the geometry definition, the SPICE data are used also to recover information for the mission planning, a topic that is covered in the next chapter.

Cosmographia [28] is a software that produce 3D visualisations of planet ephemerids, spacecrafts trajectories and instruments field of view. The data rely on the SPICE kernel system, and this tool is used to visually verify the scenarios simulated. The following figure shows an example of a Cosmographia screenshot.

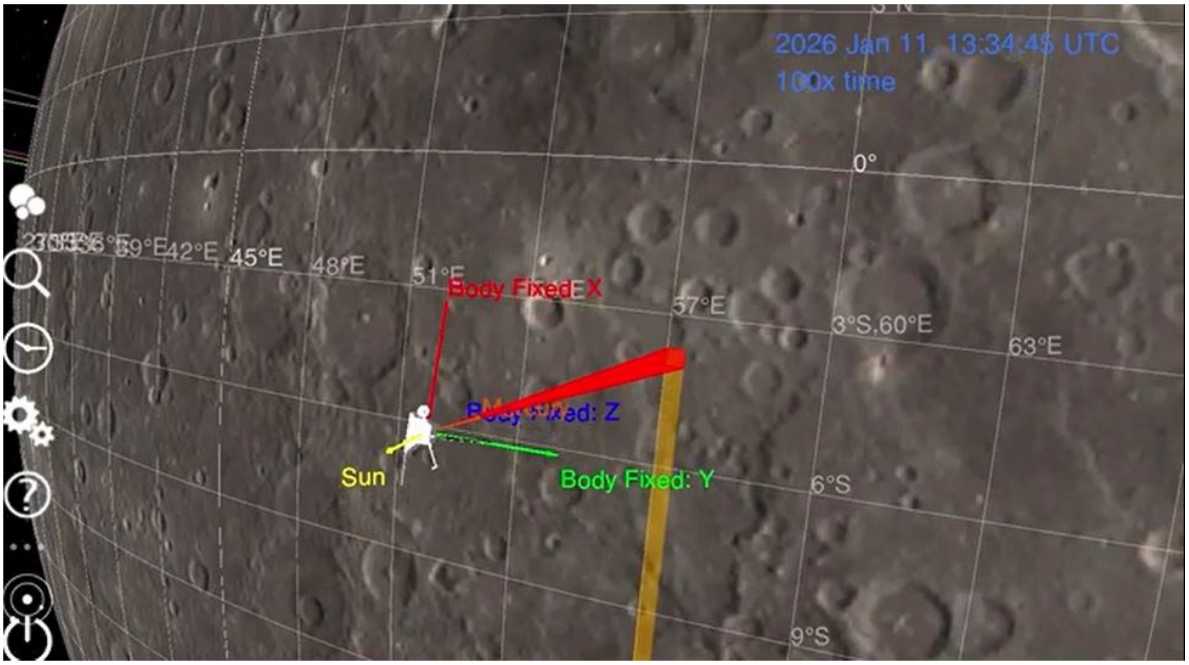

Fig 29 Cosmographia example

4.2 Simulation of 3D models

This section describes the procedure to obtain 3D models from images of the surface of a planet. The necessary algorithms developed make use of the data of the BepiColombo mission and SIMBIO-SYS suite.

Different elements are necessary to obtain the final result, in particular:

- A target to simulate. A 3D element that virtually define the surface of the planet. Meshes retrieved from planetary images of other missions are used.
- Position of the camera. SIMBIO-SYS is integrated in the MPO spacecraft, thus its position in time is linked to the orbit of the spacecraft. In order to simulate an acquisition, it is necessary to know the exact position and attitude of the spacecraft in the specific moment of the acquisition itself. This information is retrieved using SPICE kernels.
- Parameters of the camera. Extrinsic and intrinsic parameters of the camera are necessary to create a projection matrix that describes the characteristics of the simulated images.
- Synthetic images. It is necessary a raytracing software capable of rendering synthetic images that simulate the real acquisitions.
- A stereo couple. A stereo couple is formed by two images of the same target taken from different perspectives.
- A software capable to triangulate the images in order to obtain the 3D model.
- Once the 3D model (DTM) is generated from a photogrammetric pipeline starting from the synthetic images, its quality, in terms of vertical accuracy, is evaluated from a comparison process the involves the original target model used as ground truth. The entire workflow is summarized in the following flowchart.

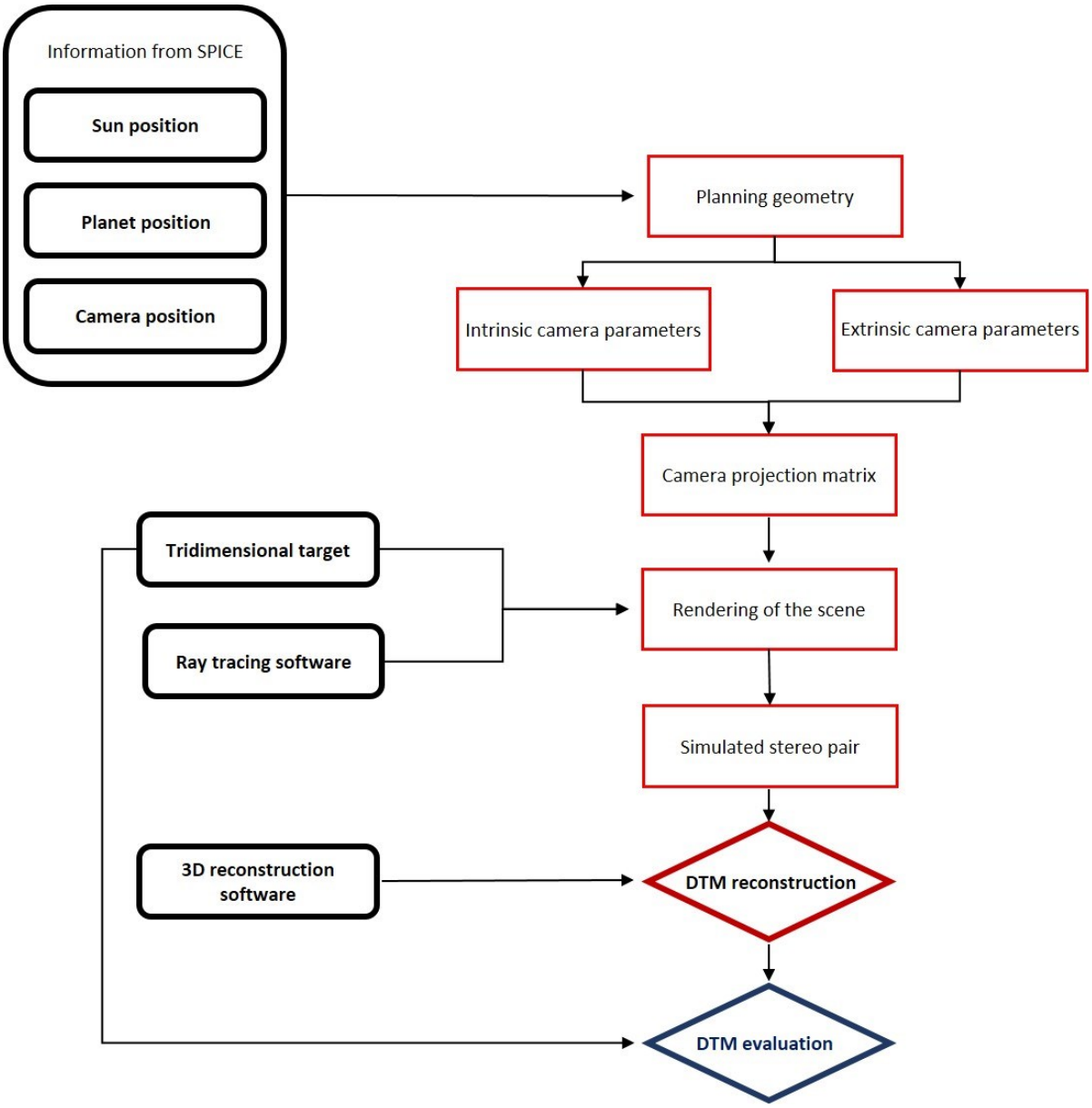

Fig 30 DTM reconstruction flowchart

The output of the workflow is a 3D point cloud representing the target. The quality of the result is influenced by different factors as:

- Solar incidence angle. It is the angle between the normal of the surface and the position of the Sun. This parameter influences the shape and dimension of the shadows on ground, with longer shadows at higher angles and vice versa. The presence of shadows can enhance or hide the features present on the surface, changing the levels of detail of an image.
- The convergence angle. It is the sum of the two acquisition angles of the two simulated images: in fact, each stereo couple is formed by two images taken from different

perspectives, defined by the angles between the boresight of the camera and the nadir direction.

- Pixel dimension on ground. This factor is linked to the altitude of the spacecraft, where a higher altitude results in a lower pixel dimension on ground.

4.3 Input elements

4.3.1 Target

SIMBIO-SYS will acquire images of the surface of Mercury. In order to simulate in advance these acquisitions, it should be chosen a target much similar as possible to the surface of Mercury. The model should have dimensions at least comparable with the footprint on ground of the camera sensor and resolution comparable to the resolution of the real images of BepiColombo instruments.

The simulated targets are meshes obtained from Digital Elevation Models (DEM) of planetary surfaces derived from other missions. Ideally, models of Mercury's surface should be used for the maximum realism, but the models provided by the previous mission MESSENGER are not good enough in term of resolution to simulate SIMBIO-SYS acquisitions. For this reason, models of the surface of the Moon have been chosen. The Moon presents morphological characteristics similar to Mercury and by now is the celestial body that can better represent the surface of Mercury. It is important to remind that for the work presented in this thesis only a general shape of a planetary surface is necessary, without considering the real morphologic elements that are located on the surface of the planet. In addition, DEMs of Mars are used as well, as the models are large enough to contain the footprint of the channel STC.

The two channels of SIMBIO-SYS, HRIC and STC, have different characteristics in terms of resolution and area covered with a single acquisition. Concerning just the panchromatic filter, HRIC has a maximum footprint size of 40×10 km^2 (during the low resolution phase) and the best resolution of 5 m/px (during the high resolution phase), while STC has a maximum footprint size of 140×60 km^2 (during the low resolution phase) and the best resolution of 50 m/px (during the high resolution phase). The two channels clearly have opposite characteristics: finding a proper target for HRIC is more challenging from the point of view of the resolution, while for STC the biggest concern is the extension, but still maintaining a good level of precision. A model with the size of the STC footprint and the resolution of HRIC could be used

to simulate acquisitions for both channels. Unfortunately, models with these characteristics do not exists, as planetary data are normally divided in extended targets mapped in low resolution, normally provided by wide angle cameras, and small targets mapped in high resolution provided by high resolution cameras. Thus, for the simulation of HRIC and STC images, different targets are used.

The real surface of Mercury presents elements of different dimensions, from giant boulders and craters to impalpable dust. It is clear that reproducing small elements in a model with a size of the order of kilometers is impossible, because the data volume of the models would become prohibitive. Moreover, this operation would be useless in any case, as the elements smaller than the resolution of the camera would not be visible anyway. For this reason, the resolution of the mesh is chosen to be of the same order of magnitude of the resolution of the camera that will be used to acquire the images.

For the HRIC simulation it was used lunar DTMs based on data from the NAC system for the LROC (Lunar Reconnaissance Orbiter Camera) [29] on the NASA's Lunar Reconnaissance Orbiter (LRO) instrument [30] downloaded from (http://wms.lroc.asu.edu/lroc/rdr_product_select).

The GSD (Ground Sample Distance) is around 2 m. It was assumed that the bidirectional reflectance distribution function (BRDF) of the Moon is best described by an Hapke model [31] [32] [33].

One example of the input used is the NAC_DTM_A17SIVB_E042S3476 DTM model has a size of 2541 × 14340 pixels and covers an area of 5082 × 28680 m^2.

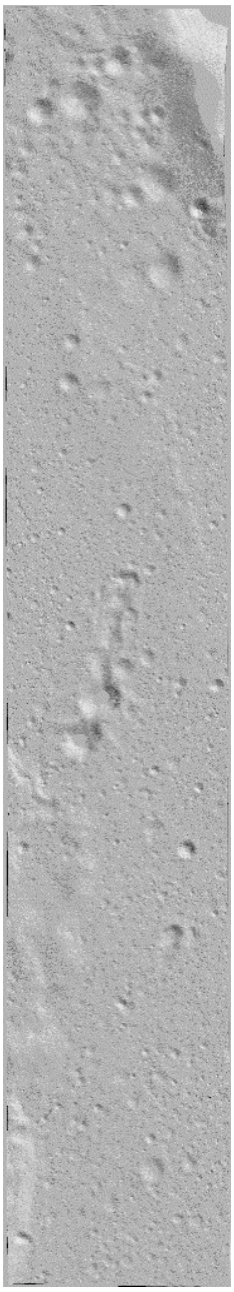

Fig 31 NAC_DTM_A17SIVB_E042S3476 DTM model from the LRO mission

For the simulation of the STC acquisitions different dataset are used.

For the first dataset, still some lunar DTMs were used but they were produced, in this case, starting from the Japanese lunar explorer Kaguya (SELENE) [34] images.

One of the DTM used is the DTM_MAP_02_N00E030S03E033SC (https://darts.isas.jaxa.jp/planet/pdap/selene/) of 11539 × 12245 pixels size, GSD is around 7 m/px covering an area of 85380 × 90613 m^2. While the mesh is created, the GSD is scaled down to 25 m/px in order to reduce the data volume of the samples.

Fig 32 DTM_MAP_02_N00E030S03E033SC DTM model from the Kaguya SELENE mission

For the second dataset DTMs of Mars were used, in particular the h2028_0000_dt4 and h3210_0000_re4 from the HRSC camera [35] onboard the MEX mission [36]. The GSD is 50 m/px and the dimension is large enough to contain an entire footprint of STC.

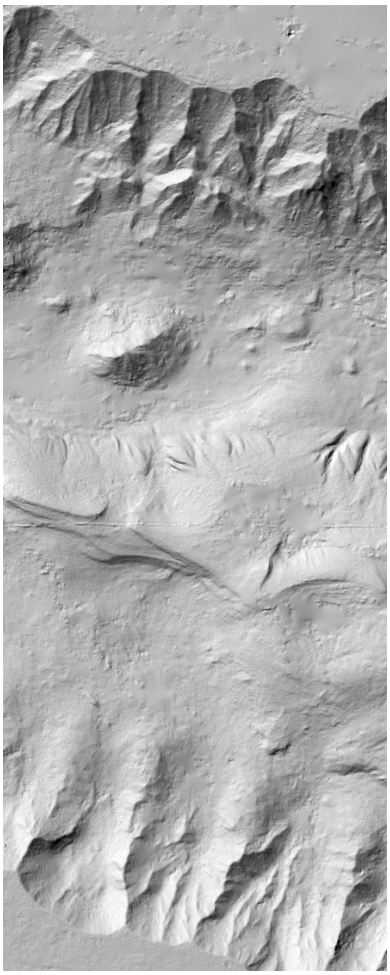

Fig 33 h2028_0000_dt4 DTM from MEX mission

4.3.2 Position of the camera

Every navigation and ancillary information of a space mission is stored in files called SPICE kernels. From these files it is possible to retrieve every useful information for performing mission planning. Several MATLAB routines have been written to calculate different orbital elements and events information, as for example camera pointings, spacecraft positions, illumination conditions and so on.

Knowing the exact position and attitude of the camera at a specific instant of time is a necessary step for the calculation of the extrinsic parameters of the camera. Along with the intrinsic parameters, this information is necessary for the creation of the 3D model.

In addition, the knowledge of the illumination conditions and altitude of the spacecraft (or the pixel dimension on ground) gives useful information for comparing the results and for evaluating the performance of the 3D reconstruction considering different configurations.

4.3.3 Simulated images

Synthetic images, in particular stereo couples, are necessary for the creation of tridimensional models. In fact, once the stereo couple is obtained, the steps described in the previous chapter are applied and the DTM is retrieved.
The simulated images are created with a ray tracing software called SurRender [37].
A huge set of images with different characteristics were simulated changing the target, the acquisition time, the illumination conditions and the position on the planet.
The target rendered is a mesh with uniform materials and consequently the effects of the albedo can be only partially simulated, limiting the realism of the images. On the other hand, the scientific realism of the images is behind the objectives of this work and do not impact the evaluation of planning an efficient acquisition strategy.

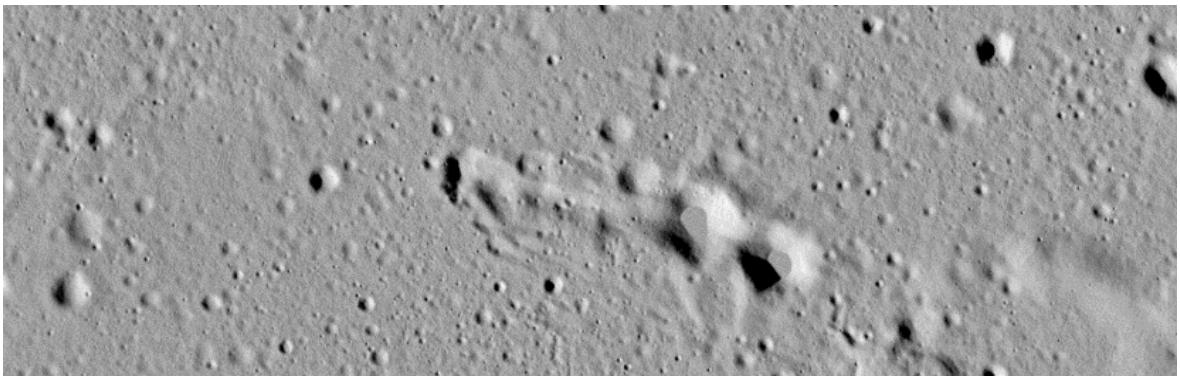

Fig 34 Example of one image rendered with SurRender. The target is the same of Fig 31 and it is possible to recognize the central part of the DTM model

4.4 SurRender

The images are simulated with SurRender software developed by Airbus. The software works with the principle of raytracing, giving realistic and physically accurate results.
Raytracing is a rendering technique that calculates the light path and simulate its encounter with a virtual object. The technique simulates the exact process of light propagation in physics, reproducing high quality and physically accurate results but with a great computational time cost. Different optical effects as reflection and refraction are taken into account in the process for the maximum realism. This technique is better suited for applications where the calculation

time is not an issue, as for example image rendering, while defects in applications where a fast rendering is essential, as for example video games.

SurRender implements a backward raytracing technique, where the ray spreads from the pixel and bounces to the object and eventually hits the light source. This method is more effective for space application where the objects are sparse.

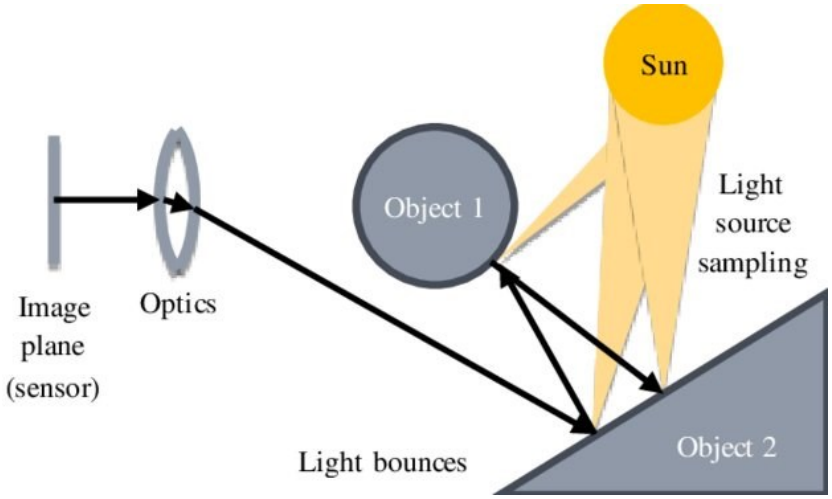

Fig 35 Principle of backward raytracing, courtesy of SurRender manual

Surface materials are customizable and are described with a bidirectional reflectance distribution function (BRDF), a four dimensional function that describes how light interacts with a particular opaque surface. Some classical BDRF functions are already coded in SurRender, as for example the Lambert and Hapke models. The Hapke model in particular is suited for the simulation of celestial bodies covered with regolith, as the Moon, and can be used with a good approximation for Mercury as well. In this way, the albedo of the surface can be simulated.

To simulate the images, the software needs basically three elements: a light source, a target to simulate and a virtual camera. The relative position and attitude of these elements are imported from the calculations made with the SPICE kernels. For the light source a synthetic Sun is simulated: its dimension, position and light power are the same as the real Sun. A customized number of rays spreading from the light source can be chosen: the higher the number, the higher the physical accuracy of the simulated image, but also at the same time the higher the calculation time. Thus, this number must be chosen as a tradeoff between good results and realistic calculation time, that can be of the order of several minutes up to hours. The number of rays used to simulate the image is chosen analyzing the image histogram of the sample. The image

histogram is a graphical representation of the tonal distribution of a digital image and plots the number of pixel for each tonal values. The number of rays is set when its increment does not affect anymore the histogram of the simulated images, meaning that two images are identical.
The target to simulate is the mesh obtained as described in the previous section. This mesh, representing a portion of the planetary surfaces, must be positioned and pointed at the correct coordinates of a hypothetical sphere representing the planet.
The virtual camera can be customized with the desired characteristics: focal length, sensor size, pixel number and dimension. Two different camera models have been created, one simulating HRIC and one simulating STC.
Once again, the camera must be positioned with its correct attitude retrieved from the SPICE kernels.
The images obtained have a dimension equal to the dimension of the footprint on ground of the sensor and a spatial resolution that depends on the distance of the sensor from the target.

4.5 3DPD

The last piece for the creation of the 3D models is a software capable to process stereo couples of images.
The 3DPD [18] [38] is a software coded for the CaSSIS camera [39] onboard the ExoMars Trace Gas Orbiter (TGO) [40] and it was developed by the scientific team of INAF of Padova. In the near future the software will be slightly modified to be adapted to the BepiColombo mission and it will be used to produce the DTMs of SIMBIO-SYS.
The pipeline of the software is shown in Fig 36: it firstly creates a mosaic of images of different framelets, then calculates a disparity map with sub-pixel precision and finally performs a triangulation in order to produce a DTM.

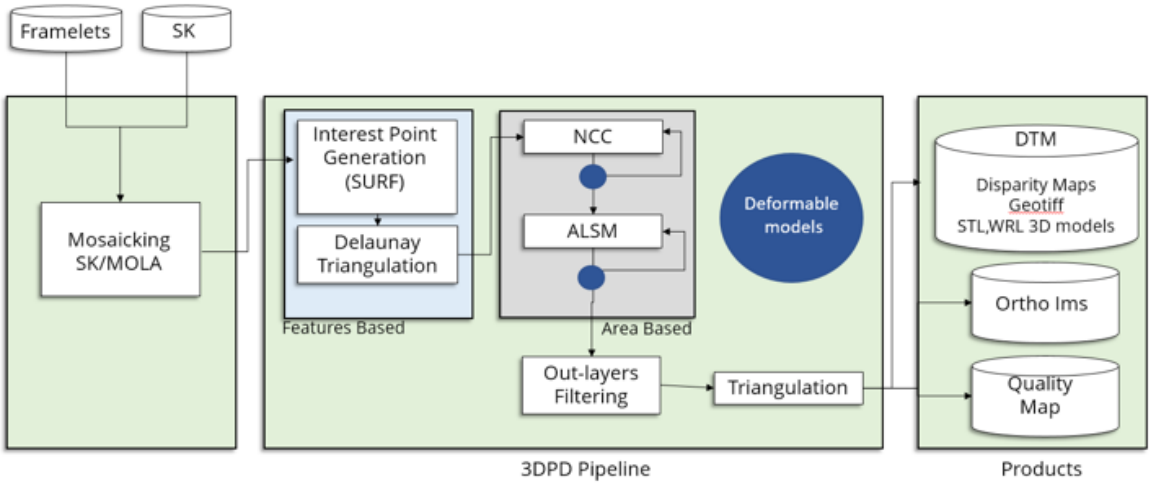

Fig 36 3DPD pipeline

The input for the 3DPD are rectified mosaicked images obtained with the CaSSIS_Reader tool, a MATLAB code written to process CaSSIS data. The mosaic is created with images of different CaSSIS framelets and the camera parameters are calculated using SPICE. Once the mosaics are obtained, the matching process can start.

The first passage in the matching process is the identification of corresponding points in the stereo pair: an interest point operator (SURF) has been used to facilitate the identification of conjugated points and a RANSAC (RANdom SAmple Consensus) [41] estimation to define a set of consistent points. The disparity map is calculated at different steps, starting with a Delaunay triangulation [42] and moving on with a Least-Squares Matching. Finally, the 3D model is extrapolated by forward ray intersection of the image coordinates. The resulting point cloud is then transformed to geographic coordinates (latitude, longitude, height) and converted in line/sample coordinates with a map projection (equirectangular or polar stereographic).

The software was validated by comparison of the results with the products of ASP software, that is considered a standard in the DTM creation for planetary science.

4.6 Mosaic

Mosaicking is a technique that permits to combine more images in a unique one. This is useful for products that have a large area that cannot be covered with just a single acquisition. In particular, mosaicking is used to produce worldwide maps, either of celestial bodies but also for the Earth as well.

In order to create a mosaic, images have to share a common area, so in other words they must overlap. For what concerns the satellite acquisitions, the along-track overlapping is obtained changing the repetition time (RT), defined as the interval of time between two acquisitions, while the overlapping cross-track is obtained acquiring images during different orbits. Fig 37 shows an example of a set of images taken in different moments that can produce a mosaic.

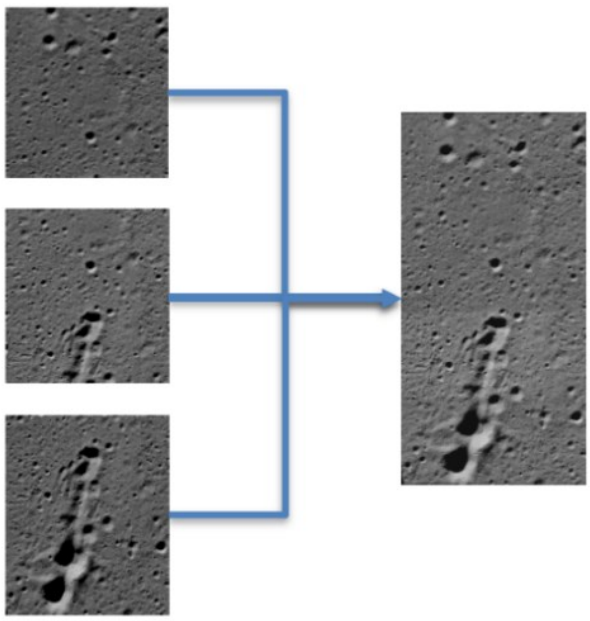

Fig 37 Example of a mosaic of three images into a unique one

A specific tool written in MATLAB code has been edited for the creation of a mosaic with HRIC images. In this way, targets bigger than the footprint on ground of the instrument becomes visible in just one image.

The procedure to create the mosaic follows these steps:

- A set of images with the associated projection matrixes has to be loaded. The projection matrix is calculated using both intrinsic and extrinsic parameters of the camera in the moment of the acquisition of the image. Other useful information, as the position of the intercept of the boresight with the surface and the position of the camera in the spacecraft's reference system, are calculated using SPICE kernels.
- A global virtual plane is created. This plane is centered in the averaged positions of the intercepts of the boresights of the camera with the surface of the planet and oriented with two axes parallel to the along-track (S-N in case of BepiColombo orbit) and cross-track (W-E) directions, while the third axis is perpendicular to the surface. In this way,

every image is rectified on the surface of the virtual plane and the height of the DTM corresponds to the surface height respect to the medium radius.

- A homography that maps the coordinates of the images in the virtual plane is calculated. The four corners of the different images are mapped in the virtual plane and the size of the mosaic is then calculated from the positions of the corners of the extreme images. Now the origin of the mosaic is shifted to the bottom left corner so that the coordinates in the mosaic increases along the x and y axes.
- The images are drawn in the virtual plane applying the homography to every pixel. A cubic interpolation is used to map the mosaic grid in the single image's pixel coordinates. The images are superimposed one upon the others, meaning that in the area shared by two images only the values of the second images are considered. No blending nor pixel values averaging is used considering that the synthetic approach does not take in account of possible misalignments as distortions or errors in pointing.
- A new projection matrix relative to the whole mosaic is calculated. The matrix is derived from the pixel size, the number of pixels and an equivalent focal length associated to the mosaicked image. In this way, the mosaic is treated as an image acquired from a "virtual" equivalent camera created ad hoc.

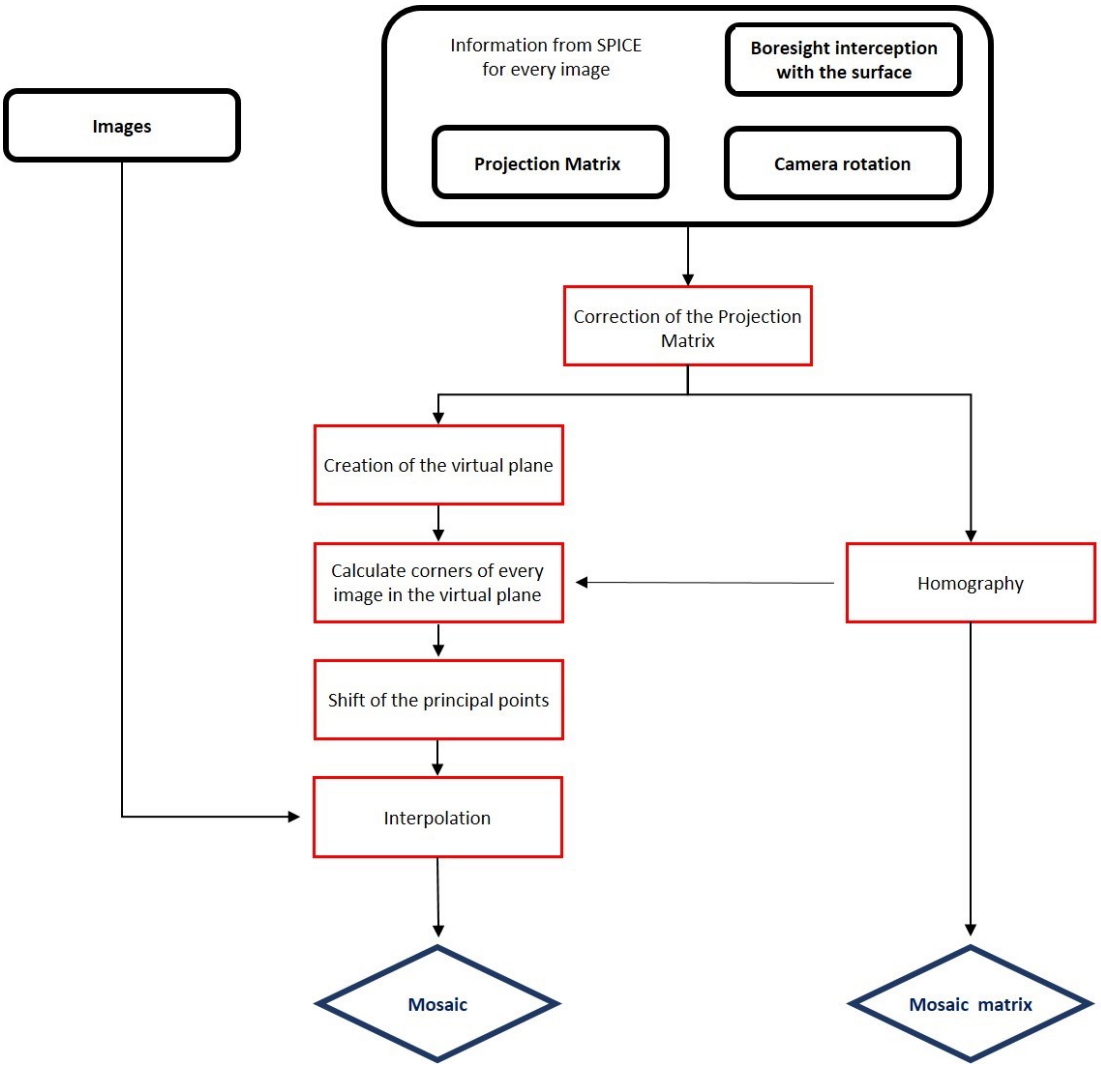

Fig 38 Mosaic workflow

Every image in the mosaic has a vertical displacement error due to the fact that images of the curved surface are all mapped in a common horizontal plane. The magnitude of the error depends on the altitude of the spacecraft while taking images and the interval of time between two acquisitions (if the interval is short the two images are more likely to lean on a common plane). In any case, the vertical displacement error is of the order of a fraction of a pixel.

The most critical parts are the junctions between the different images, where there could be a discontinuity in the pixel values.

The mosaic code can be improved by adding blending in the overlapping areas between the different picture [43]. Blending is a process of creating a continuous passage in two overlapping pictures: in the area of overlapping the values of the pixels is averaged with the values of the

pixels of the two images. In this way, the passage between the two borders should become invisible.

4.6.1 Illumination changes in the mosaics

A mosaic of images is constructed from several images acquired in different moments. Images can be combined in two directions: along the same orbit (along-track) and along the direction orthogonal to the satellite track (cross-track). In case of MPO, which has a polar orbit, the along-track direction corresponds to the North-South direction and the cross-track direction to the East-West. For simplicity, the images acquired along-track can be assumed to form the columns of the mosaic and the images acquired cross-track the lines.
The illumination conditions, expressed by the solar incidence angle, can vary inside the same patch of images that will create a unique mosaic. In particular, images on the top of the mosaic can have an illumination condition different to the images on the bottom (the same can happen with images in the left and in the right). The result can be a single image (the mosaic) affected by the different illumination conditions within, and this phenomenon is more evident on large mosaics.
The principal factors that influence the illumination conditions are the position of the target on the surface of the planet (especially the latitude) and the position of the planet respect to the Sun (expressed by the True Anomaly).
This section presents an analysis of the illumination changes inside a mosaic.

4.6.1.1 Illumination changes along-track

Images along-track are acquired along the same orbit and form the columns of the mosaic. The relative positions between two images is defined by the repetition time of the acquisitions. Depending on the position of the spacecraft, images along-track can be acquired both from South to North and from North to South, but in any case, the images closer to the poles have higher incidence angles respect to the ones closer to the equator. Thus, the incidence angle is strictly dependent from the latitude.
The second factor that influence the incidence angle is the position of Mercury respect to the Sun represented by the True Anomaly.

The following graphs show the change of the solar incidence angle, both cumulative and after consecutive images, in dependence of the number of images and the True Anomaly.

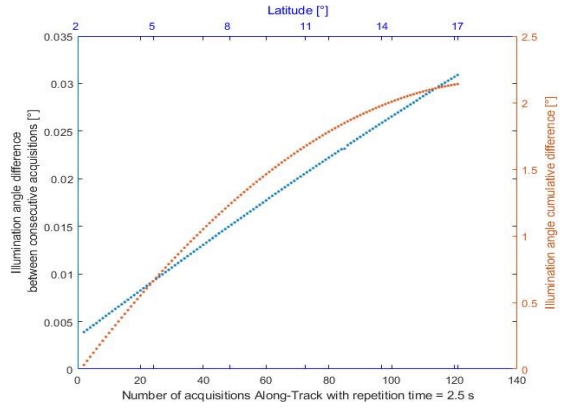

True Anomaly = 120°

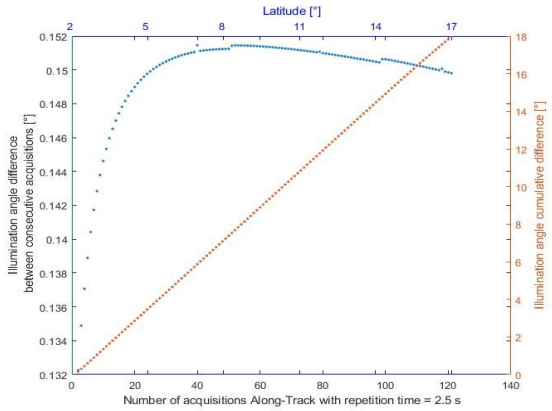

True Anomaly = 180°

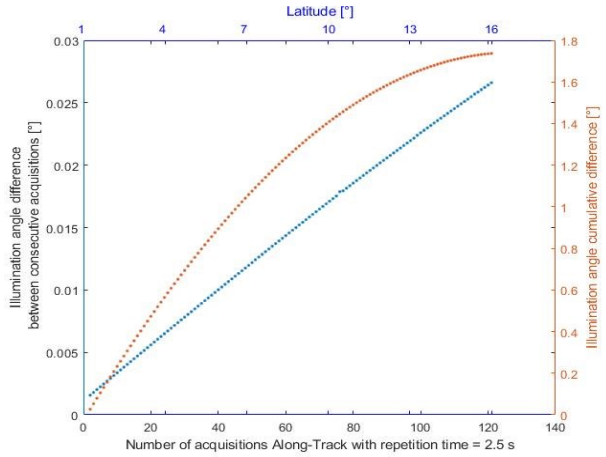

True Anomaly = 240°

Fig 39 Along-track illumination changes in a mosaic near the equator

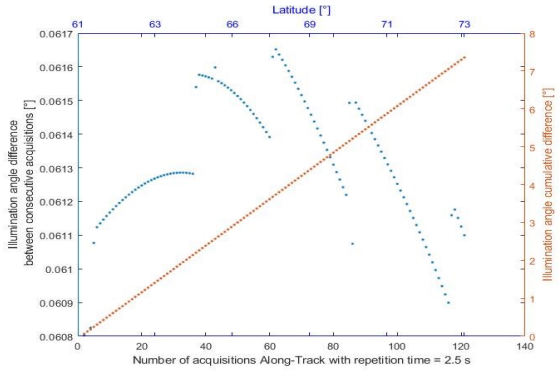

True Anomaly = 120°

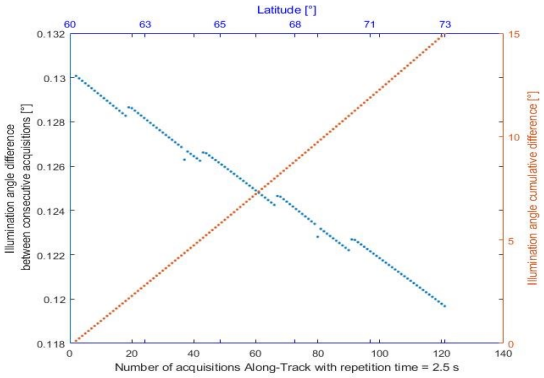

True Anomaly = 180°

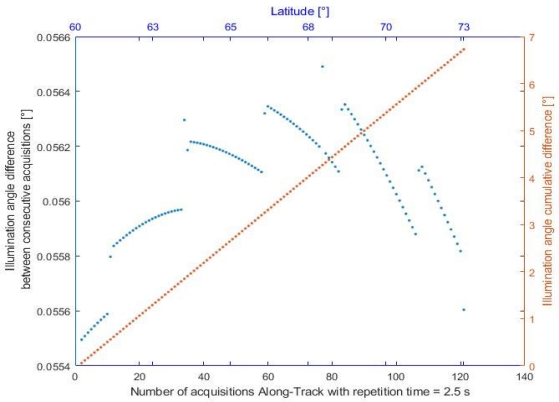

True Anomaly = 240°

Fig 40 Along-track illumination changes in a mosaic at latitude = 60°

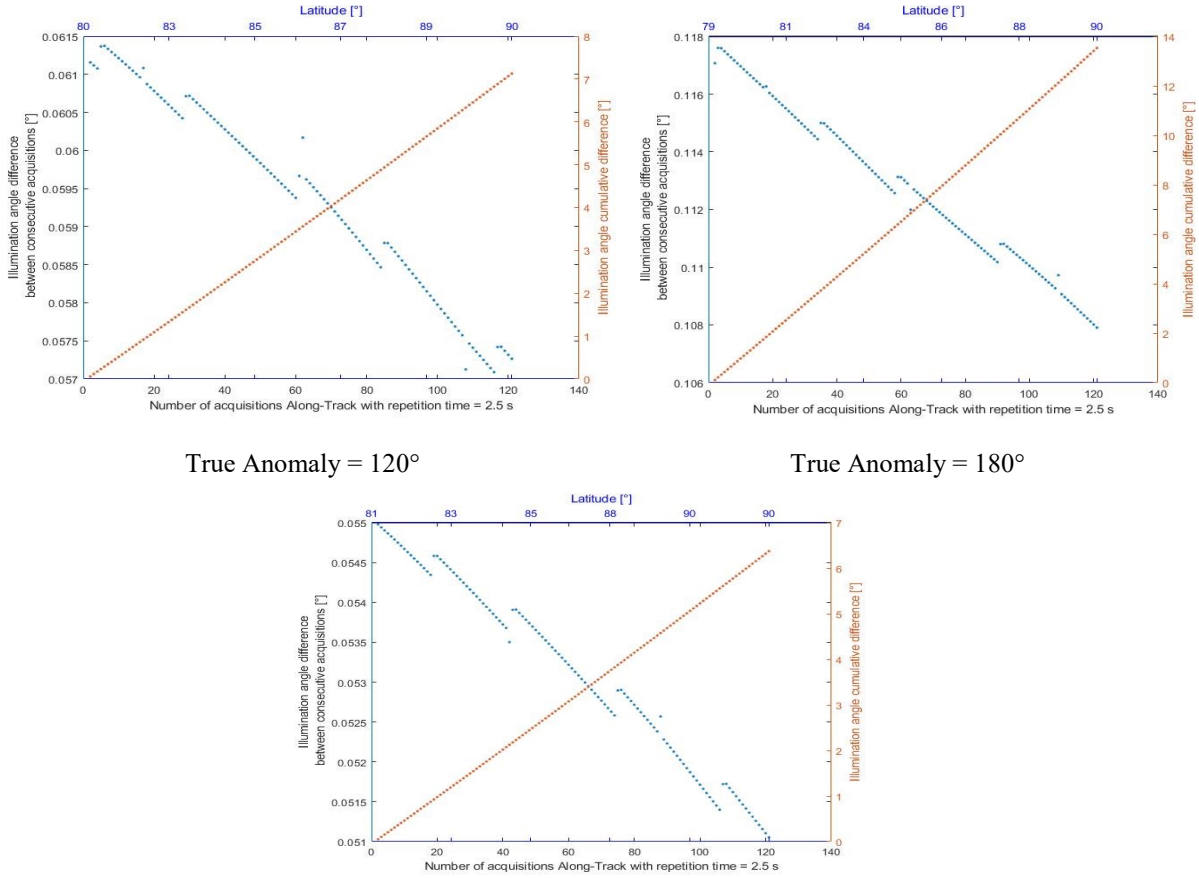

True Anomaly = 120°

True Anomaly = 180°

True Anomaly = 240°

Fig 41 Along-track illumination changes in a mosaic near the pole

Different data are acquired at different latitudes and True Anomaly, covering all the possible scenarios during the mission. Three sets of test are performed: one at the equator, one at an intermediate latitude of 60° (60° is chosen because it is the beginning of the areas where there surely is cross-track overlapping between HRIC images acquired during consecutive orbits) and one near the poles: in this way all the possible scenarios involving the different latitudes are covered.

Different values of True Anomaly are simulated as well. The two extreme values chosen for the True Anomaly, 120° and 240°, correspond to the extreme of the interval for the SIMBIO-SYS high resolution phase (in correspondence of the illuminated Periherm at the Aphelion phase). At True Anomaly 180° the planet is at the Aphelion and the illumination angle is strictly dependent on the latitude.

The next chapter describes in details the different acquisition phases of SIMBIO-SYS and the illumination changes so more details about the topic can be found there.

The tests are performed in the North hemisphere but the same results are valid for the South hemisphere as well.
The number of images for the creation of the mosaic has been chosen large (more than 100) in order to better emphasize the illumination changes. This number of images is calculated considering HRIC images, while if STC images would be considered this value is reduced. In any case the change in latitude or longitude is shown as well in order to clarity the dimension of the mosaic on the surface independently from the dimensions of the images used to retrieve it.
The blue line represents the difference of the solar incidence angle between two consecutive acquisitions, while the orange line represents the cumulative difference between the first and the last acquisition. The most important factor is the latter, because it represents the difference in the illumination between the opposite borders of the mosaic, while the former is practically constant (few seconds of repetition time do not move significantly the position of the image on the surface of the planet).
The change of the illumination in the mosaic follows the same trend described in the next chapter for the general illumination change, so a deeper analysis can be found there.
Some considerations regarding the illumination in the along-track direction of a mosaic can be extrapolated:

- The illumination change is more evident when the True Anomaly is close to 180°.
- The illumination change is more evident near the equator respect to the poles.
- For practical applications, the illumination can be assumed constant when Mercury is at the extreme of the high resolution phase, especially in the areas close to the equator.

4.6.1.2 Illumination changes cross-track

Images in the cross-track direction of the mosaic are acquired during different orbits. After a certain latitude (around 60°) the dimension of the footprint on ground of a HRIC image is large enough to obtain an overlapping with consecutive orbits. In this case, the illumination conditions remain almost invariant. On the other hand, if the dimension of the footprint is not large enough to obtain an overlapping, a gap will be present between two consecutive orbits. This gap has to be filled with other passages but in this case the illumination conditions can be very different (e.g. the illumination angle of Sun can have different sign, meaning that light is coming from right instead of left for example). More details about this aspect are explained in section 5.5 Illumination conditions

The following graphs show the change in the illumination conditions in dependence of the True Anomaly (and the corresponding shift in the longitude) at different latitudes. Every couple of graph is identical but shows on top the True Anomaly or the longitude covered with consecutive acquisitions.

The tests are performed with latitudes above 60° so that the mosaic is created with successive orbital passages without gaps.

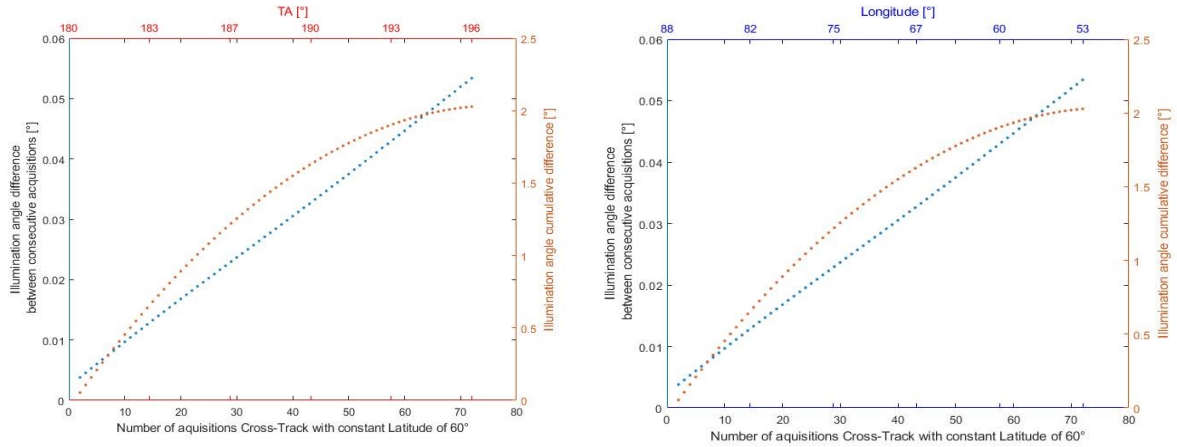

Fig 42 Cross-track illumination changes with True Anomaly = 180° and the corresponding longitude shift

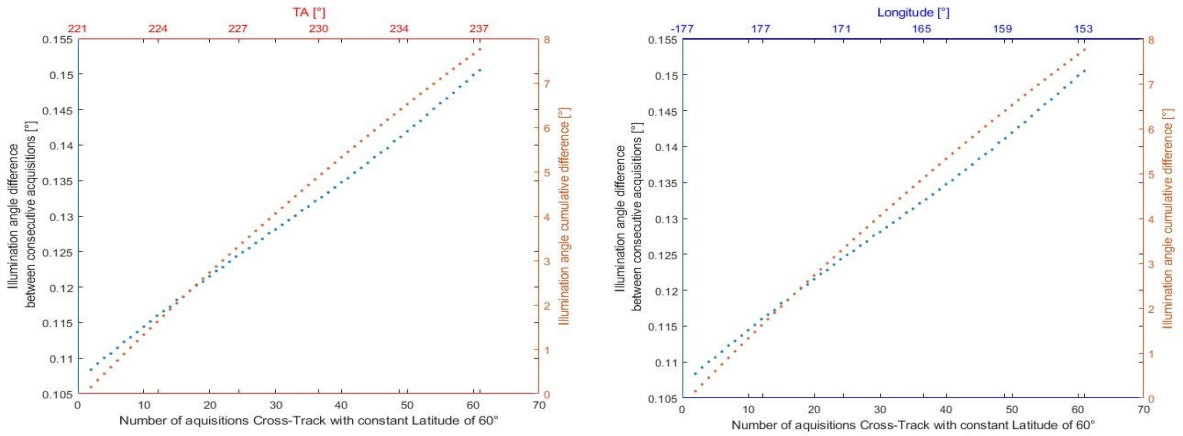

Fig 43 Cross-track illumination changes with True Anomaly = 220° and the corresponding longitude shift

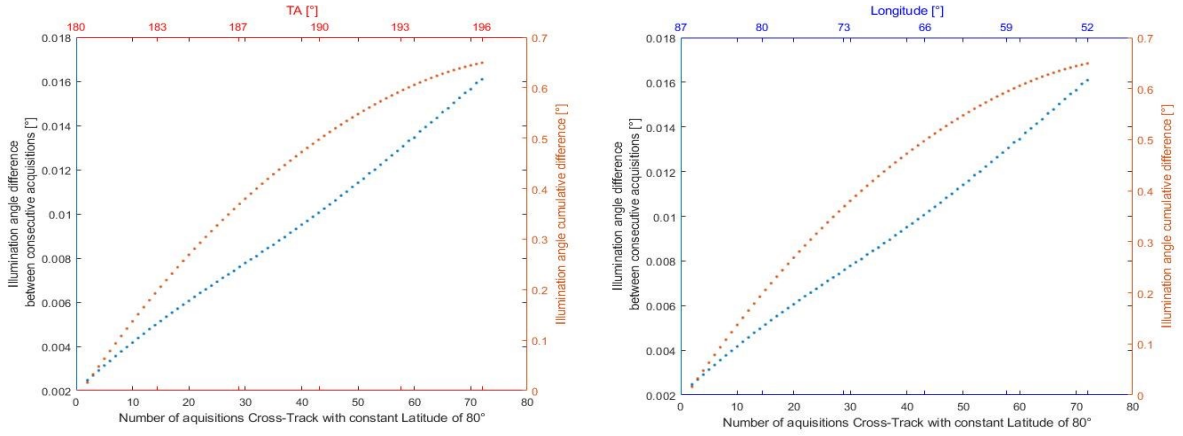

Fig 44 Cross-track illumination changes with True Anomaly = 180° and the corresponding longitude shift

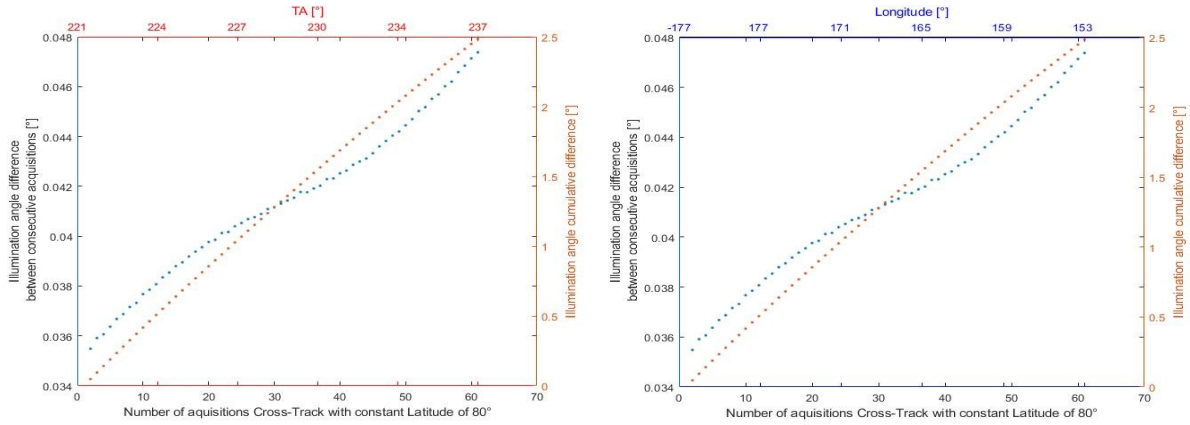

Fig 45 Cross-track illumination changes with True Anomaly = 220° and the corresponding longitude shift

Some considerations regarding the illumination in the cross-track direction of a mosaic can be extrapolated:

- The illumination change is more evident when the True Anomaly is close to 180°.
- The illumination change is more evident in positions distant from the poles.
- The illumination change is smaller respect to the change in the along-track direction.
- Most of the time the illumination can be considered constant, especially near the poles.
- Mosaics with images acquired in consecutive orbits can be performed only from a certain latitude (60°).

Chapter 5: Mission Planning

Scope of the analysis of this chapter is to collect information useful for the science working team of SIMBIO-SYS in the definition of the main interesting targets to be planned. Major attention is reserved to HRIC, but the same evaluations can be applied to STC and VIHI as well.

The scope of mission planning is to facilitate to coordination between the different segments of the mission (scientific objectives, attitude control, instrument acquisitions, working teams…) and to envision the best scenarios for the maximization of the scientific output. Concerning SIMBIO-SYS in particular, the mission planning has to predict: when the targets are visible, which are the acquisition characteristics for the targets, how to maximize the scientific output.

Firstly, general information about some mission parameters like illumination conditions and resolution on ground are calculated. Secondly, a possible configuration scenario for the exploration of the poles is evaluated: the idea is to use data from both STC and HRIC for the creation of DTMs. Finally, some practical examples of targeting with HRIC are shown.

The data used for the analysis have been extracted using customized MATLAB routines working with SPICE kernels.

5.1 HRIC target planning

HRIC will operate during the BepiColombo nominal mission to perform targeted high resolution observations of specific areas of interest selected according to the scientific objectives with the goal of covering almost the 20% of Mercury's surface. Several ranges of solar incidence angles and latitudes will be taken into account according to the specific objective of the observations.

HRIC will operate in push-frame mode covering a specific target mainly with the panchromatic filter; also the colour mode of the same region could be used by means the other three colour filters if necessary. During the mission, it is scheduled to perform some off-pointing manoeuvres, giving the possibility to HRIC to acquire stereo pairs and to observe the same

surface area with different stereo view angles. From these off-nadir pointing it will be possible to obtain high resolution DTMs of the surface of Mercury.

Being SIMBIO-SYS rigidly integrated on the S/C, off-nadir pointing is needed to acquire the target by a roll or a pitch of the S/C during the same orbit or the following. These special pointings need to be carefully planned to minimise the impact on the other nadir pointing instruments and to maintain the radiator away from the direct light of the Sun.

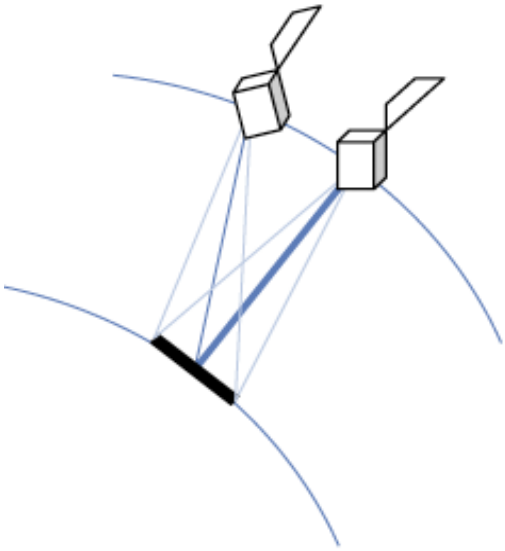

Fig 46 MPO off-pointing for HRIC DTMs

HRIC is a high resolution camera with a narrow FOV, so it will be able to completely cover a target extended both in a range in latitude and longitude only in particular ranges of coordinates. In fact, the HRIC panchromatic filter 2048 × 640 pixels size with a focal length of 800 mm and a cross-track FOV of 1.47° will provide different covering extensions in accordance with the mission phase that depends on the distance of MPO from the surface and on the argument of the Periherm.

If a target has an extension bigger than the area covered by a single acquisition, it is worth considering to perform a mosaic of different pictures that can be acquired during successive orbits or during specific orbits during the mission. More details about mosaicking issues are given in section 4.6 Mosaic

The next part of the chapter covers the principal aspects related to mission planning of BepiColombo, with particular focus to the change of orbital parameters and illumination conditions.

5.2 MPO orbit change

MPO moves around Mercury with an elliptical and polar orbit. This orbit is inertial so it does not move with respect to the planet and the change of the pointing towards the surface is due to the rotation of the planet itself above the spacecraft. This means that the spacecraft maintains also the same orientation respect to the Sun, pointing always the solar panel towards it and the radiator in the opposite direction. In order to maintain this configuration, MPO has only to perform a rotation of 180° degrees around its z axis in the position of the Perihelion and Aphelion. Fig 47 represents the MPO orbit.

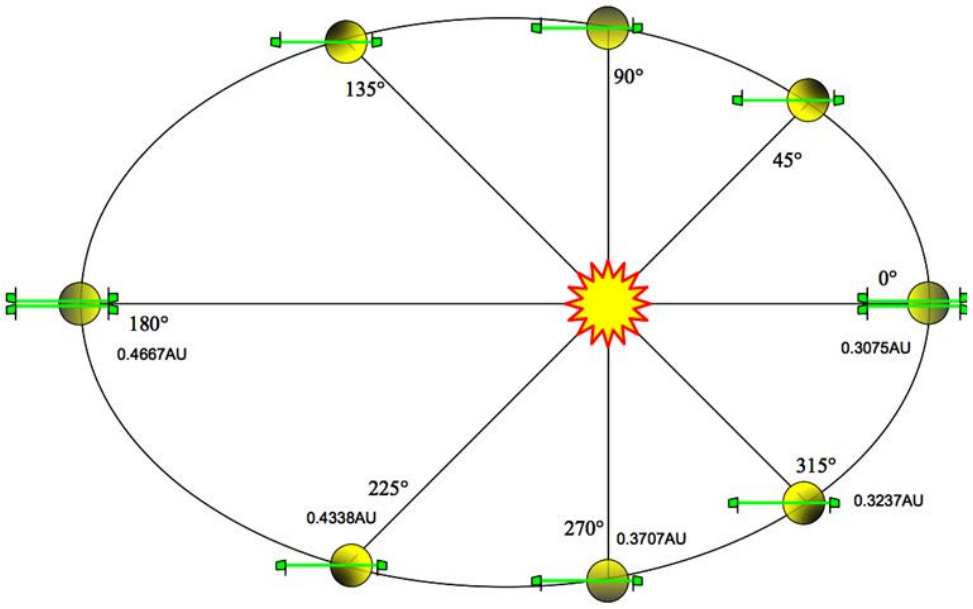

Fig 47 The solar system is visualized from above and the green segment represents the MPO orbit. The orbit maintains the same orientation respect to Mercury and the Sun and performs a rotation of 180° around the z axis in the Aphelion and Perihelion, where the true anomalies are respectively 180° and 0°

Even if the orbit is inertial and consequently theoretically fixed, in practice it changes slightly in time because of inevitable perturbations as: Mercury non-uniformity gravity field, the Sun third body perturbation and the solar pressure. The solar pressure can be considered negligible in comparison to the other two.

The principal effects of the perturbations are two: the Periherm changes the argument and the altitude.

The change of the argument of the Periherm is expressed in rad/sec by the following expression:

$$\dot{\omega} = -\frac{3}{4} J_2 n \left(\frac{r_M}{p}\right)^2 2(5\,cos^2\,i - 1) \qquad (16)$$

Where n = $\sqrt{\frac{\mu M}{a^3}}$ is the mean motion and p = a(1 - e^2) is the semi-latus rectum. The mean motion of MPO results to be approximately $\dot{\omega}$ = -25.4°/year.

The ellipse that the orbit follows rotates changing the position of Periherm and Apoherm: in particular, the Periherm shifts (see Fig 48) from latitude around 16° at the beginning of the mission to a latitude of about -18° at the end of the first year (nominally the end of the mission). If the mission continues for another year, the Periherm continues to move south reaching about -50° latitude. At the same time the altitude of the Periherm decreases in time. This is caused by the change of the eccentricity of the orbit due to perturbations. These two factors have important consequences for the mission planning, changing the resolution and spatial cover of SIMBIO-SYS.

At the same time, the semi major axis and the period of the orbit do not change. Just a small oscillation of the orbital period is present, as it can be noticed in Fig 50, but the overall duration of the period remains constant.

The next sections will focus on the consequences of the orbit's change and on important concepts related to the mission planning.

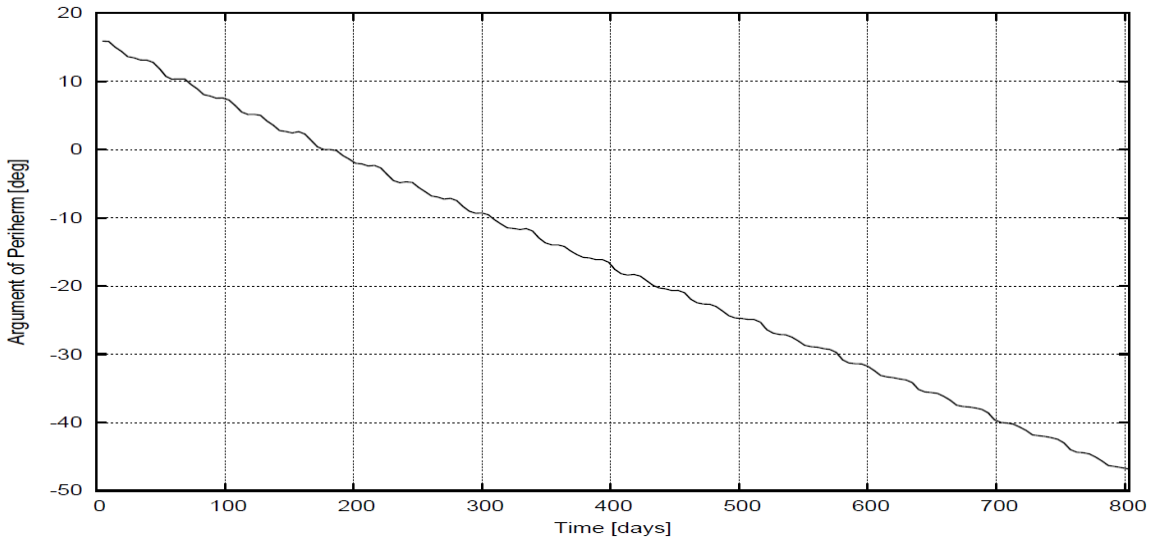

Fig 48 MPO argument of Periherm [deg] evolution over 800 days

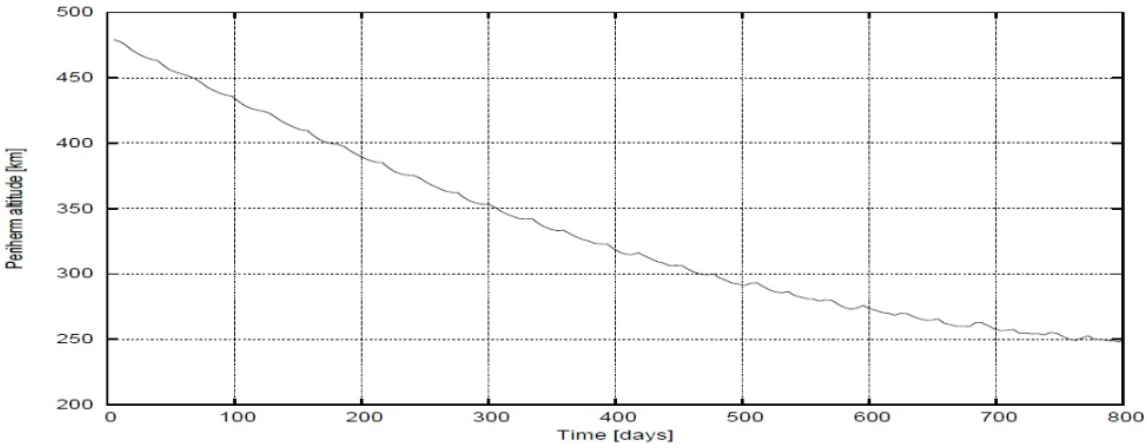

Fig 49 MPO argument of Periherm [km] evolution over 800 days

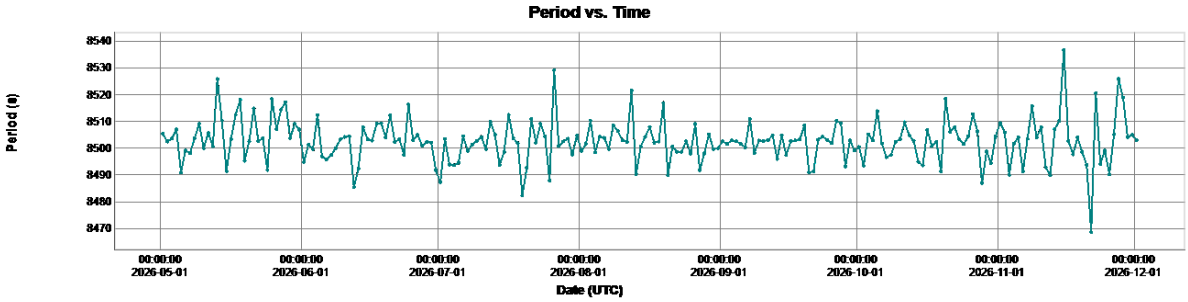

Fig 50 MPO orbital period as a function of time. A small oscillation of few seconds in the period is present, but is negligible in comparison to its overall stability during time

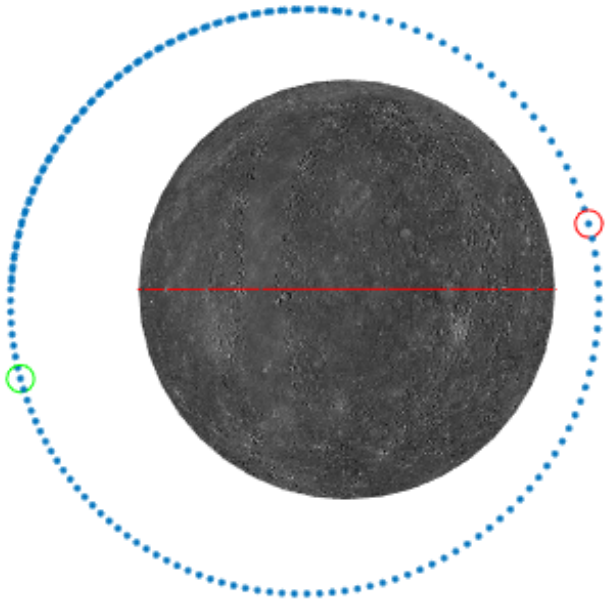

Fig 51 MPO orbit at the beginning of the mission - 16 March 2026, green circle: Apoherm = 1500 km, red circle: Periherm = 480 km

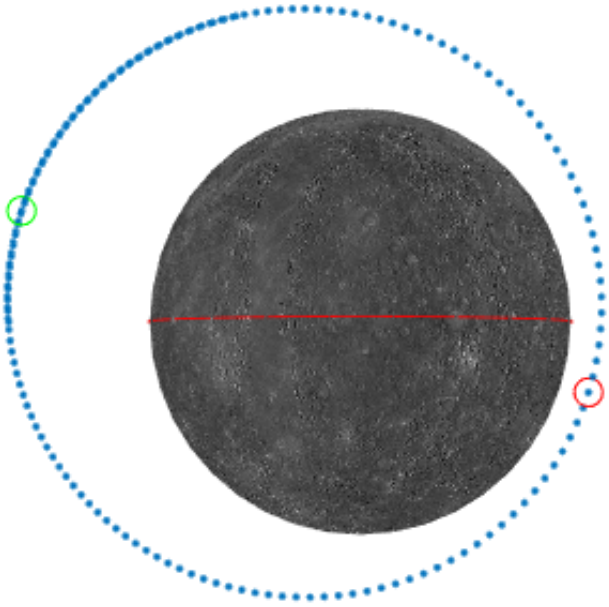

Fig 52 MPO orbit at the end of the nominal mission - 1 May 2027, green circle: Apoherm = 1666 km, red circle: Periherm = 314 km

5.3 Resolution phases

On-ground resolution depends on the altitude of the MPO while orbiting around Mercury: the maximum resolution is reached at the minimum altitude (Periherm) and the minimum resolution at the maximum altitude (Apoherm).

Mercury rotates around the Sun, reaching a minimum distance at the Perihelion and a maximum distance at the Aphelion.

The identification of different resolution phases is driven by the combination of the MPO and Mercury orbits.

The mission architecture has been planned taking into account the extreme hot temperature of the surface of the planet, that can damage the instruments distorting some of their components with thermal deformations. With the current mission configuration, the spacecraft is close to the planet when the planet is far from the Sun and consequently the surface temperature is lower, and vice versa.

The operative modes for HRIC are two, High Resolution (HR) and Low Resolution (LR).

Several acquisition phases (passes) can be considered for each of the two main operative modes: High Resolution with MPO near the Periherm (with Mercury near the Aphelion) and Low Resolution with MPO near the Apoherm (with Mercury near the Perihelion).

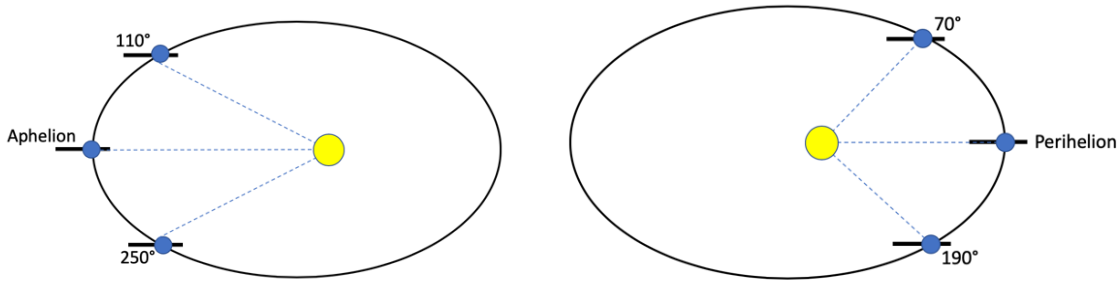

Fig 53 HRIC resolution phases. On the left: the HRIC HR phase is comprised between 110° and 250° of True Anomalies. on the right: the HRIC LR phase is defined in the ranges of True Anomalies between 70°and 190°

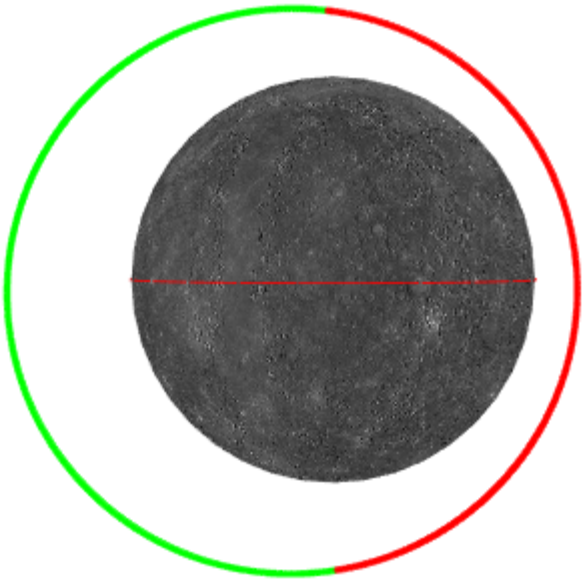

Fig 54 Representation of the segment of High Resolution Phase (in red) and the segment of Low Resolution Phase (in green) during a MPO orbit (beginning of the mission)

The starting date of the analysis has been considered correspondent with the starting of the commissioning phase (15 March 2026) and the period considered is the first terrestrial year of the nominal mission (1 May 2027).
Furthermore, the HR phase has been divided in 5 sub-phases:

1. 15 MAR 2026 - 27 APR 2026
2. 8 JUN 2026 – 24 JUL 2026
3. 4 SEP 2026 – 20 OCT 2026
4. 1 DEC 2026 – 16 JAN 2027
5. 27 FEB 2027 – 14 APR 2027

in the LR phase 5 sub-phases have been analysed:

1. 6 MAY 2026 – 30 MAY 2026
2. 2 AUG 2026 – 26 AUG 2026
3. 29 OCT 2026 – 22 NOV 2026
4. 25 JAN 2027 – 18 FEB 2027
5. 23 APR 2027 – 17 MAY 2027

5.4 Footprint on ground

As explained in the previous section, MPO orbit is elliptical, so the altitude of the spacecraft varies during time while orbiting around the planet. This has different consequences for the images taken with SIMBIO-SYS: the resolution, the dimension of the footprint and the repetition time vary.

The dimension of the HRIC footprint reaches a maximum at the Apoherm (around 40 × 12 km^2 for HRIC FPAN) and a minimum at the Periherm (12 × 4 km^2 for HRIC FPAN), while the resolution follows an opposite behavior.

Phase	**Position**	**Latitude [°]**	**Altitude [km]**	**Velocity of the S/C [km/s]**	**Pixel on ground [m/px]**	**Footprint dimension FPAN [km^2]**
Beginning of the mission	Periherm	15.9	480	2.94	6	12.31 × 3.84
	Apoherm	-15.8	1500	2.18	18.7	38.48 × 12.02
End of the first year mission	Periherm	-18.3	316	3.09	3.95	8.10 × 2.53
	Apoherm	18.4	1666	2.07	20.8	42.73 × 13.35

Tab 14 Information about Periherm and Apoherm at the beginning and end of the mission

Plotting the footprint on ground is a good method to evaluate the coverage for a target. It is visually helpful for checking how many passages are necessary to cover the entire target, or in any case to check the overlapping of subsequent acquisitions.

The following images show different example of footprints. It is notable the apparent augmentation of the dimension of the footprints near the poles: in reality this phenomenon is due mostly to the decreasing distance between two points at the same latitude along the longitude while moving towards the poles, rather than the increment of the dimension of the footprint. Still, the area covered by the filter also increases (of a factor around 2) because the altitude of the orbit near the poles is higher than the altitude near the equator (of a factor around 2).

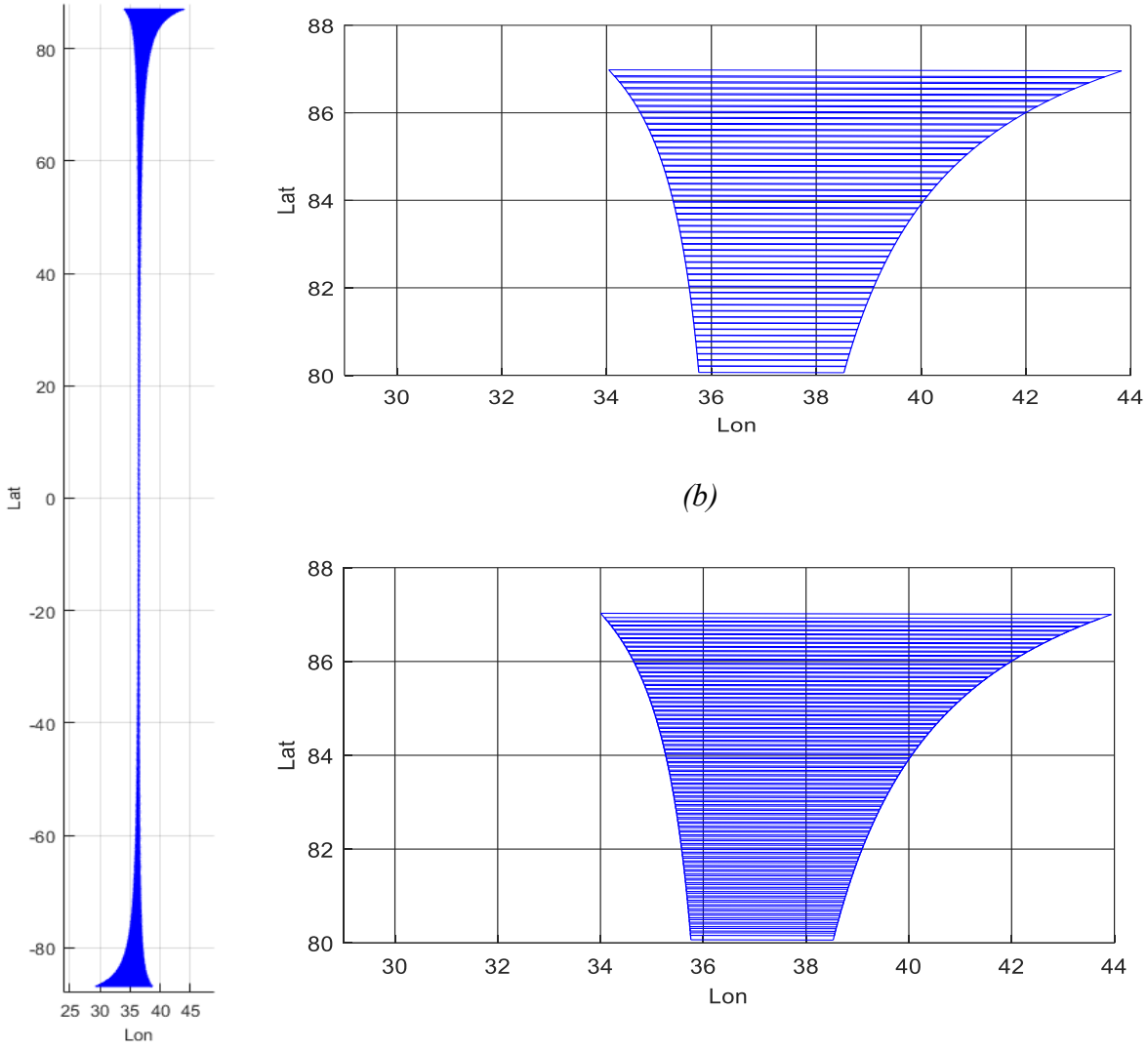

(a) *(b)* *(c)*

Fig 55 a) HRIC FPAN footprint of a single obit from pole to pole b) footprint overlapping near the pole with repetition time of 3 seconds c) footprint overlapping with repetition time of 2 seconds, the overlapping percentage along track of two consecutive acquisitions increases

Fig 56 shows different footprints of HRIC FPAN during three successive orbits during the same day. The footprints start to overlap around 53° of latitude.

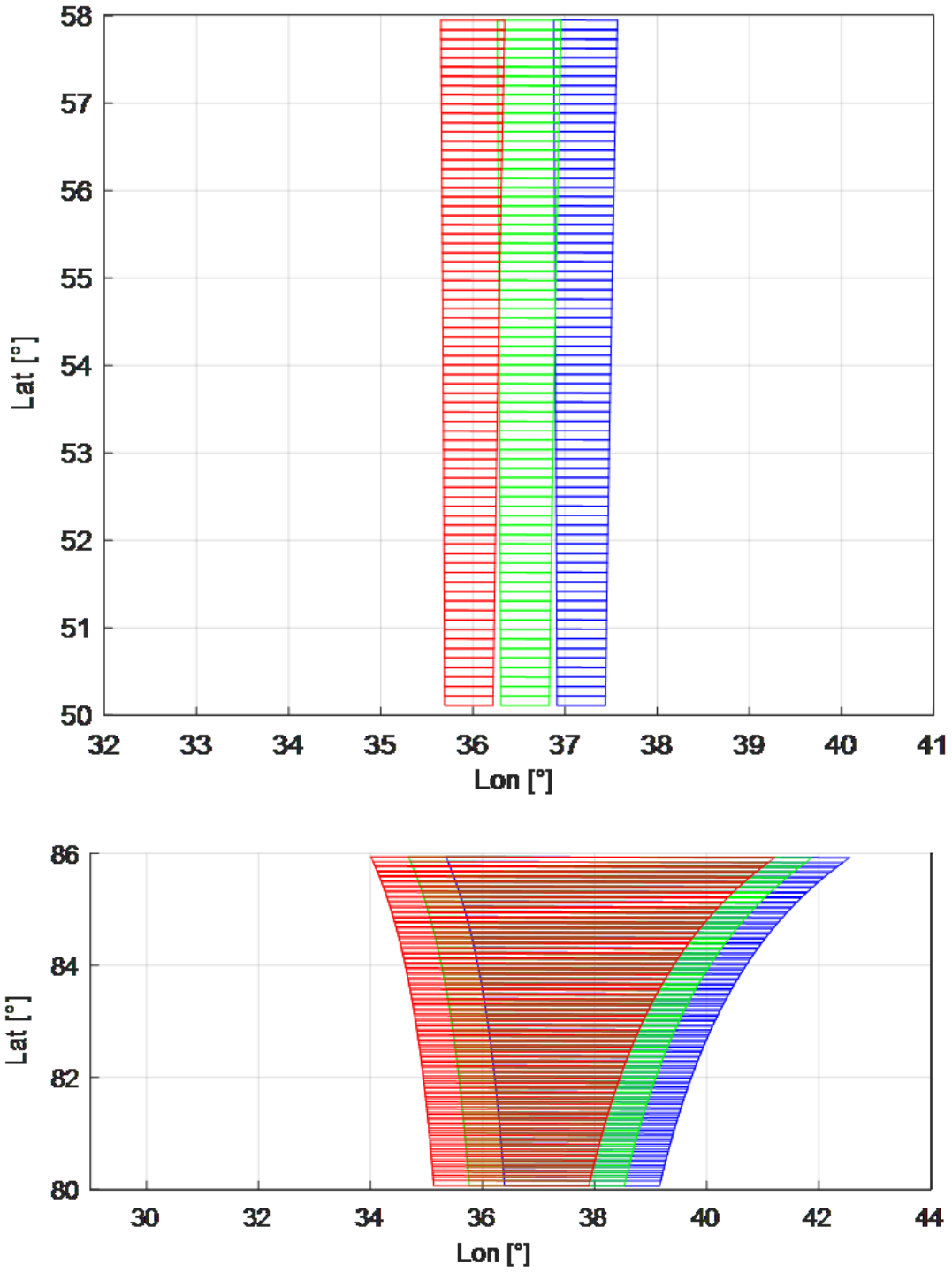

Fig 56 HRIC FPAN footprints of three successive orbits. The blue is the first orbit, the green the second and the red the third. The order can be understood by the fact that the planet is rotating counterclockwise while MPO orbit is fixed, resulting that the footprint moves towards west (left in this case) after every passage

5.5 Illumination conditions

The solar incidence angle is defined as the angle between the normal of the surface of the planet and the direction of the Sun.

The solar incidence angle depends on two variables: the position of Mercury respect to the Sun (True Anomaly) and the position of the selected point on the surface of Mercury in terms of latitude (Solar azimuth). For high latitude positions, e.g. polar regions, the solar incidence angle becomes almost independent from the position of Mercury, differently from the low latitudes where the incidence angle is strongly dependent from the position of Mercury. For intermediate regions the two phenomena coexist.

A particular illumination condition can be required for a specific objective. It is important to highlight that for a target in a specific position some illumination conditions are never achieved during all the mission time. For example, a target near the poles will never be illuminated with a low incidence angle.

The illumination affects the matching between images and it is an important factor for the 3D reconstruction [44] [45] [46].

The following graph shows different solar incidence angles of some random points chosen on the Mercury's surface at different latitudes seen from MPO in a range of time corresponding to the high-resolution image acquisition phase.

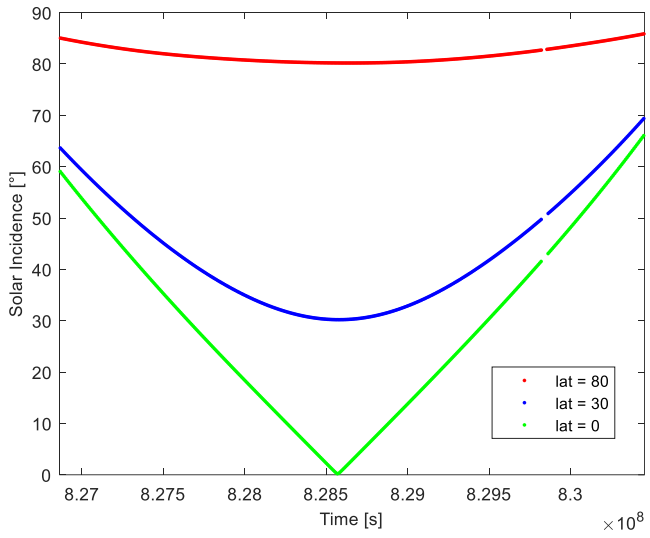

Fig 57 The graph shows the solar incidence in dependence to the latitude of the target. The simulation is performed during one window of time for high resolution acquisition (15 March 2026 – 26 April 2026)

The graph suggests that, at low latitudes, the differences in the solar incidence angles are more evident: near the equator the solar incidence angle varies from 0° to 60°, while for latitudes around 30° the solar incidence angle varies from 30° to 65°. In fact, in this area the incidence angle is mostly dependent on the True Anomaly of Mercury. The procedure of pairing imaging is consequently more affected by the change of the solar inclination at low latitudes than at high latitudes because the polar regions are always characterized by high incidence angles.

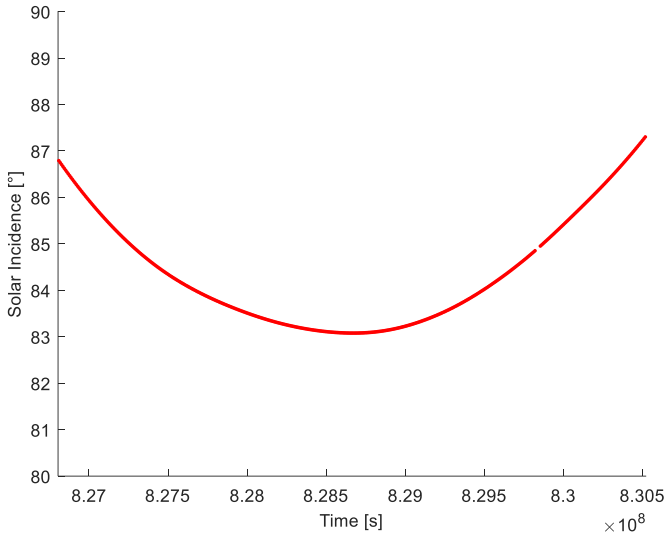

Fig 58 Solar incidence angle for the polar region (Lat > 80°), where the change is very small

Concerning the polar regions, the incidence angle can be assumed constant in time (changes of few degrees shall not have a significant relevance while matching the images). This is a positive fact, because images taken during different orbits and time will always have similar illumination conditions, facilitating the matching between them. On the other hand, it is clear that for high incidence angles (e.g. > 80) the shadows are long and the interior of the craters can be completely lacking of information: in this case this portion of the surface cannot be reconstructed in the 3D model, as it is impossible to find recognizable features, and the model presents holes. In conclusion it can be assumed the following: the matching of images at low latitudes must be carefully planned as images taken in different instant of time can have significant differences in illumination conditions, while for polar regions the illumination conditions are more constant.

In any case it is important to remind that the relative position of the Sun respect to Mercury changes when the planet is in the positions with True Anomaly 0°-180° respect to the positions

with True Anomaly 180°-360°, so an image of the same area acquired in different moment can have the light coming from opposite directions.
The following figure shows the same target acquired in different moments and consequently under different illumination conditions.

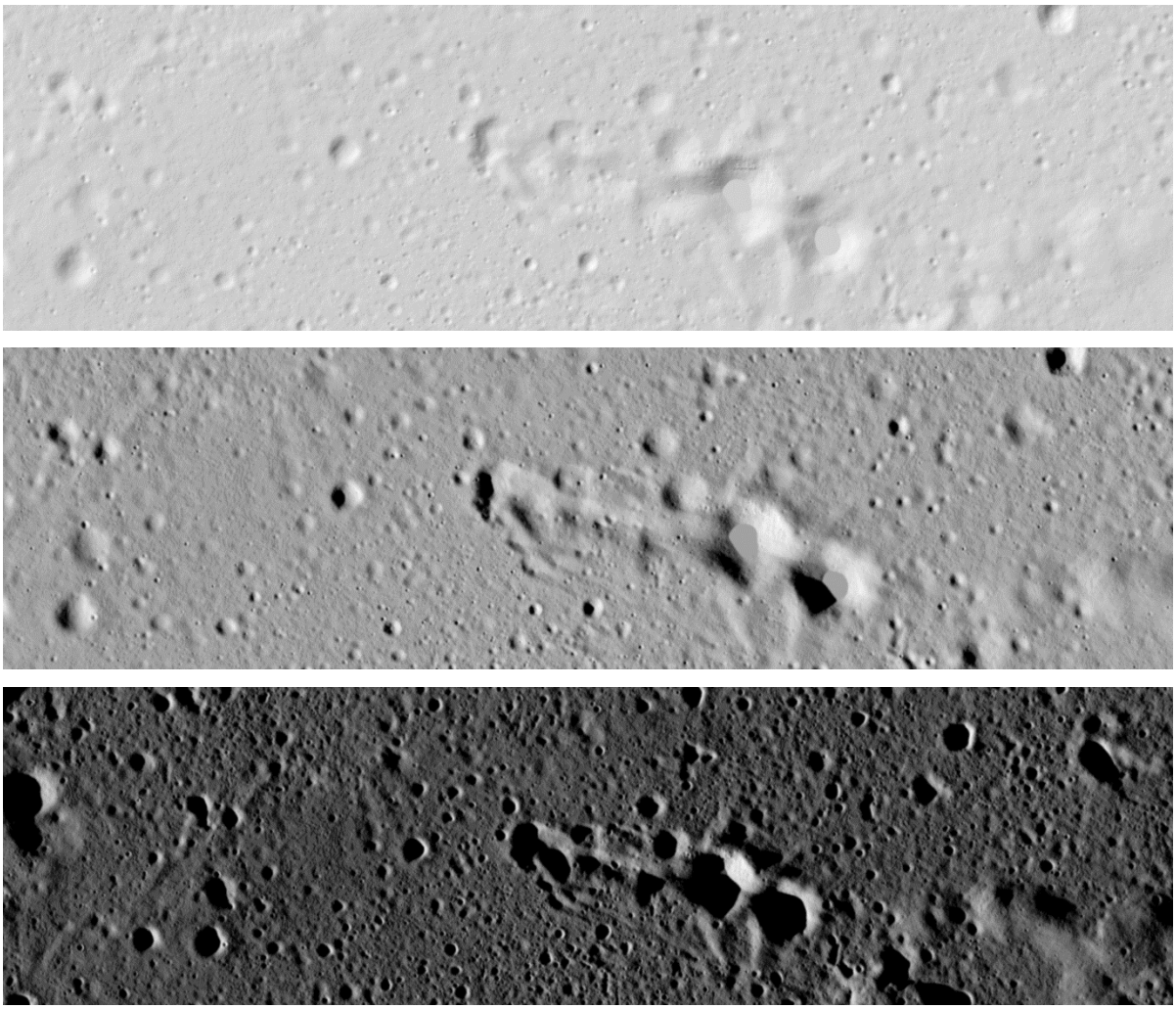

Fig 59 The same target acquired under different illumination conditions. Solar incidence angles from top to bottom: 20°, 45°, 75°

5.6 Resolution on ground and overlapping factor

In this section the change of resolution on ground and overlapping factor during the different mission phases are analyzed.
In the following graphs the pixel on ground dimensions have been computed varying the latitude for each of the sub-phase identified.

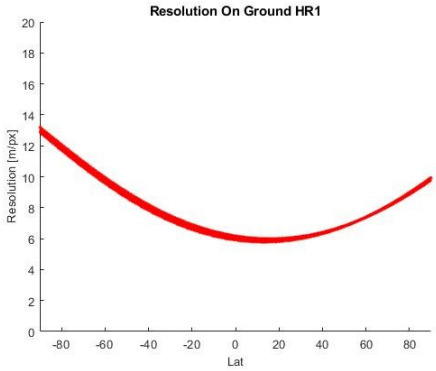
Resolution On Ground HR1
Resolution [m/px]
Lat

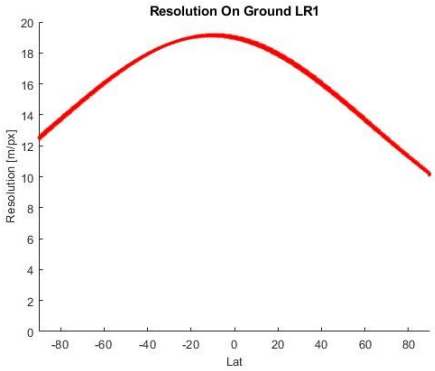
Resolution On Ground LR1
Resolution [m/px]
Lat

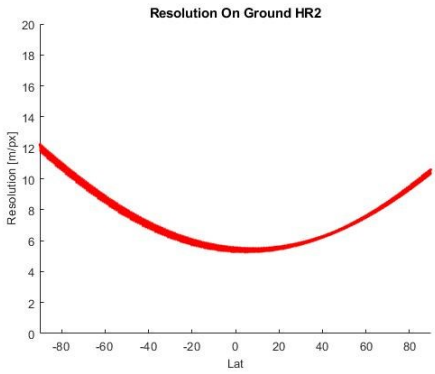
Resolution On Ground HR2
Resolution [m/px]
Lat

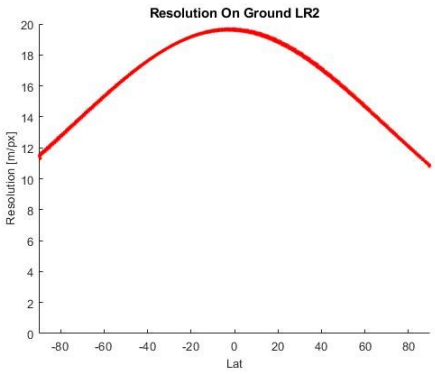
Resolution On Ground LR2
Resolution [m/px]
Lat

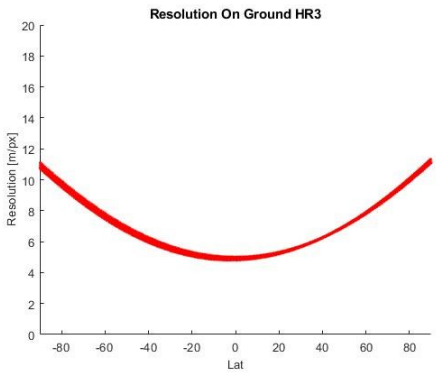
Resolution On Ground HR3
Resolution [m/px]
Lat

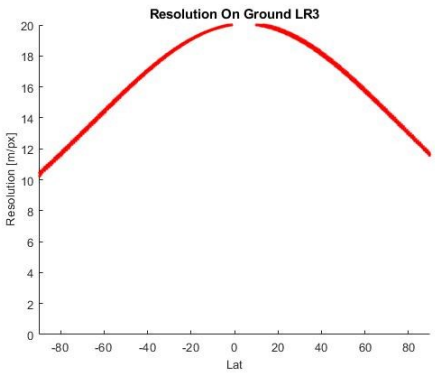
Resolution On Ground LR3
Resolution [m/px]
Lat

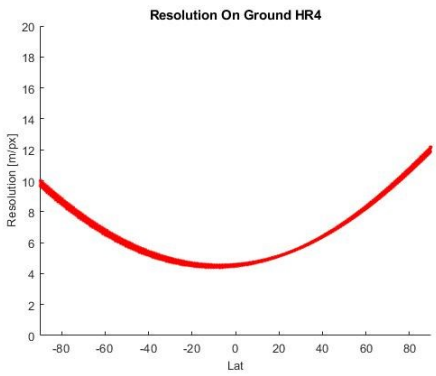
Resolution On Ground HR4
Resolution [m/px]
Lat

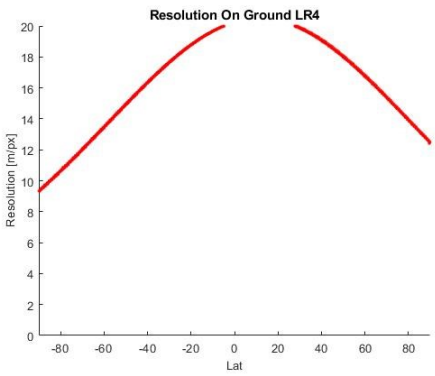
Resolution On Ground LR4
Resolution [m/px]
Lat

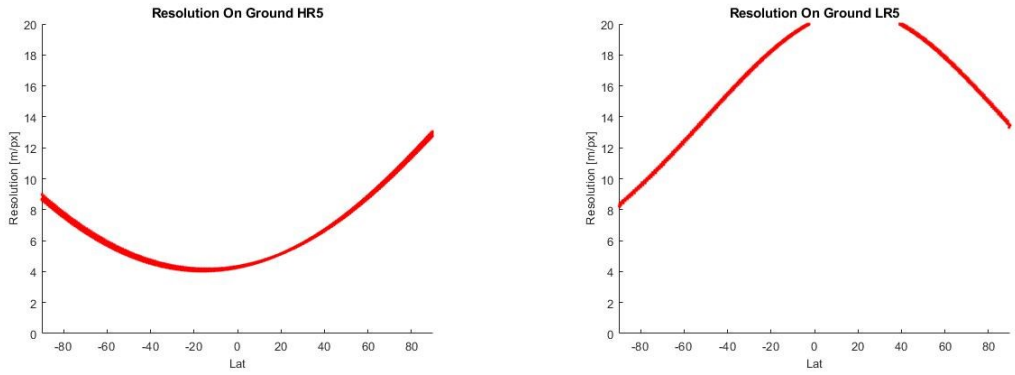

Fig 60 Pixel on Ground: On the left columns, HR phases; on the right columns, LR phases. The plots have been generated for each of the sub-phases (1,2,3,4,5)

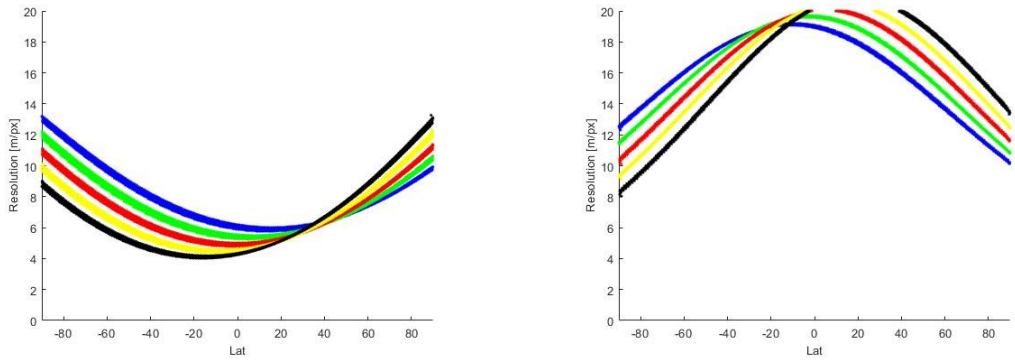

Fig 61 Cumulative graphs of the pixel on ground: On the left for HR, on the right for LR. In blue: HR/LR 1, in green: HR/LR 2, in red: HR/LR 3, in yellow: HR/LR 4 and in black HR/LR 5.

The change of the pixel scale during different phases is due to the change of the MPO orbits along time. The argument of the Periherm migrates towards the South and consequently the ellipsis of the orbit rotates, and at the same time the altitude of the Periherm diminishes. This produces a decreasing of the pixel on ground dimension moving towards the South of the planet for consecutive sub-phases.

It is clear that the pixel on ground dimension reaches a minimum (highest resolution) near the equator during the HR phases (MPO is at the closest point from the planet at the equator), while during the LR phases the minimum is at the poles (MPO is at the farther point from the planet

near the equator). Fig 51 and Fig 52, that show the position of MPO during HR and LR phases, can help to clarify these concepts.

In the following graphs the FOV cross-track dimension has been plotted varying the latitude for each of the HR sub-phases.

The Mercury rotation (0.595°/orbit) fixes the limit beyond which subsequent orbit acquisitions guarantees the overlapping between the HRIC acquisitions at the same latitude. A rotation of 0.595° corresponds to a displacement of around 25 km at the equator for two consecutive orbits. The overlapping is performed between subsequent orbits when the swath cross-track exceed the Mercury rotation. This characteristic is valid for the whole duration of the mission, because the period of the orbit remains constant, and obviously also the velocity of the rotation of Mercury around its axis remains constant.

Beside the cross-track FOVs, the overlapping factor (in the right columns) is complementary to the left side graphs: the overlapping percentage increases with the increasing of the latitude starting from the intersection between the limit imposed by the rotation of Mercury and the amplitude of the cross-track swath.

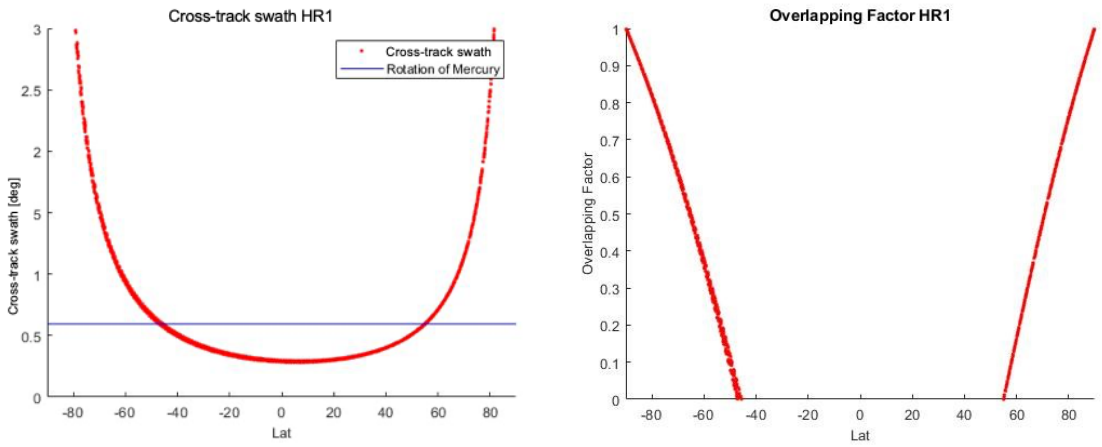

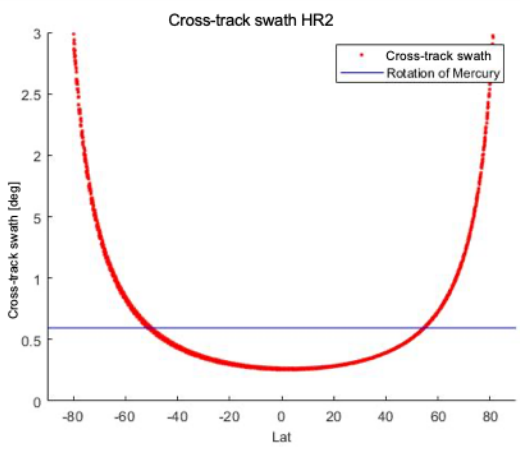
Cross-track swath HR2
Cross-track swath
Rotation of Mercury
Cross-track swath [deg]
Lat

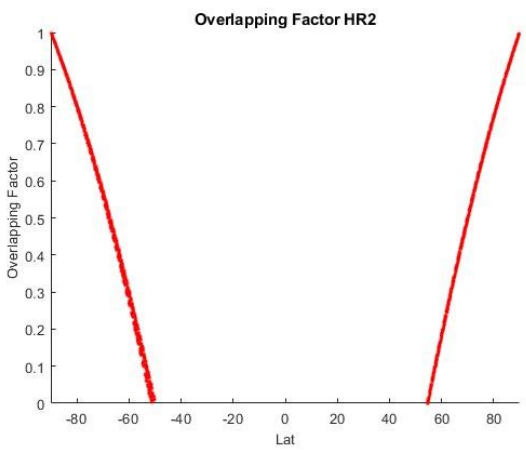
Overlapping Factor HR2
Overlapping Factor
Lat

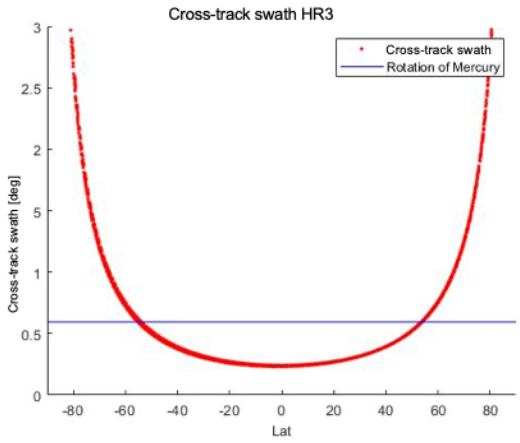
Cross-track swath HR3
Cross-track swath
Rotation of Mercury
Cross-track swath [deg]
Lat

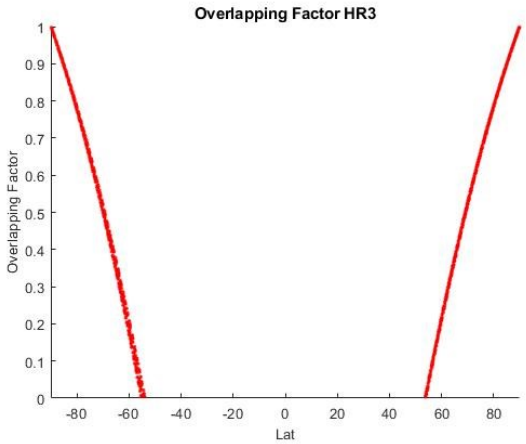
Overlapping Factor HR3
Overlapping Factor
Lat

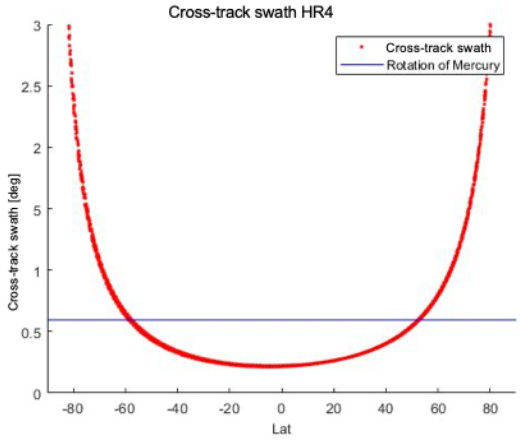
Cross-track swath HR4
Cross-track swath
Rotation of Mercury
Cross-track swath [deg]
Lat

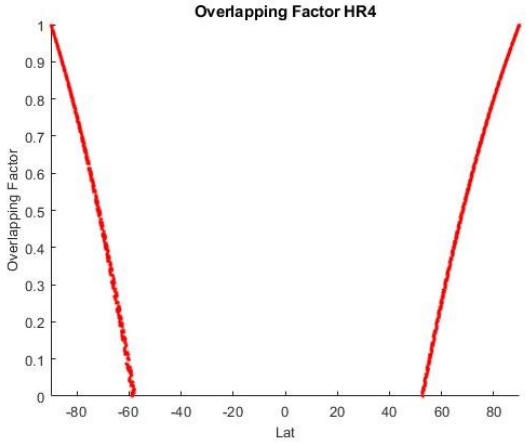
Overlapping Factor HR4
Overlapping Factor
Lat

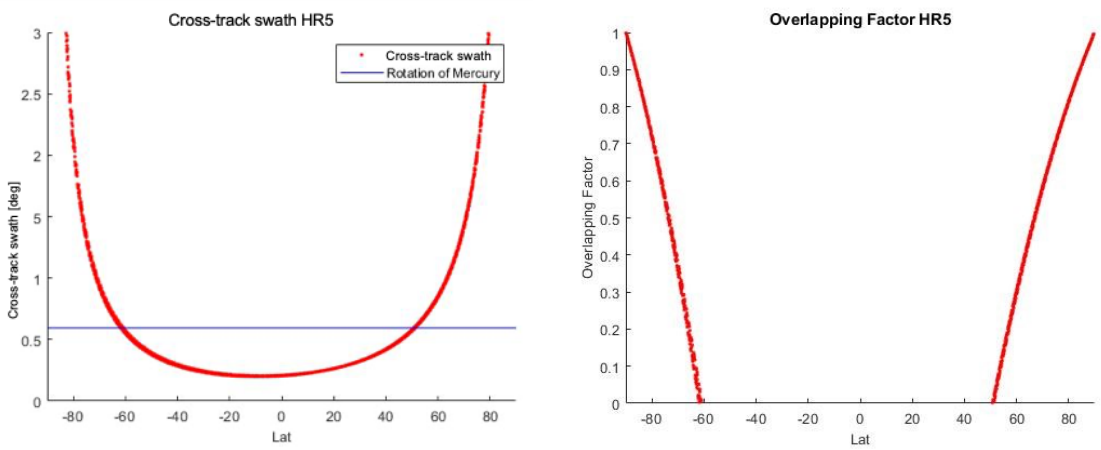

Fig 62 Graphs for HR, on the left: In red, Cross-track swath with respect to the limit imposed by the rotation of Mercury in each orbit (in blue); on the right: the Overlapping percentage varying with the latitudes.

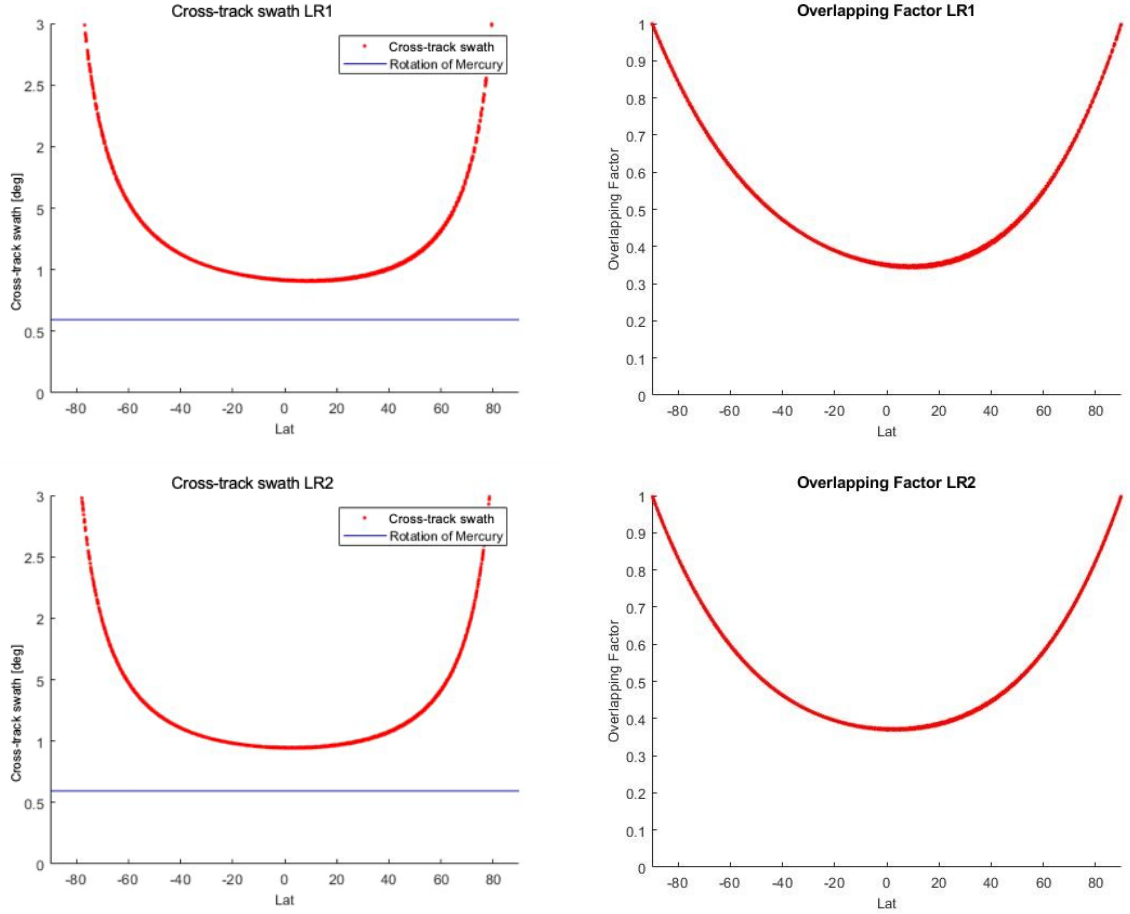

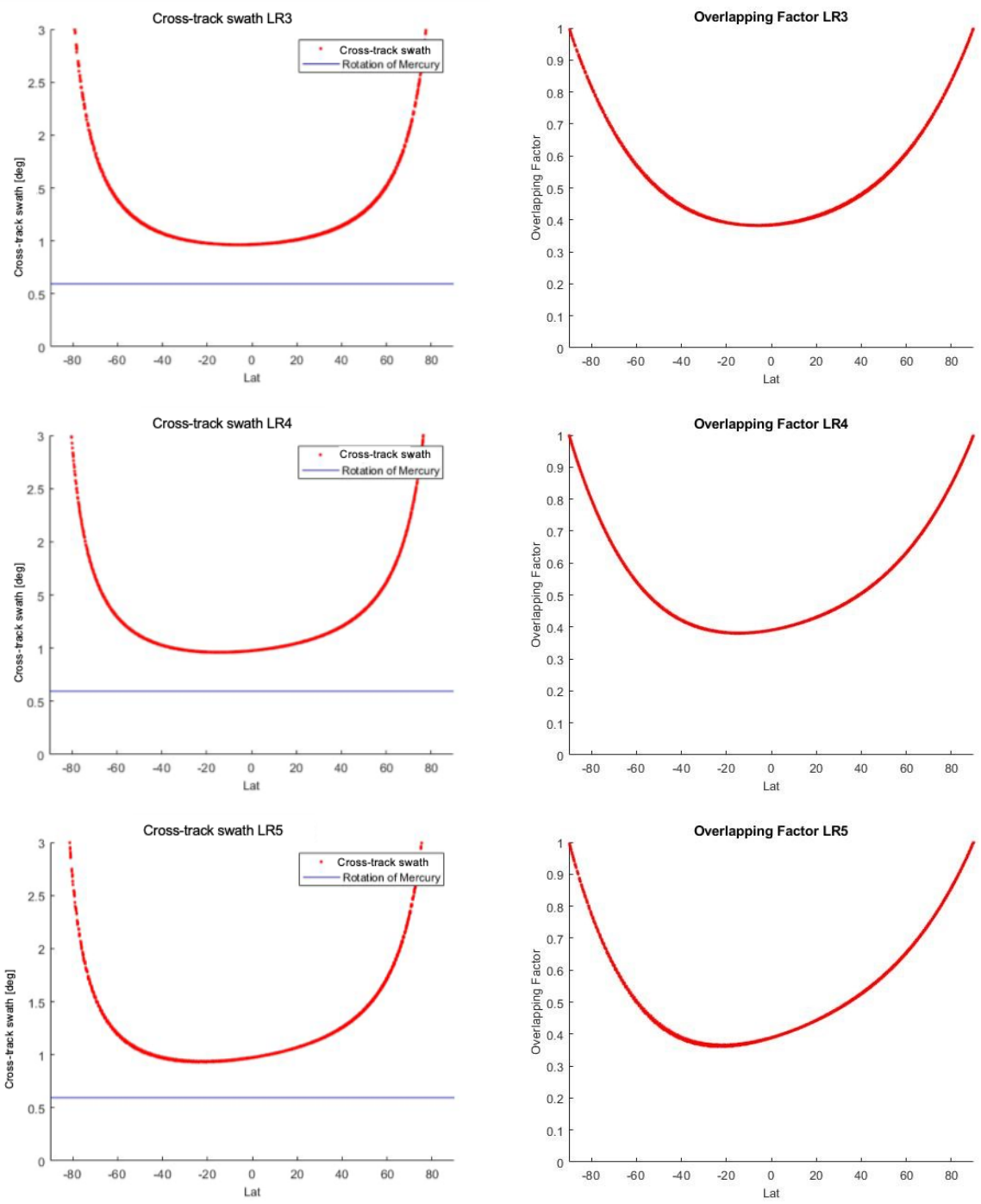

Fig 63 Graphs for LR, on the left: In red, Cross-track swath with respect to the limit imposed by the rotation of Mercury in each orbit (in blue); on the right: the overlapping factor varying with the latitudes.

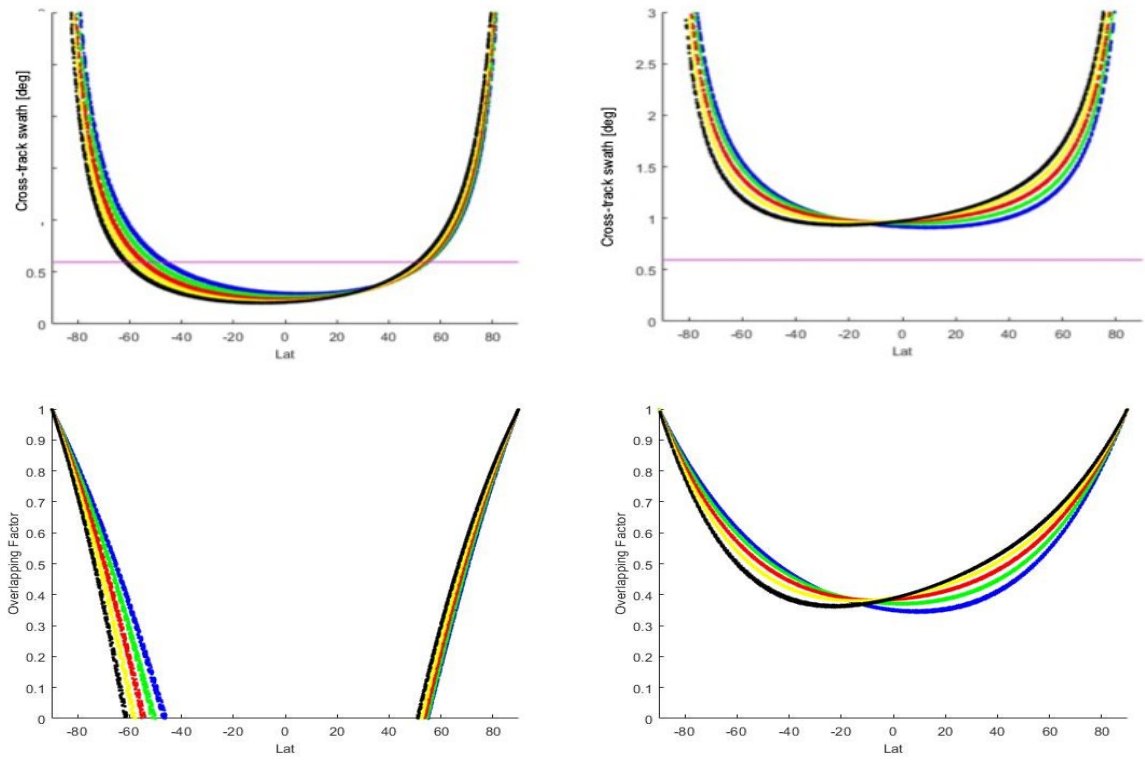

Fig 64 Cumulative graphs: on the top the Cross-track swath amplitude for HR (left), LR (right) and below the overlapping percentage for HR (left) and LR (right).
In blue: HR/LR 1, in green: HR/LR 2, in red: HR/LR 3, in yellow: HR/LR 4 and in black HR/LR 5.

The change of the MPO orbit along time can be noticed in these graphs as well. The movement of the Periherm towards the South decreases the overlapping percentage in the southern hemisphere among consecutive phases.
In terms of pixel scale, the northern hemisphere is better covered at the beginning of the mission (for the southern hemisphere is the opposite).
In terms of overlapping, instead, for the northern hemisphere the percentage does not change particularly during the mission, differently from the southern hemisphere where the change is more evident. In conclusion, for the southern hemisphere the overlapping is better at the beginning of the mission but accomplished with a lower spatial resolution.
What can be noticed from the graphs is that for the LR case, the percentage of overlapping between consecutive orbits is always performed between 30% and 100% going towards the poles, differently from the HR case where the overlapping is allowed only in the ranges beyond the + 50° /- 40° of latitudes.

The following table summarizes the area that can be covered with successive orbits (limited by MIN Lat and MAX Lat) and the minimum Pixel on Ground (PoG) value achievable with the corresponding latitude.

	MIN Lat (Hem. North) [°]	**MAX Lat (Hem. South) [°]**	**Lower PoG [m/pix] (corresponding latitude [°])**
HR1	~ 55	~ - 46	~ 5.7 (16°)
HR2	~ 54	~ - 50	~ 5.3 (3°)
HR3	~ 53	~ - 55	~ 4.8 (-6°)
HR4	~ 52	~ - 58	~ 4.3 (-10°)
HR5	~ 51	~ - 61	~ 4 (-17°)
LR1	~ 0	~ 0	~ 10.2 (North Pole)
LR2	~ 0	~ 0	~ 11 (North Pole)
LR3	~ 0	~ 0	~ 10.6 (South Pole)
LR4	~ 0	~ 0	~ 9.5 (South Pole)
LR5	~ 0	~ 0	~ 8.2 (South Pole)

Tab 15 Summary table of the different resolution phases of HRIC

5.7 Target oriented strategy

HRIC has a target-oriented strategy, mapping about 20% of the surface of the planet by selecting specific targets. The targets are chosen for their scientific importance and are sparse all over the planet.

During the mission, every target becomes visible for a specific amount of times and under specific conditions. Knowing a-priori this information is definitely useful for an efficient planning and helps scientists in the selection of the most interesting targets.

Speaking of illumination conditions, it happens that some targets are always visited under the same condition, while for others the illumination condition varies. This aspect is dependent on the longitude of the target and it is enabled by the rotation of Mercury around the Sun.

The following figure helps to clarify this phenomenon: the number upon represents the number of possible illumination conditions a target can be subjected on during the first year of mission. This means that even if a target is revisited more than one time, it can happen that either the

illumination condition remains the same or changes: for example, near 0° of longitude 3 different illumination conditions can occur, between 0° and 315° 2 conditions occur while between 315° and 225° only one condition occurs. This factor can be either positive or negative in dependence of what the user wants to obtain, meaning that different illumination scenarios are necessary or not.

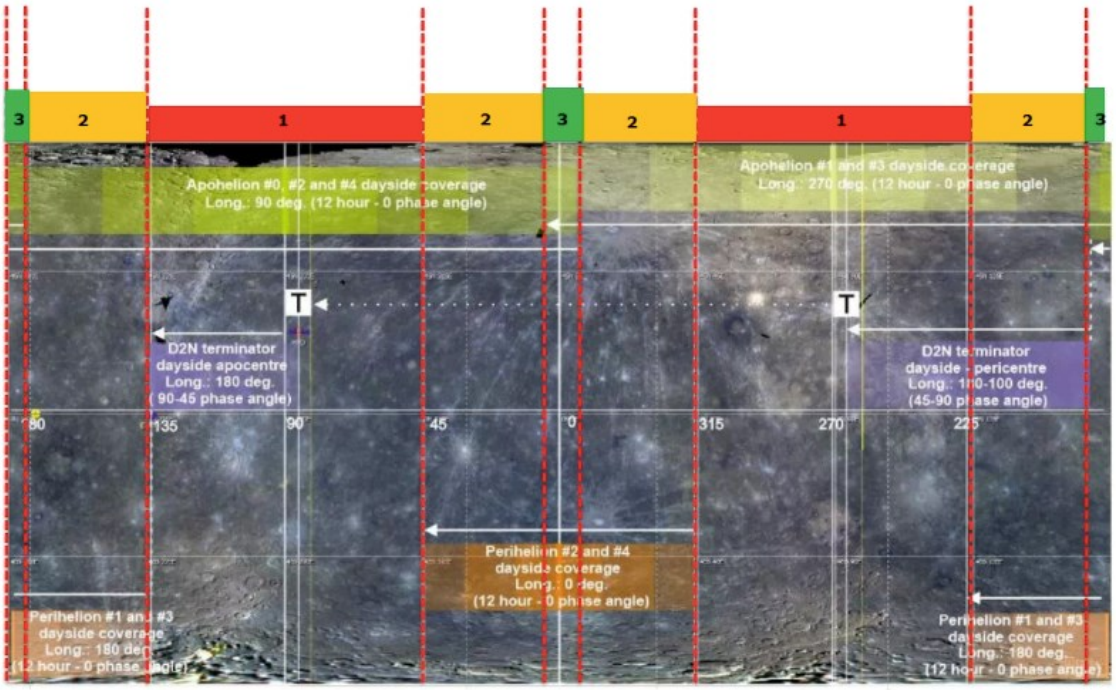

Fig 65 Different illumination conditions

The SIMBIO-SYS scientific working group (SCWG-Surface and Composition) selected a list of around 500 preliminary targets so far. The list includes the name of the target, its position on the surface and the desired acquisition conditions in terms of incidence angle and spatial resolution. Using the information stored in the SPICE kernels and some customized MATLAB routines, a prediction of the acquisition conditions has been calculated. For every target it is possible to verify the number of times that is visible, the time of the possible acquisition, the incidence angle and the resolution on ground. From this list of information every user can verify if the desired acquisition conditions of the specific target are met.

The following example shows how to check the characteristics of the acquisition for the target 500001. Clearly, this procedure can be applied for every target.

The first extract of the table indicates the name, position, dimension and desired acquisition conditions of the selected target.

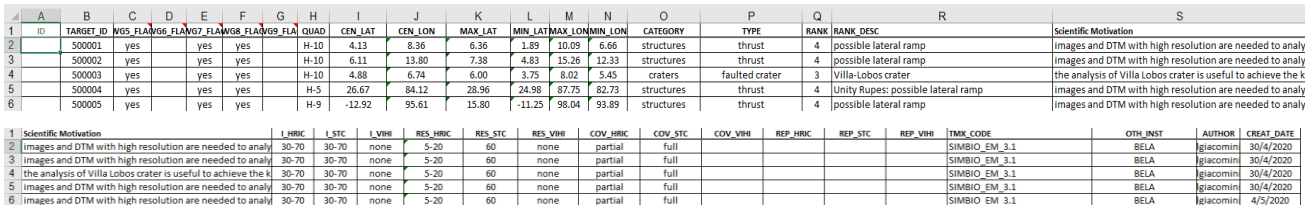

ID	TARGET_ID	WG5_FLA	WG6_FLA	WG7_FLA	WG8_FLA	WG9_FLA	QUAD	CEN_LAT	CEN_LON	MAX_LAT	MIN_LAT	MAX_LON	MIN_LON	CATEGORY	TYPE	RANK	RANK_DESC	Scientific Motivation
	500001	yes		yes	yes		H-10	4.13	8.36	6.36	1.89	10.09	6.66	structures	thrust	4	possible lateral ramp	images and DTM with high resolution are needed to analy
	500002	yes		yes	yes		H-10	6.11	13.80	7.38	4.83	15.26	12.33	structures	thrust	4	possible lateral ramp	images and DTM with high resolution are needed to analy
	500003	yes		yes	yes		H-10	4.88	6.74	6.00	3.75	8.02	5.45	craters	faulted crater	3	Villa-Lobos crater	the analysis of Villa Lobos crater is useful to achieve the k
	500004	yes		yes	yes		H-5	26.67	84.12	28.96	24.98	87.75	82.73	structures	thrust	4	Unity Rupes: possible lateral ramp	images and DTM with high resolution are needed to analy
	500005	yes		yes	yes		H-9	-12.92	95.61	15.80	-11.25	98.04	93.89	structures	thrust	4	possible lateral ramp	images and DTM with high resolution are needed to analy

Scientific Motivation	I_HRIC	I_STC	I_VIHI	RES_HRIC	RES_STC	RES_VIHI	COV_HRIC	COV_STC	COV_VIHI	REP_HRIC	REP_STC	REP_VIHI	TMX_CODE	OTH_INST	AUTHOR	CREAT_DATE
images and DTM with high resolution are needed to analy	30-70	30-70	none	5-20	60	none	partial	full					SIMBIO_EM_3.1	BELA	lgiacomin	30/4/2020
images and DTM with high resolution are needed to analy	30-70	30-70	none	5-20	60	none	partial	full					SIMBIO_EM_3.1	BELA	lgiacomin	30/4/2020
the analysis of Villa Lobos crater is useful to achieve the k	30-70	30-70	none	5-20	60	none	partial	full					SIMBIO_EM_3.1	BELA	lgiacomin	30/4/2020
images and DTM with high resolution are needed to analy	30-70	30-70	none	5-20	60	none	partial	full					SIMBIO_EM_3.1	BELA	lgiacomin	30/4/2020
images and DTM with high resolution are needed to analy	30-70	30-70	none	5-20	60	none	partial	full					SIMBIO_EM_3.1	BELA	lgiacomin	4/5/2020

Tab 16 List of preliminary targets for HRIC

The second extract of the table (Tab 17) indicates instead the characteristics of every possible acquisition of the target 500001 taken as example.

For each target, the following information are displayed:

- Position: the coordinates of the centre of the target on the planetary surface. If the target is bigger than the footprint of the camera, then it is only partially visible with just one acquisition. Acquisitions during successive orbits can be used to fill eventual gaps and create a mosaic of images that covers the entire target. This possibility is specific for every target and depends on its position and dimension, so a further specific investigation is needed to retrieve a complete planning scheme.
- Date: the date in which the target results visible from the orbit. This list takes into account only the positions in which the target is illuminated, so the target is excluded if it is in the dark side of the planet.
- True Anomaly: the True Anomaly of Mercury (its position) at the moment in which the target is visible.
- Altitude: the altitude of MPO at the moment in which the target is visible.
- Resolution: resolution on ground of HRIC and STC images at the moment in which the target is visible.
- Solar incidence: the solar incidence angle at the moment in which the target is visible.

TARGET	LAT	LON	DATE	TRUE ANOMALY[°]	ALTITUDE [KM]	RESOLUTION HRIC [M/PX]	RESOLUTION STC [M/PX]	SOLAR INCIDENCE ['
500001	4.13	8.36	2026 MAR 19 11:15:47.71	133.6284875	487.9711983	6.099639979	51.3653893	46.62041889
500001	4.13	8.36	2026 JUL 14 16:26:18.09	217.9667308	424.1787747	5.302234684	44.65039734	38.02385149
500001	4.13	8.36	2026 JUL 14 18:48:00.96	218.2693257	424.1588257	5.301985321	44.64829744	38.32554076
500001	4.13	8.36	2026 AUG 12 23:04:13.89	350.9860144	1563.571255	19.54464069	164.5864479	10.01417704
500001	4.13	8.36	2026 AUG 13 01:25:56.76	351.6071185	1563.594475	19.54493094	164.5888921	9.468196351
500001	4.13	8.36	2026 SEP 11 08:12:18.11	133.4169761	400.0137118	5.000171398	42.10670651	46.68614476
500001	4.13	8.36	2026 SEP 11 10:34:00.92	133.7335575	399.9950737	4.999938421	42.1047446	46.3695435
500001	4.13	8.36	2027 JAN 06 15:44:21.06	218.068994	363.8360642	4.547950803	38.29853308	38.26921821
500001	4.13	8.36	2027 MAR 06 07:30:03.35	133.5220613	354.3215914	4.429019892	37.29700962	46.43858025
500002	6.11	13.8	2026 MAR 18 14:00:55.87	130.7571455	485.6731859	6.070914824	51.12349325	49.63197775
500002	6.11	13.8	2026 JUL 13 19:11:25.16	215.2652487	424.2484518	5.303105647	44.65773177	35.56287211

Tab 17 List of the acquisition characteristics for every target

The target 500001 is seen 9 times (see the dates in the previous table) during the first year of mission. The number of times can vary from target to target and depends on its position on the surface.

Some of the constrains are met in every acquisition, for example the HRIC resolution required (5-20 m/px), while others are not in some of the acquisitions, for example the illumination condition (30-70° required, but 10°- 9° on 2026 August 12 23:04:13 and 2026 August 13 01:25.56).

In conclusion, this tool is useful to check a-priori the characteristics of the different acquisitions of every target.

5.7.1 Example at the Poles

As previously explained, the footprint on ground near the poles is bigger (lower resolution) because of the higher altitude of MPO. Around the latitude of 60° (-60°) the footprints of two consecutive orbits start to overlap. In this case, if the target is bigger than the area covered by a single acquisition, it is just necessary to acquire other images during the successive orbits to cover the cross-track area. For the along-track area instead, it is just necessary to set a proper repetition time in order to obtain to desired overlapping percentage. The result is a set of images that overlap both cross and along-track between them. From these images is possible to obtain a mosaic that covers the entire area of the selected target.

Target 600035 can be useful to explain to the procedure to cover it.

Here the position and dimension are summarized:

TARGET_ID	QUAD	CEN_LAT	CEN_LON	MAX_LAT	MIN_LAT	MAX_LON	MIN_LON	AREA
600035	H-14	-66.68°	76.16°	-68.70°	-65.50°	79.00°	75.00°	156 × 134 km^2

The target size is 156 km along the longitude (cross-track dimension) and 134 km along the latitude (along-track dimension).

The image shows a representation of six consecutive orbits that map the target. The first available acquisition is available on 3 July 2026.

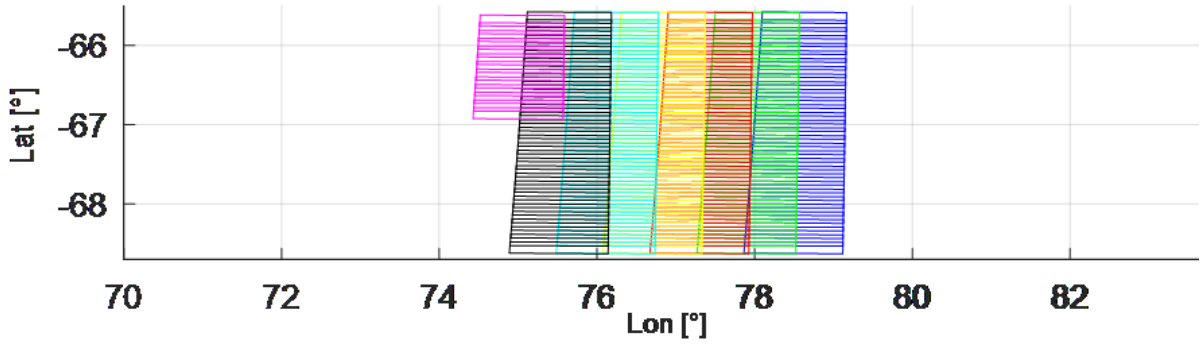

Fig 66 Representation of six consecutive orbits mapping target 600035. The order of the orbits is: blue, green, red, yellow, cyan, black, magenta.

In this case, the overlapping cross-track factor for two consecutive orbits is high (around 50%). Probably, for this example it is sufficient to acquire images every two orbits instead of every one. In this case only blue, red and cyan footprints would be considered but on the other hand, the overlapping decreases and can be null in some areas.

The repetition time is chosen in dependence of the overlapping percentage needed along-track. The formula to calculate it is the following:

$$repetition\ time = \frac{\text{along}_{\text{track}}\text{dimension of the image} - \text{along}_{\text{track}}\text{dimension of the overlapping}}{\text{velocity of the spacecraft}} \quad (17)$$

For this example, a conservative repetition time of 2 seconds have been taken into account.

5.7.2 Example near the equator

Target 500001 can be useful again to explain to the procedure to completely cover it with different acquisitions.

Here the position and dimension of the target are summarized:

TARGET_ID	QUAD	CEN_LAT	CEN_LON	MAX_LAT	MIN_LAT	MAX_LON	MIN_LON	AREA
500001	H-10	4.13°	8.36°	6.36°	1.89°	10.09°	6.66°	144 × 187 km^2

In this case the footprints of two consecutive orbits do not overlap because the altitude of MPO is low and the dimension of the footprint is too small. Thus, for this target it is necessary to take successive acquisitions in different periods of time to fill the gaps between the footprints. The following image shows the result, with in blue the first sequence of orbits (on 19th of March 2026), in red the second sequence of orbits (on 14th of July 2026) and in green the third sequence of orbits (on 11th of September 2026). From these different sequences of images is possible to create a mosaic.

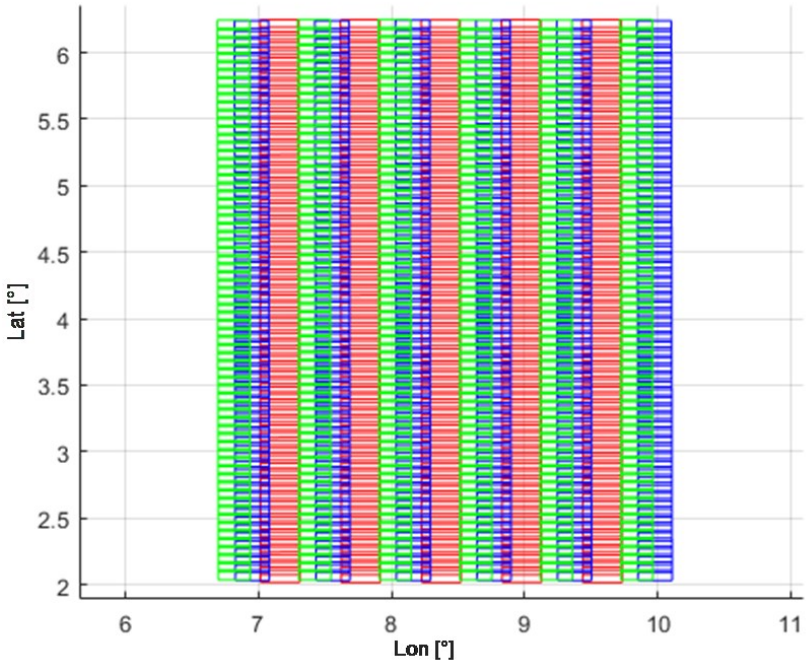

Fig 67 Representation of three sequence of orbits necessary to map the entire target 500001 close to the equator. The sequence order is: red, blue, green

This target represents a particular case where two orbital passages happen during the same Aphelion: the first passage is at the beginning of the high resolution phase (TA = 133°), the second one at the and (TA = 218°). In this way two different acquisition conditions occur.
For other targets, the ones acquired in the middle of the high resolution phase (TA around 180°), the revisitation condition occurs after one Aphelion (one orbit of Mercury around the Sun) and in this case the two acquisition conditions are the same from the point of view of the illumination, as the planet is in the same position respect to the Sun.
This situation presents a disadvantage in the creation of the mosaic with respect to the one described at the poles for two different reasons: the images are taken at different moments and under different conditions, so the resolution and incidence angle change for every sequence of orbits. These conditions are summarized for this particular case:

ORBIT PASSAGE	DATE	RESOLUTION [m/px]	ILLUMINATION ANGLE [°]
First (red)	2026 MAR 19	6	46
Second (blue)	2026 JUL 14	5.3	38
Third (green)	2026 SEP 11	5	46

Tab 18 Example of three different orbital passages to cover the target 500001

The difference in terms of resolution and incidence angle produces a mosaic with different characteristics inside it.
The cross-track footprint dimension reaches a minimum when the spacecraft is at the Periherm. This value changes in time because of the orbital change but can be approximated to 10 km of width as worst case scenario. Reminding that at the equator the distance between two consecutive orbits is around 25 km, it means that a maximum of four passages of different orbits are necessary to completely cover every gap in a target, but in most of the cases two or three passages should be sufficient.

5.8 Observation strategy at the poles

The Poles are the most interesting regions from a scientific point of view, but are also the most difficult areas to explore, as the average altitude of MPO is higher than equatorial regions due

to the elliptical orbit (lower resolution) and incidence angles are higher than 80° (long shadows and high occlusions). Polar regions identify the area between ± 83° of latitude and the poles. The MESSENGER mission saw something that appeared to be water ice inside the craters near the poles [47]. Reminding the elevate temperature of the surface of Mercury, that can reach 450°C, this discover was kind of surprising. On the other hand, the rotation axis of the planet is perpendicular to the orbital plane: in such way, the rays of the Sun cannot enter directly inside the craters in the polar regions and consequently the temperature remains low, allowing the possible presence of water. By the way MESSENGER did not detect directly the presence of water, and this important discover can be hopefully confirmed by the instrumentation on board MPO, in particular by the images and the spectroscopic analysis provided by SIMBIO-SYS. But in case the presence of ice would be confirmed, another question arises: where does it come from? Some theories suggest that the water does not came from Mercury directly, but more probably from asteroids that collided with the surface for millions of years. BepiColombo will hopefully find an answer to this question.

Near the Poles the altitude of MPO is higher respect to the equatorial regions and this factor has two important consequences for the stereo products of STC: firstly, the pixel on-ground dimension, strictly liked to the altitude of the spacecraft, increases; secondly, the baseline between two different acquisitions increases up to the point to decrease the performance in the matching process of image pairs. These two aspects influence the quality of the DTMs reconstructed with STC stereo pairs, resulting that the DTMs quality depends on the position of the target on the planet, with better results in the equatorial regions respect to the Poles.

A different approach for the image acquisition can be considered to avoid this problem.

One possibility is to use HRIC to produce the second image for the stereo pair. In this way the 3D reconstruction of the surface will be recovered from a nadir pointing image of HRIC and an inclined image of STC. This strategy can undoubtedly provide useful results but also presents some critical aspects that have to be examined.

Some of the issues related to this strategy are the following:

- HRIC and STC have different FOV and sensor size, causing a different resolution and footprint dimension on ground. It is necessary to uniform the two outputs of the cameras in order to compare them, e.g. mosaicking of different images of HRIC to obtain an image with dimensions comparable to the one of STC; reducing the resolution of HRIC images to a level comparable to STC.
- Evaluate the 3D reconstruction performance with a nadir-inclined stereo pair.

- Define a strategy for mosaicking the HRIC images, e.g. calculate the repetition time along-track and the overlapping value cross-track after one or more orbits of MPO.
- Evaluate the illumination conditions in the polar regions, e.g. to facilitate the matching process, stereo pair images should have similar illumination conditions.
- Estimate the data volume necessary to explore the poles with the HRIC-STC configuration.

5.8.1 Image acquisition

HRIC works with a pointed-oriented strategy and can be activated at will when necessary. Theoretically, it can be activated during every orbit after MPO passes the ±83° of latitude, to completely map all the area included from 83° to 90°.
Moving towards the poles, the overlapping percentage of two images acquired in consecutive orbits increases. The following graphs show the cross-track swath of HRIC panchromatic filter on the surface of Mercury.

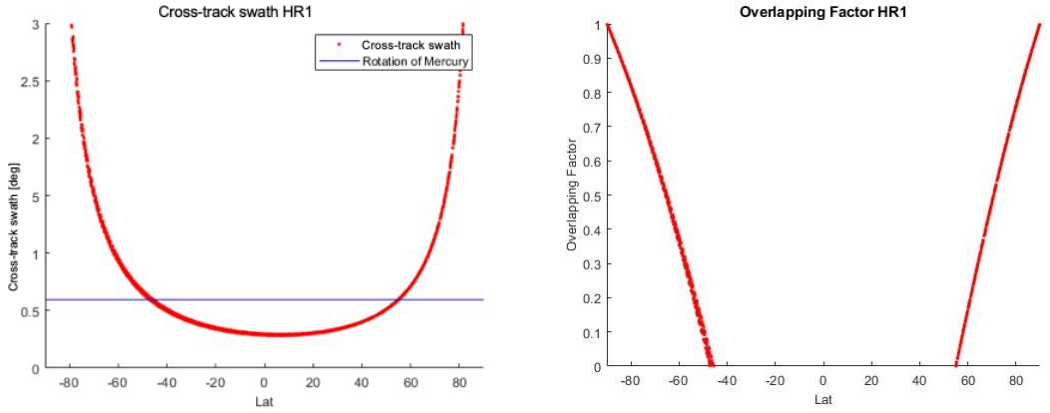

Fig 68 Cross-track swath and overlapping factor for the phase HR1

From the graphs is clear that the overlapping of two consecutive orbits starts around +- 55° of latitude, reaching 100% at the Poles. This study concerns only the polar regions so hereafter only regions above ± 83° of latitude will be considered. Here the percentage of overlapping of two consecutive orbits is higher than 90%: such a high value is not necessary, and images can be acquired with a gap of some orbits between one and the other. In this way a smaller number of images are necessary, decreasing the total data volume. The following graph shows the overlapping percentage for different orbits.

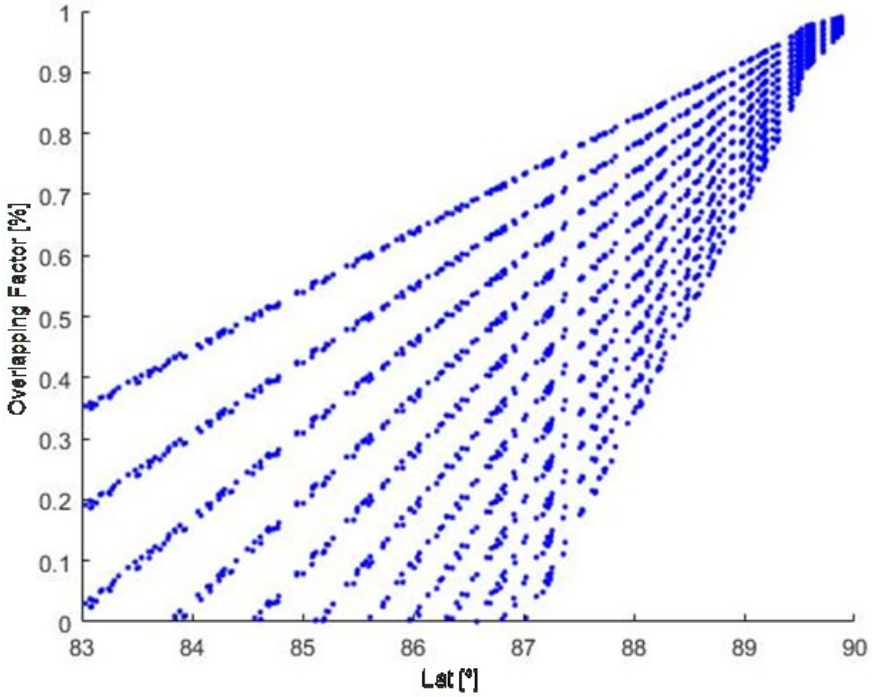

Fig 69 Overlapping percentage changing the acquisition step between orbits in dependence of the latitude. The different lines show the overlapping for a step from 4 to 15 orbits, moving from the top (highest percentage) to the bottom (lowest percentage). For example, at latitude of 86°, the overlapping percentage corresponds to 60% with an acquisition step of 4 orbits, and to 10% with an acquisition step of 10 orbits

As the overlapping percentage increases very rapidly moving towards the Poles in these high latitudes, two strategies can be planned:

1) Images are acquired after a fixed step between orbits (every four orbits for example) and this step is maintained constant for every latitude. In this way, images of areas closer to the Poles will have a higher overlapping percentage, as the distance between the tracks on ground of the orbits decreases. The number of images and the consequent data volume will be increased as well. On the other hand, fixing only one step facilitates the acquisition operation. To better clarify this aspect let us consider this example: MPO is moving towards the north pole and when it passes 83° of latitude HRIC starts to take a sequence of images with the chosen repetition time. It continues to take acquisitions until reaching the pole, and then repeats the same procedure after the chosen number of orbits. The result is a strip of sequenced images from 83° to 90° latitude at every step of orbits.

2) Different steps are chosen depending on the latitude (for example the step can be changed for every latitude between 83° and 90°). In this way the overlapping and the data volume will be optimized, but the complexity in the acquisition operation increases. In this case, as the number of acquisitions varies in dependence on the latitude, it is not possible to acquire sequenced images with the technique described above. In the end, planning the acquisition times and creating the final mosaic can be more challenging.

Another factor to take into consideration is the orientation of the footprint of the cameras. Let us suppose to take images at a certain latitude every orbit and repeat the acquisitions all around the planet covering 360°: the images form a circle around the planet along the same parallel. Viewing from the top of the pole this figure is a polygon with a number of sides equal to the number of images (assuming an infinite number of acquisitions the polygon will match a perfect circle). Increasing the step between orbits, which means decreasing the number of images, makes two consecutive images to be less aligned. This can lead to difficulties in the matching process. This phenomenon becomes more relevant moving towards the poles. The following figure can help to grasp the problem: the blue and red parallelograms represent the HRIC footprint on ground, and the interval between the acquisition is equal to 5, 10, 15 orbits for figure (a), (b), (c) respectively. The overlapping percentage clearly decreases while augmenting the interval (more orbits) between the two acquisition, but it can also be noticed how the two images are less parallel (the blue and red sides are more aligned in figure (a) than in (c)).

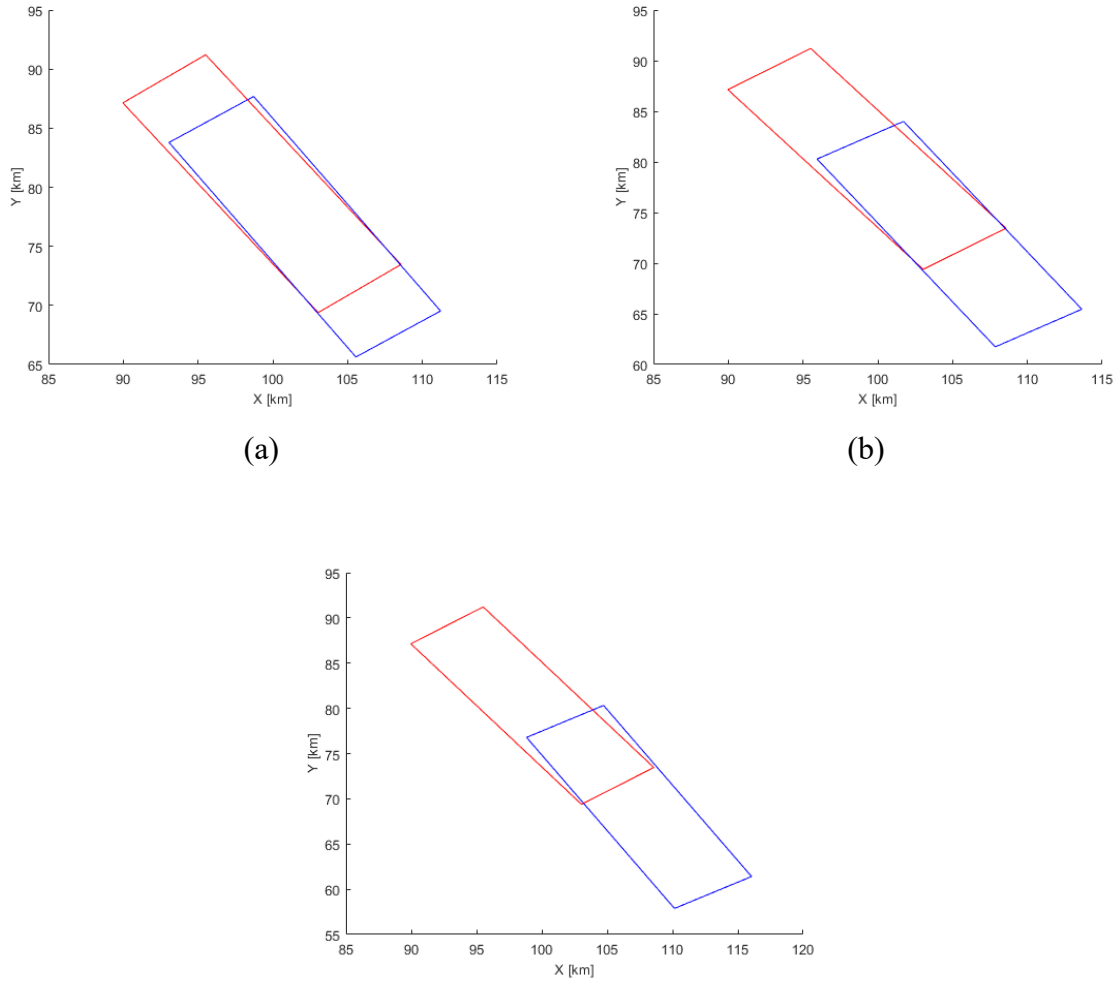

Fig 70 Footprint of two images, in red the first image and in blue the acquisition after 5 orbits (a), 10 orbits (b) and 15 orbits (c). The footprints are displayed in Cartesian coordinates x and y. It is notable how the two images are less aligned in the case c respect to the case a.

5.8.2 Along-track repetition time

While cross-track overlapping depends on the latitude and the sensor size, along-track overlapping depends only on repetition time. Strictly speaking, repetition time depends on the velocity of the spacecraft, that depends on its altitude and consequently on the latitude. On the other hand, the velocity of the spacecraft while flying the polar regions is almost constant, so

the repetition time can be considered practically independent from the latitude in a first approximation.

The panchromatic HRIC filter has a dimension of 2048 × 640 pixels and a FOV of 1,47 × 0,49 degrees. In the polar regions its footprint has an average size of 25,5 × 8,5 km^2 (again, this value depends on the latitude but can be assumed constant). Assuming for example a 20% of overlapping, in the sensor it corresponds to 262144 pixels, or an area of 2048 × 128 pixel. With a resolution on ground of around 10 m/px, the overlapping in the along-track direction corresponds to 1,3 km. The average velocity of the spacecraft is 2,55 km/s. The repetition time can be approximated to a conservative value of 2,5 s, obtaining an overlapping of 20% for consecutive along-track images.

The repetition time for SIMBIO-SYS has not been fixed yet and the 20% presented here is just a conservative assumption. A comparison can be made with the CaSSIS camera, which has characteristics very similar to STC, where the overlapping is 30 pixels width. With this assumption, the repetition time for HRIC images increases to 3,2 s using formula (17). Increasing the repetition time leads to the acquisition of a smaller number of images, with a consequent decrease in the data volume.

5.8.3 Data volume

In this section a rough estimation of the total number of images required to cover entirely the polar regions is calculated. The polar region considered is defined by all the area included from 83° to 90° of latitude.

The number of images of both HRIC and STC are calculated for both of the techniques described above, with a fixed step and a flexible step between orbits. The calculations are conservative and represent a worst case scenario, with an overlapping area probably higher than the one required.

5.8.3.1 Calculation with fixed orbital step

Here the number of images of HRIC and STC necessary to cover the polar regions are estimated. In this first approximation the orbital step between consecutive HRIC acquisition is assumed constant at every latitude inside the polar regions.

Supposing a fixed orbital step of four orbit, two HRIC images share a 20% of overlapping at 83° of latitude. With a conservative repetition time along-track of 2.5 seconds, five sequenced images are necessary to cover 1° of latitude. The number of acquisitions cross-track to cover all the circumference of the planet is 121. The total number of HRIC images necessary to cover the two poles results to be 8400.

The procedure to calculate the number of STC images necessary is the same as the one for HRIC, with the difference that the FOV of STC is bigger and consequently only 420 acquisitions are necessary.

If the image overlapping is limited to 30 pixels, 6562 HRIC images and 328 STC images are necessary.

5.8.3.2 Calculation with flexible orbital step

Here the number of HRIC and STC images necessary to cover the polar regions are calculated assuming a flexible orbital step between successive HRIC acquisitions.

The procedure for the estimation is the same described in the previous section but here the data are shown with tables to facilitate the explanation.

Latitude	Orbit step	Number of acquisitions
83	5	121
84	6	100
85	7	86
86	8	76
87	9	67
88	10	60
89	11	55
		TOT: 565

Tab 19 Number of HRIC acquisitions to cover one pole

Reminding that five images are necessary to cover 1° of latitude along-track, the total number of HRIC images necessary to cover the poles with this acquisition strategy is 5650.

For STC:

Latitude	Orbit step	Number of acquisitions
83	20	30
84	24	25
85	28	21
86	32	19
87	36	17
88	40	15
89	44	14
		TOT: 141

Tab 20 Number of STC acquisitions to cover one pole

Total number of STC images necessary to cover two poles is 242.

Assuming just 30 pixel of overlapping, the total number of images decreases to 3530 for HRIC and 190 for STC.

To better understand these numbers, it is useful to make some comparisons with the total number of images that will be acquired during the mission.

The total number of STC acquisitions during a single orbit (excluding the polar area) is estimated to be 370-518 images. Thus, the number of STC images necessary to cover the polar regions is similar to the number of acquisitions for every single orbits.

HRIC has to map 20% of the surface in high resolution, with a flexible pointed oriented strategy of image acquisition. The area covered by the two polar regions correspond to less than 1% of the total surface of Mercury. Because of the overlapping required to perform the mosaicking, the total images necessary to map the polar regions is increased. Even assuming a conservative average overlapping percentage of two images of 20%, the number of images necessary will increase, corresponding to a “virtual” 1,2% of the planetary surface, a value that is quite small if compared to the expected 20% (reminding that in the 20% of the total planetary surface the polar regions are included as well). In addition, for the polar regions a binning factor and a high compression factor can be applied, decreasing the total size of the data volume. It can be concluded that the data volume necessary to map the poles in stereo mode is significantly

smaller than to the total data volume of the entire mission. Moreover, it is important to remind that the polar regions are the most interesting areas from a scientific point of view so it is worth to reserve to them a considerable part of the total data volume.
Images are taken at 14 bits/pixel, so a single image of HRIC and STC has a size of 2,2 Mb and 0,6 Mb respectively. In the worst case scenario with 8400 HRIC images and 420 STC images the total data volume is around 19 Gb, a small value (around 2,5 %) compared to the total data volume expected for SIMBIO-SYS for the entire mission (750 Gb planned for the first year). The calculation here does not take into account binning or compression factor, that can reduce significantly the data volume.

5.9 HRIC and STC integration

The configuration described above makes use of images both of HRIC and STC for a stereo pair: STC will normally take images with an angle of 20°, but the second image of HRIC is nadir pointing [48]. In this way the convergence angle is smaller, nominally the half of two STC images. Consequently, the dimension of the baseline between the two images decreases as well.
This innovative configuration proves to be more effective for the exploration of the planet, in particular of the polar regions where it is easier to obtain a mosaic with HRIC.
Fig 71 shows a comparison of the DTM precision for the two configurations measured by the standard deviation of the distance of the DTM and the ground truth. This topic is covered with more details in chapter 6. The illumination condition is assumed to be the same inside the different HRIC images that compose the mosaics, so every strip of images is assumed to be acquired after one (or few in case of the poles) orbit so the illumination remains constant.
The tests are performed both at the North and South hemisphere and at the beginning and end of the mission, covering all the possible mission scenarios.
The following conclusions can be extrapolated:

1) The quality of the DTM is always better at the end of the mission respect to the beginning. This is explicable because the altitude of MPO decreases in time and consequently the resolution on ground increases.
2) The quality of the DTM is better in the South hemisphere respect to the North hemisphere. This is explainable because the altitude of MPO is lower at the South hemisphere respect to the North.

3) The hybrid configuration HRIC-STC generally produces better results.
4) The difference of DTM quality reconstruction with the two configuration is more evident in the North hemisphere. Probably this is due to the fact that the resolution in the North hemisphere is lower so that finding correspondence points between the two images is more challenging and the matching results more difficult. For this reason, the matching process produces better results for the HRIC-STC configuration where the difference of the two images of the stereo pair is lower.
5) In the North hemisphere there is a minimum in the STD value in the regions between 50° - 60° of latitude. This is expected because of the illumination conditions, that are more favorable for the reconstruction of DTM when the solar incidence angle is around 40° - 50°. This trend instead is not recognizable in the South hemisphere. This tendency can be explained by the higher resolution in the South hemisphere that compensate the lack of information due to the high incidence angles present near the equatorial regions of the planet.

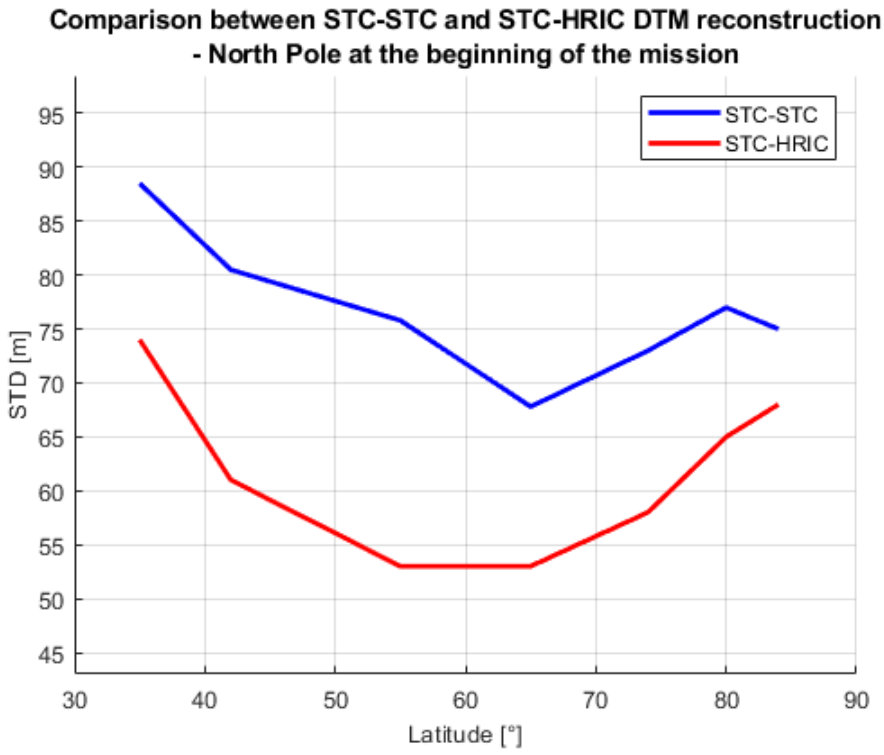

(a)

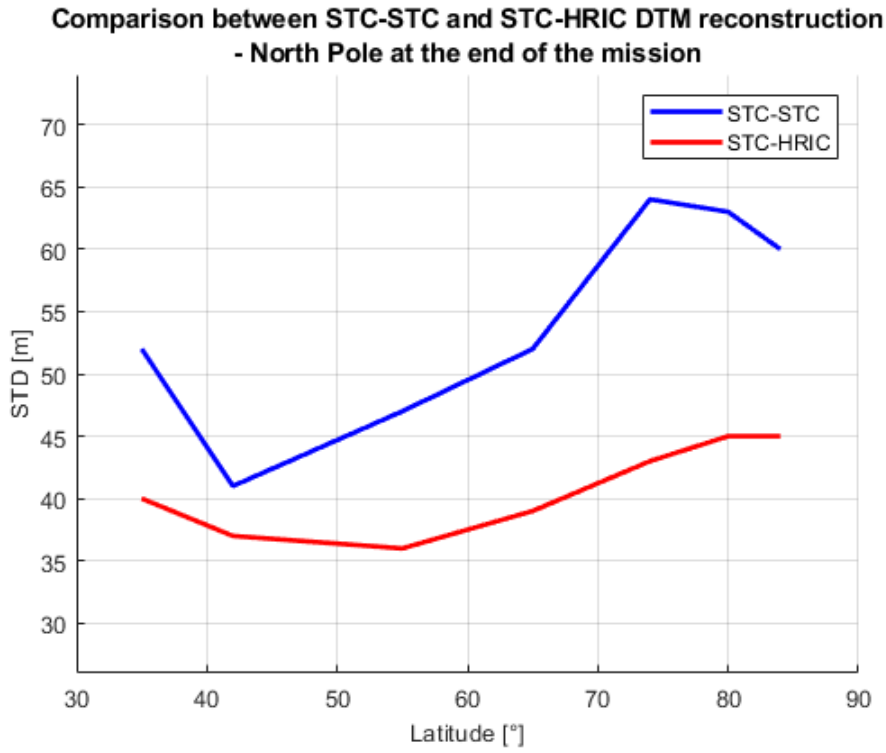
Comparison between STC-STC and STC-HRIC DTM reconstruction
- North Pole at the end of the mission
STC-STC
STC-HRIC
STD [m]
70
65
60
55
50
45
40
35
30
30
40
50
60
70
80
90
Latitude [°]

(b)

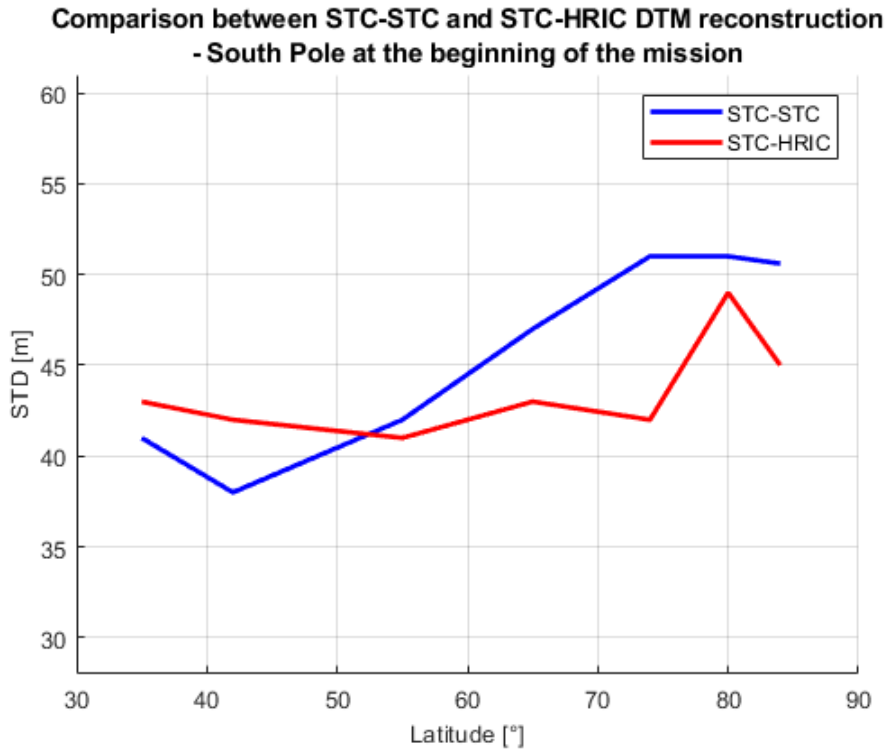
Comparison between STC-STC and STC-HRIC DTM reconstruction
- South Pole at the beginning of the mission
STC-STC
STC-HRIC
STD [m]
60
55
50
45
40
35
30
30
40
50
60
70
80
90
Latitude [°]

(c)

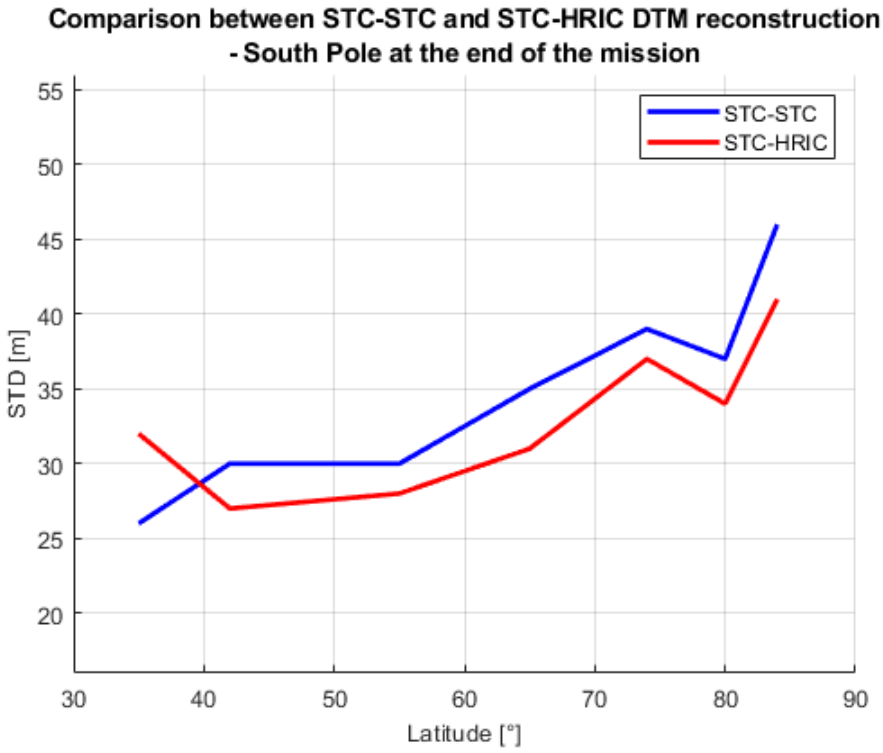

(d)

Fig 71 Comparison between STC and STC-HRIC DTM reconstruction

The estimation of the 3D reconstruction is therefore lightly better with the HRIC-STC configuration than the normal STC configuration. This conclusion is also proved by using the formula of the expected precision:

$$Vertical\ accuracy = \Delta p \frac{H}{B} \frac{H}{c} \frac{cos^2(FOV/2)}{cos^2(FOV/2 + e)} \tag{18}$$

In particular, the different inputs are: Δp the matching error measured in pixels, H the altitude of the acquisition, B the baseline, *c* the focal length of the camera, *e* the emission angle and FOV the field of view.

This formula calculates the expected vertical precision of a DTM derived from a given stereo pair, taking into account two different factors, the matching error and the geometric error. Here the matching error is assumed constant with a value of 0.2 px (rule of thumb) and only the geometric error is calculated. In this way, the impact of the change of the geometrical properties of the stereo pair obtained with the different configuration is evaluated. More details about the topic can be found in the next chapter.

The results are shown in the following graphs, where the expected precision is always better in the HRIC-STC configuration.

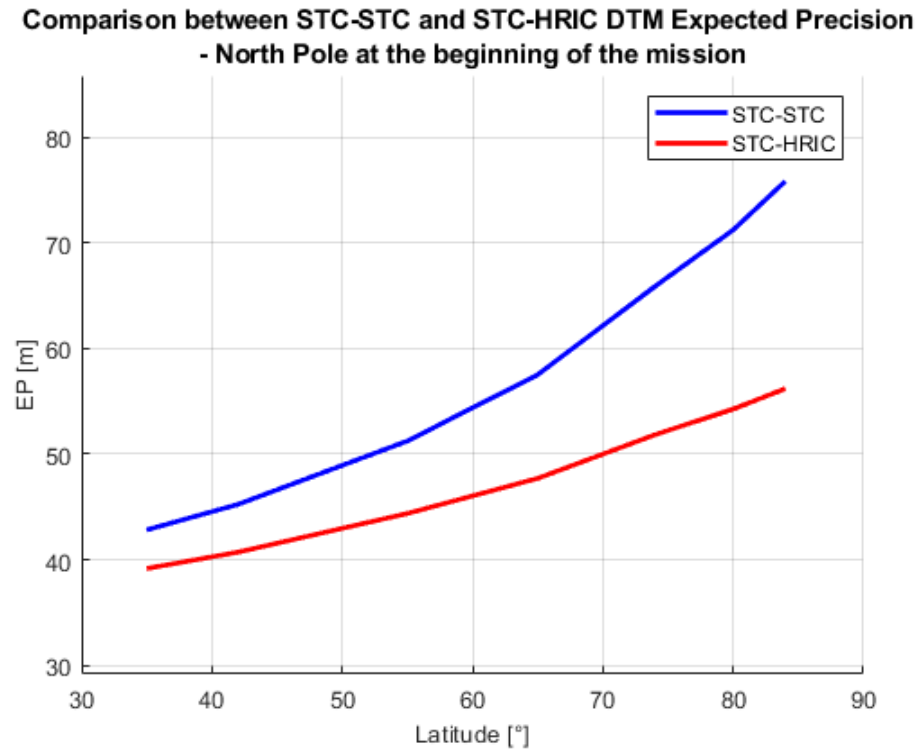
Comparison between STC-STC and STC-HRIC DTM Expected Precision
- North Pole at the beginning of the mission
STC-STC
STC-HRIC
EP [m]
Latitude [°]
30
40
50
60
70
80
90

(a)

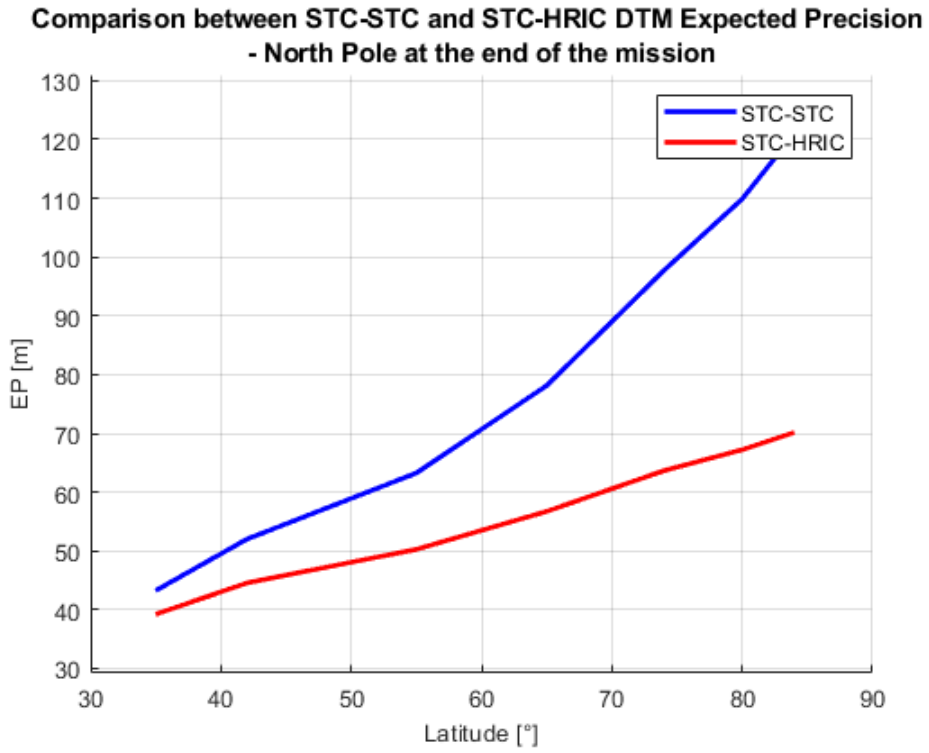
Comparison between STC-STC and STC-HRIC DTM Expected Precision
- North Pole at the end of the mission
STC-STC
STC-HRIC
EP [m]
Latitude [°]
30
40
50
60
70
80
90
100
110
120
130

(b)

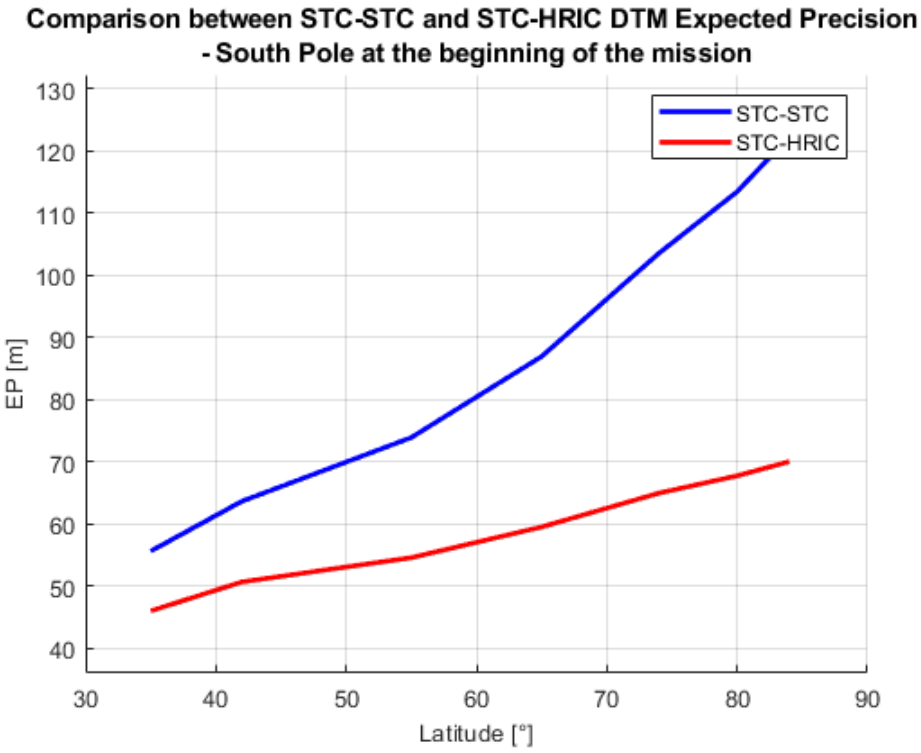

(c)

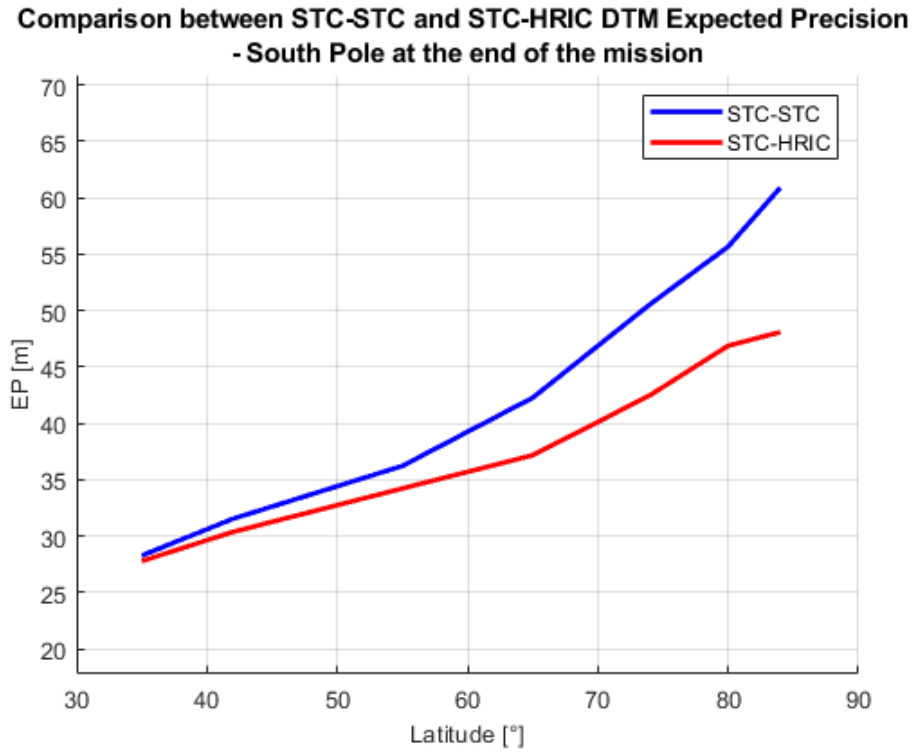

(d)

Fig 72 Comparison between the expected vertical precision of the STC-STC and HRIC-STC DTM reconstruction

In the creation of the stereo pair, it is suggested to utilize as master image the image acquired at lower altitude (higher resolution). In dependence of the mission scenario, for the STC-STC configuration it can one or the other of the images of the two channels of STC, while for the HRIC-STC configuration is always the HRIC image.
This observation strategy is only feasible thanks to the possibility for the different channels of SIMBIO-SYS to work together, increasing the quality of the scientific outputs.
In conclusion, it is suggested to adopt the HRIC-STC configuration proposed in this work for the 3D reconstruction of the polar regions, where the creation of HRIC mosaics is easier.
It has to be noticed that HRIC is required to operate in the nominal nadir configuration for this observation strategy, so the spacecraft has not to be rotated and can operate in the nominal mission conditions. Moreover, in the polar regions the swath between two consecutive orbits is small enough to always guarantee an overlap of the HRIC images, facilitating the production of mosaics.

5.9.1 Mosaic of HRIC images

One of the major upside of the SIMBIO-SYS package lays on the possibility to work with the different channels together. In this way, the data collected with one channel can be compared and eventually integrated with the data retrieved with another channel.
Images obtained with STC and HRIC can be successfully compared after small adjustments. The principal difference of two sets of images are the dimensions and the resolution on ground. The two panchromatic filters of HRIC and STC have different size and consequently produce different footprints on ground. The HRIC PAN is 2048 × 640 pixels and FOV 1,47 × 0,46 degrees. The STC PAN is 896 × 384 pixels and FOV 5,39 × 2,31 degrees. Therefore, STC PAN is approximately 3,6 times bigger than HRIC PAN in the horizontal dimension and 4,7 times in the vertical dimension. These values can be approximated to 4 × 5 times or 5 × 6 times when evaluating the number of HRIC images necessary to reach the size of a single STC image. Depending on the overlapping percentage, the number of HRIC images can increase.
An example of a HRIC mosaic can be seen in the following image.

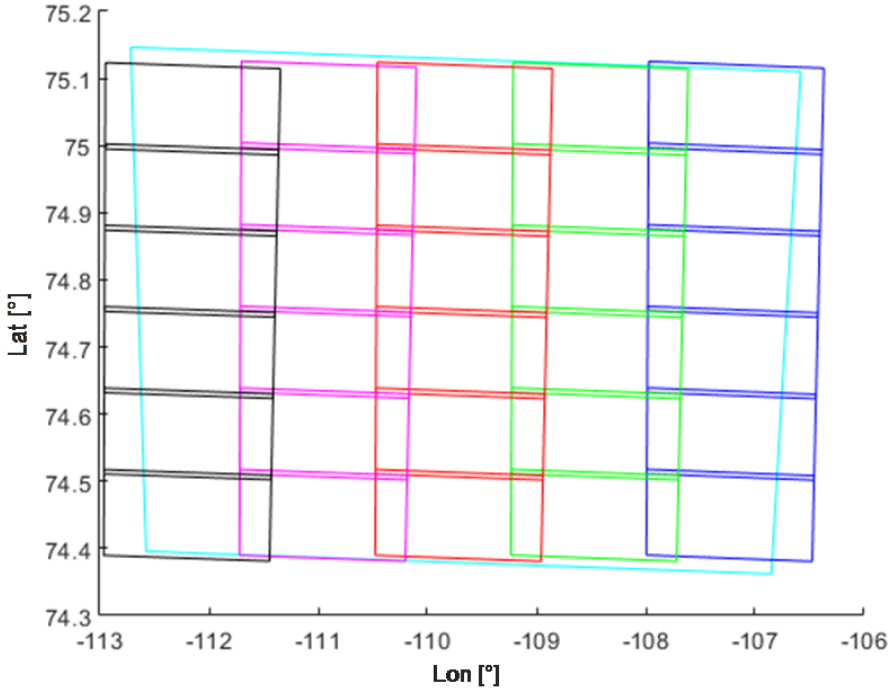

Fig 73 HRIC images mosaic. In cyan the footprint of a single acquisition of STC. In blue, green, red, magenta and black the sequence of images of HRIC. Repetition time = 2,4 s; HRIC acquisition every orbit. In this example 30 images of HRIC are necessary to mostly cover the area of a single STC image

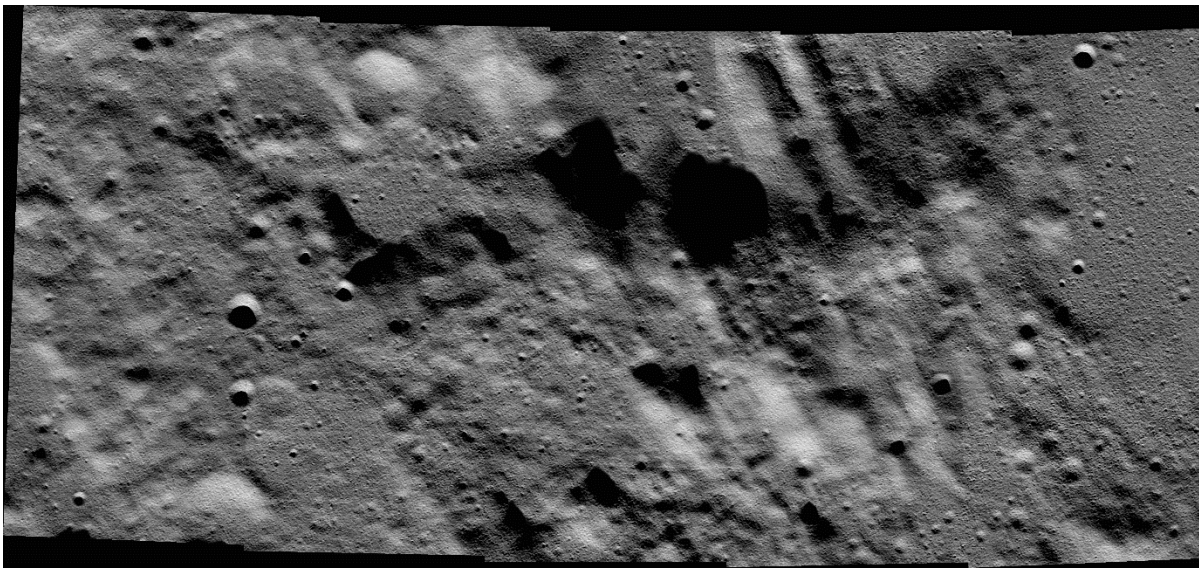

(a)

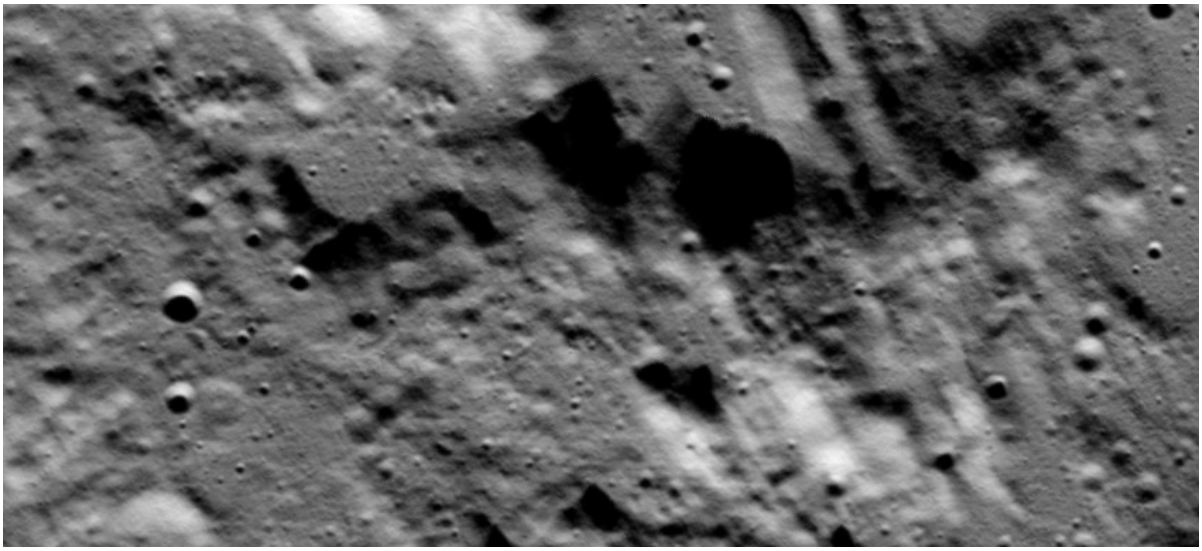

(b)

Fig 74 a) mosaic of 30 HRIC images to approximately cover an area of one STC image b) the STC image for the equivalent area. It is important to notice that the mosaic presents more details as the resolution is higher

The mosaic obtained from the HRIC images is formed by a high number of pixels per row and column, roughly equal to the sum of the pixels of all the images that compose it. Calling R the number of rows of images and C the number of columns of images and without considering the image overlapping, a mosaic is composed by 640 × R and 2048 × C pixels.

The following figure shows the footprints of the HRIC images used to retrieve the mosaic in Fig 74.

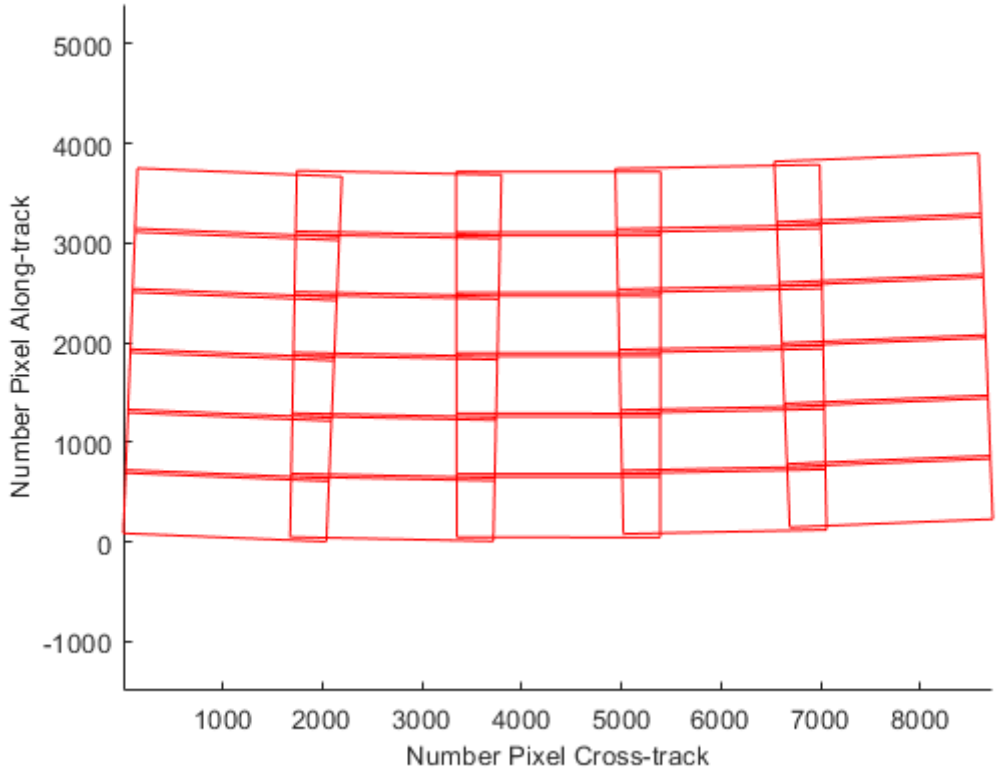

Fig 75 Footprints of 30 HRIC images that compose a mosaic and the corresponding cross-track and along-track dimensions in pixels

In order to obtain an image with pixel size comparable to the pixel size of a STC image the mosaic must be resampled. There are two ways to obtain a resampling: applying a binning factor while acquiring images with HRIC (preprocessing) or resampling the mosaic obtained post processing. Operating post processing is easier because there is no intrinsic limit in the resampling factor, while instead the binning factor is limited to 4 or 16. Thus, the mosaic is processed reducing the number of pixel and increasing their size at the same time. The result is an image with size and resolution comparable to the STC images. After the resampling, a greater number of details is present in the mosaic respect to the equivalent STC image, as the higher HRIC resolution allows to capture details that are not captured by STC. Thus, even after the resampling, the additional details are still visible (see Fig 74).

In any case, it is possible to acquire the HRIC images using a binning factor and later resampling the mosaic post processing. In this way the data volume is reduced.

A new projection matrix is calculated and associated to every mosaic. The intrinsic parameters of the new projection matrix are calculated using the number of pixel after the resampling and the equivalent focal length calculated knowing the altitude of the observation. The extrinsic parameters are calculated using as position of the camera and direction of pointing the average of the positions of the cameras and the average directions of pointings of the various images that compose the mosaic.

5.9.2 3D reconstruction performances

STC is the stereo channel of SIMBIO-SYS specifically designed to obtain DTMs from the planetary surface. It is formed by two channels inclined by ± 20°. This angle is called stereo angle and is fixed as it is part of the geometry of the channels of the camera. While the spacecraft is moving in its orbit, the forward channel takes an image of a certain area on the surface, then the backward channel takes a second image of the same area from a different perspective. These two images form a stereo pair useful to crate DTMs.

Because of the elliptical MPO orbit, the convergence angle of the stereo pair (that depends both on the geometry of the two channels but also on the latitude) varies along the orbit. The convergence angle (or intersection angle) is defined as the sum of the two emission angles of the two channels while pointing at the same target. The emission angle is the angle defined as the effective pointing direction of the boresight of the channel, and corresponds to the stereo angle (fixed) plus a variable part that depends on the position of the spacecraft in the orbit.

The convergence angle of the two channels of STC is shown in Fig 77: image (a) represents the two boresights of STC from orbit while pointing on ground, image (b) quantifies the convergence angle.

The convergence angle affects the matching performance of the two images, because for a higher value corresponds a larger baseline. As shown in the graphs, the accuracy on ground of this configuration decreases moving towards the polar regions [49].

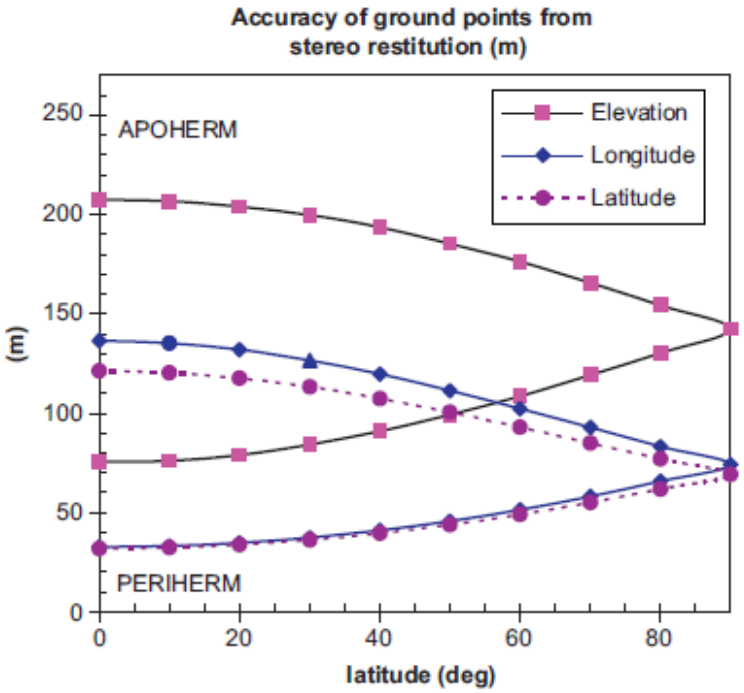

Fig 76 Expected accuracy of the ground point in function of the latitude. The lowest three lines refer to the Periherm, the highest three lines to the Apoherm. The Periherm, corresponding to the High Resolution phase, should be the case to be considered. It is notable how the accuracy decreases moving towards the poles

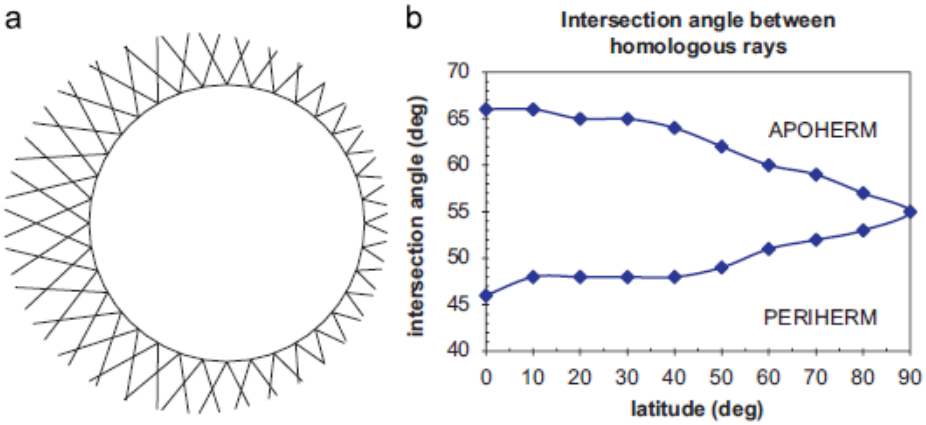

Fig 77 (a) representation of the intersection rays of the two channels of STC from orbit, (b) intersection angle of the two channels of STC in function of the latitude. Even if the stereo angle of STC is fixed at 20°, the interception angle is dependent on the altitude of the spacecraft

While matching the two images for the creation of the stereo pair, it is suggested to use the image acquired at lower altitude (higher resolution) as the master image. In dependence of the mission scenario, it can be either the image acquired with the L or H channel. Following this procedure will increase the quality of DTM reconstructed. This factor is more evident near the Poles where the change of MPO elevation is more evident.

In conclusion, the configuration of STC is optimized for the equatorial regions, while it has a worse performance in the polar regions. This is due to high convergence angles (and large baselines) between rays of the two channels, increasing the difficulty in the matching process as the target is visible from very different perspectives.

5.9.3 Different resolution

HRIC and STC have different resolution on ground, with HRIC that has a resolution around 10 times better than STC. Maintaining this difference in the resolution of the data retrieved with the two cameras is not necessary while matching images. In addition, higher resolution images require a higher data volume, and mapping the whole polar region in high resolution can be prohibitive.

To avoid these problems, HRIC samples should be taken with a lower resolution. This can be achieved increasing the binning factor while imaging. Binnig consists in combining a cluster of pixel in a single pixel while acquiring one image. This procedure is used to increase the signal to noise ratio, defined as the ration of the strength of an electrical signal carry information respect to the unwanted disturbance. While binning, the SNR increases (positive outcome) but the resolution decreases (normally negative outcome, but in this case is positive) and consequently also the data volume. HRIC can acquire images with a binning factor of 4 (2 × 2) and 16 (4 × 4).

HRIC can work in different operative mode, applying different binning and compression factors.

An optimized combination of these two factors can be chosen to be applied to HRIC images, in order to increase the matching performance with STC images and decrease the total data volume. A post processing operation is still suggested to homogenize the data from HRIC and STC.

Chapter 6: DTM Evaluation and specific applications

In this chapter the evaluation of the quality of the HRIC DTMs and a comparison of the results are presented. The quality of the results depends on different factors: illumination conditions, stereo angles, length of the baseline and altitude of the spacecraft. Taking into account these factors, an optimal acquisition condition is extrapolated.
An error budget is computed: this error affects every acquisition and depends on the knowledge of the position and orientation of the spacecraft and pointing error of SIMBIO-SYS.
The libration phenomenon is examined and is correlated with the use of DTMs, that can improve the precision of the experiment deigned to calculate the libration amplitude.
In addition, some examples of applications which use DTMs are given, as for example the co-registration with the instrument BELA.

6.1 Result comparison

The objective of the image simulation and the consequent 3D models creation is to acquire information for planning stereo acquisitions with SIMBIO-SYS, with particular focus on HRIC. Hereafter, only DTMs created from HRIC stereo pairs are examined: these high resolution DTMs have higher resolution (around 10 times better) with respect to the standard DTMs with STC (or the HRIC-STC configuration previously described, which resolution is only slightly better than the STC-STC configuration).
The evaluation of the results is made by comparing the DTMs obtained with the original mesh from which the images were taken. The software CloudCompare was used for this purpose [50]. The original mesh is used as ground truth and the resulting 3D model is superimposed on it.
The following figure shows the comparison of a DTM (colored area) with its original ground truth (gray area). The different colors represent the STD of the difference between the two models.

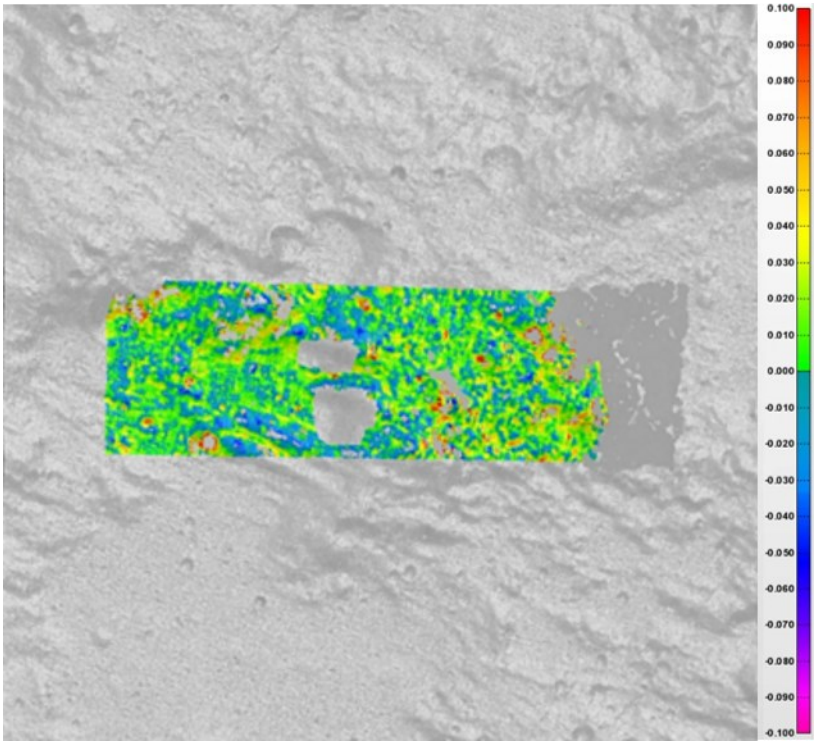

Fig 78 DTM quality evaluation in STD

The quality of the DTM is measured by the mean distance (MD) and the standard deviation (STD) of the distance of the points of the two models.

$$STD = \sqrt{\sum_{i=1}^{n} \frac{\left(DTM_{ref} - DTM\right)^2}{N}} \tag{19}$$

$$MD = \left[n^{-1} \sum_{i=-1}^{n} \left(DTM_{ref} - DTM\right) \right] \tag{20}$$

In most of the triangulated models it happens that some points are positioned far away from the surface: these points are outliers and are cut off, so they will not affect negatively the standard deviation calculation. Consequently, the resulting model after the outliers' removal is formed by a smaller number of points and the ratio between the number of points after and before the cuts can be used to evaluate the quality of the result.

A theoretical vertical accuracy of a DTM can be calculated in a first approximation with the formula [51]:

$$Vertical\ accuracy = \Delta p \frac{H}{B} \frac{H}{c} \frac{cos^2(FOV/2)}{cos^2(FOV/2+e)} \tag{18}$$

Where Δp is the RMS stereo matching error in pixel units (0.2 pixel often used as a rule of thumb) and depends on the illumination conditions and the difference in the perspective of the stereo pair, H is the height of the center of perspective, B is the baseline of the stereo block, *c* is the focal length, FOV is the field of view of the camera and *e* the emission angle (or the sum of the emission angles of the two acquisitions). It is clear that the vertical accuracy depends on two factors: a matching factor (Δp) and a geometric factor (H and B, that are correlated together). While increasing the baseline B seems always a good idea, in reality it will affect negatively the matching factor because decreases its precision: for this reason, a tradeoff between these two aspects should be chosen. This is the reason while the HRIC-STC configuration proved to be more efficient than the normal STC configuration in most cases: the two images are acquired with more similar perspective and this enables a better matching even if the baseline of the stereo pair is reduced.

For the creation of high resolution DTMs, a set of different HRIC images under different acquisition conditions has been simulated. Different factors influence the acquisition conditions, in particular:

1) The incidence angle.
2) The convergence angle.
3) The baseline.
4) The altitude of the spacecraft.

The incidence angle depends on two factors: the latitude of the targets and the True Anomaly of Mercury. The rays of the Sun are more perpendicular to the surface of the planet near the equator, and become more inclined moving towards the two poles. At the same time, rays are more perpendicular when the planet is close to the Perihelion (TA = 0°) and Aphelion (TA = 180°) and become more inclined in intermediate positions.

The acquisition of one set of HRIC images is simulated along the same orbit, while MPO is moving toward the north pole. In this way the position of the planet is fixed and the change of illumination is due only by the change of the latitude of the target.

At the same time, moving toward the pole, the altitude of the spacecraft increases and consequently the resolution on ground diminishes.

The convergence angle corresponds to the sum of the two angles of the boresights of the two cameras while pointing at the surface. Its change is simulated in two ways: in the first way, one camera is assumed fixed in a nadir position (the nominal attitude of MPO) while the second is inclined at different angles (MPO is assumed to rotate); in the second way both cameras are inclined (MPO is assumed to rotate in both cases). MPO is assumed to rotate around its y axis,

moving its pointing along the along-track direction. Images simulated in these two ways differ for the different perspective, as in the first case the master image is maintained the same while only the slave is changing, whereas in the second chase both are changing.

The baseline is the distance between the two cameras of a stereo couple. Increasing the convergence angle means increasing also the baseline.

The last factor that influence the DTM quality is the altitude of the spacecraft that increases always moving towards the poles, independently from the position of Mercury around the Sun and the convergence angles. In reality, the altitude of the spacecraft respect to the same coordinates on the surface changes in time as the orbit of MPO changes in time, but this aspect does not influence deeply the comparisons performed here.

The following considerations concerning the incidence angles can be extrapolated from the results:

- Minimum incidence angle. The minimum incidence angle to obtain acceptable results can be identified around 20°. At inferior angle the shadows are practically absent and the images are uniformly bright. The matching process between the two images is not able to identify the features, and the result is a very noisy point cloud. Low incidence angles characterize the areas near the equator, where the rays of the Sun hit the surface almost perpendicularly.
- Maximum incidence angle. While the precision of the reconstruction of the 3D model decreases for high incidence angles, there is not a clear upper bound that limits drastically the performance. On the other hand, it is notable that for high incidence angles (e.g. > 80) the shadows are long and the interior of the craters can be completely black: in this case this portion of the surface cannot be reconstructed in the 3D model, as it is impossible to find recognizable features, and the model presents some holes. In any case, the reconstruction of the areas outside the holes has a precision comparable to the one obtained at lower incidence angles.
- Optimum angle. The incidence angle that gives better results in the reconstruction of the 3D model can be identified around 40°-50°. This value is reached for latitude around 40°-50°, but also in the equatorial area, when the planet is in a favorable position. The example in Fig 79 helps to clarify this aspect. The two series of images (position (a) and position (b)) were taken at the same position on the surface of the planet, Latitude = -2° and Longitude = -40°, but in different moments. In position (a), Mercury is close to the Aphelion (True Anomaly = 157°) and the rays arrive more perpendicular to the surface

(solar incidence = 22°), while in (b) the planet is distant from the Aphelion (True Anomaly = 244°) and the rays arrive more inclined (solar incidence = 64°).
Now it is clear that a good mission planning can optimize the acquisition time for every target, selecting the best illumination conditions for better outcomes.

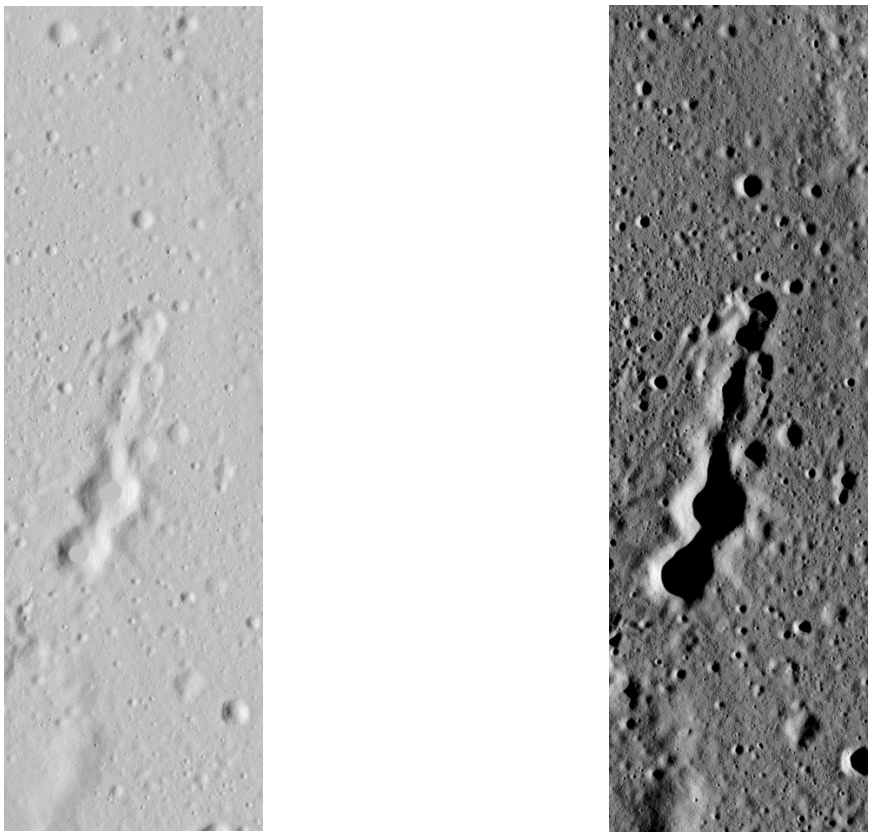

(a) (b)

Fig 79 Two acquisitions taken in the same place on the surface but at different times. (a): TA = 157°, incidence angle = 22°; (b): TA = 244°, incidence angle = 64°.

The second factor that influences the quality of the 3D model is the convergence angle between the acquired images. This angle corresponds to the rotation applied on MPO to obtain an off-pointing configuration. The tests were performed with different convergence angles, nominally 5°, 7°, 10°, 15° and 20° divided in two categories: in the first set one angle is maintained 0° as the nominal nadir pointing and the other is changed; in the second set both are changed. The two couples of stereo angles are then the following: 0°/5°, 0°/7°, 0°/10°, 0°/15°, 0°/20° for the

first set and 2°/-2°, 2°/-5°, 5°/-5°, 7°/-7°, 10°/-10° for the second set. The sign of the angle represents the direction of the rotation of the spacecraft: the pointing on ground is changed in the along-track direction, so a positive or negative rotation discriminates whereas the pointing is moved forward respect to nadir or backward. The situation described is symmetric in the along-track direction.

The two sets of angles differ for the perspective of the target. Considering the couple nadir-inclined, one of the image remains always the same and only the other one is acquired with a different perspective. On the contrary, in the other case with both images inclined, the perspective on the target is changed in both images.

The simulated stereo couples are always obtained in the along-track direction for the sake of simplicity. In the real scenario, the stereo pair can be acquired in two different ways: in-orbit and inter-orbit. For the in-orbit stereo observations the sequence is the following: 1) ahead pointing in along-track; 2) nadir pointing; 3) backwards pointing in along-track. Inter-orbit stereo observations are performed from subsequent MPO orbits with the sequence: 1) cross-track pointing at orbit 1; 2) nadir pointing at orbit 2; and 3) cross-track pointing at orbit 3, where the rotations 1) and 3) have opposite signs and point towards the nadir pointing of orbit 2.

The convergence angle in-orbit depends only on the rotation applied to MPO while the angle inter-orbit depends on the cross-track distance between the different orbits.

The following graph shows the cross-track angle between two consecutive orbits in dependence of the latitude and consequently on the altitude of the spacecraft: the angle represents the rotation that must be imposed to MPO to point at the same target of the following (previous) orbit. It is clear that the stereo angle is dependent on the geometry of the acquisition and cannot modulated at will. On the other hand, it is possible to perform the acquisitions after (before) more than one orbit, in this way summing (or multiplying) the value of the cross-track angle. For example, at a latitude of 20°, the angle cross-track is 3,5° after one orbit, 7° after two orbits, 10,5° after three orbits and so on.

The graph is calculated at the beginning of the mission and the values slightly change during the mission because of the change of the MPO orbit in time.

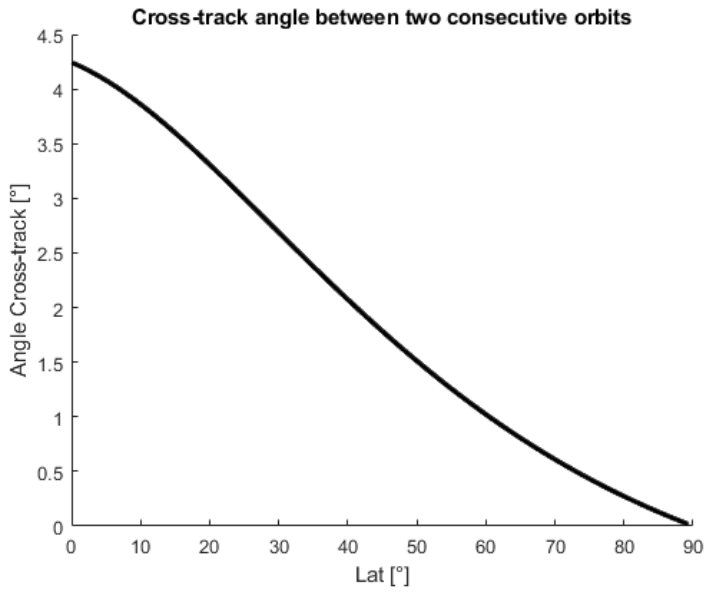

Fig 80 Cross-track angle between two consecutive orbits

The results prove that the best performances are obtained with convergence angles around 10°, with a clear deterioration for smaller and higher angles.

Comparing the outcomes obtained in the nadir-inclined and inclined-inclined cases, the inclined-inclined case results more effective in most of the cases. Taking in mind that every off-pointing must be carefully planned and that most of the time the two results are very similar, it is suggested to adopt the configuration that better suits with the mission's constraints.

The baseline is always coupled with the convergence angle, as it is impossible to have small convergence angles with large baselines and vice versa. The same considerations made for the convergence angle are valid for the baseline as well.

The last factor that influences the 3D reconstruction is the resolution on ground. As the resolution on ground is linked to the orbit of the spacecraft, this factor cannot be modulated at will, but follows the constrains of the geometry of the mission. Images taken with better resolution are more detailed and consequently the DTM could be generally more detailed. On the other hand, the other factors like illumination and convergence angle are more influent in the precision of the creation of the DTM.

The following graphs show the precision of the HRIC DTMs in dependence of the convergence angle and the illumination conditions. For every position on the planet two sets of data are displayed: one represents the nadir-inclined configuration (in blue, called nadir for simplicity) and the other the inclined-inclined configuration (in red, called inclined for simplicity).

During the different simulations it can happen that some points are missing: in these cases, the point cloud obtained after the triangulation was affected by some errors, e.g. it was too noisy to compare to the ground truth, thus the result is not representative of the real situation. But even with the gaps, a general trend in the reconstruction performance can be noticed.

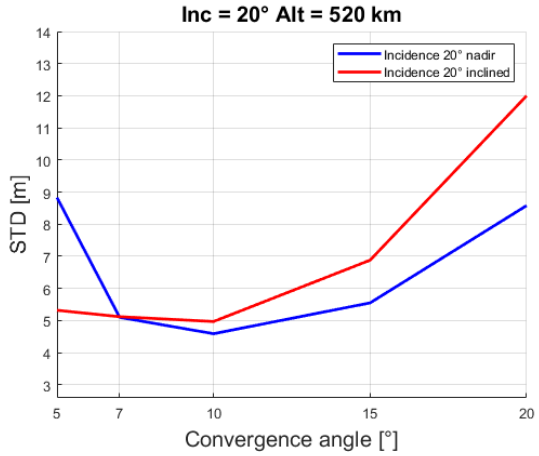

(a)

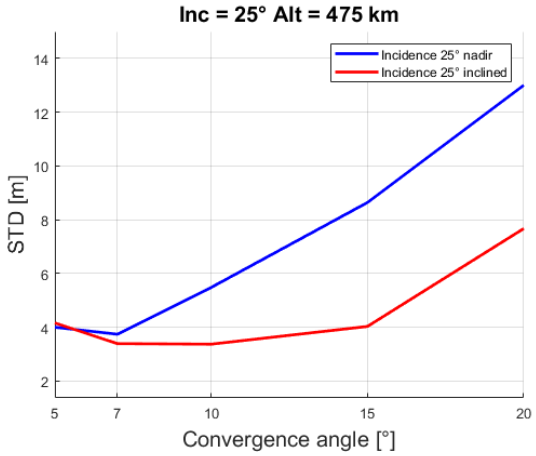

(b)

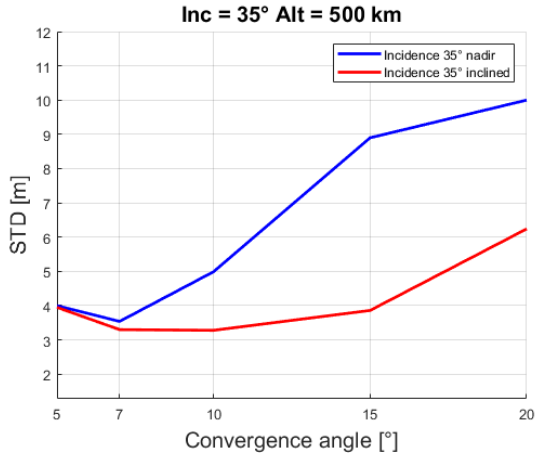

(c)

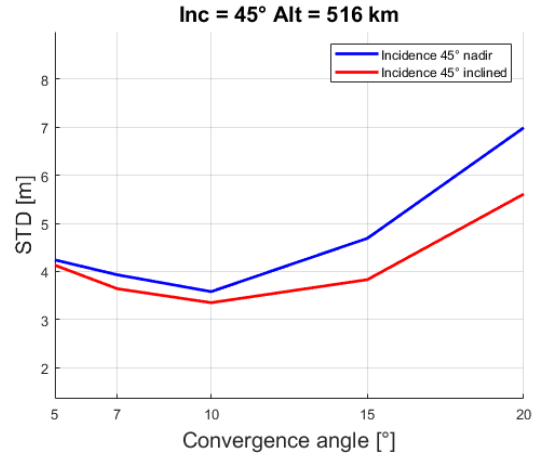

(d)

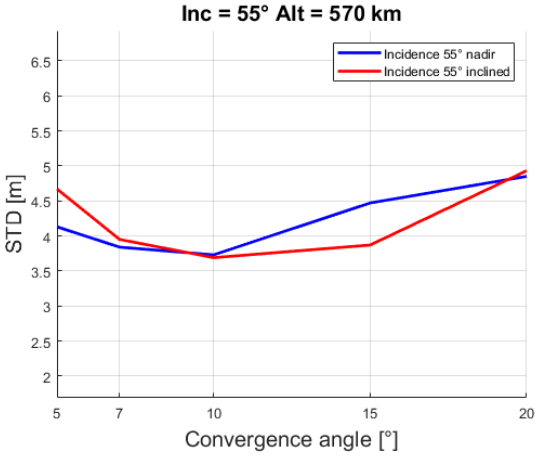

(e)

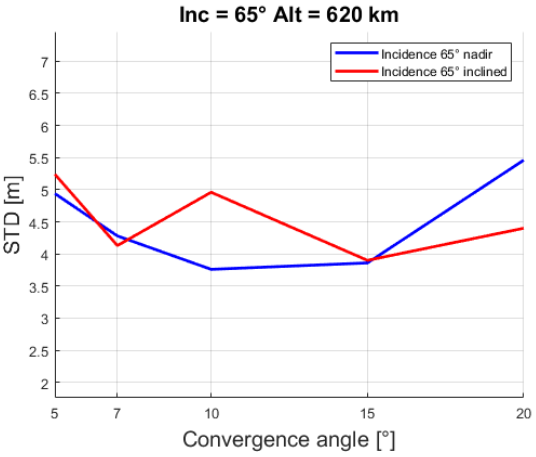

(f)

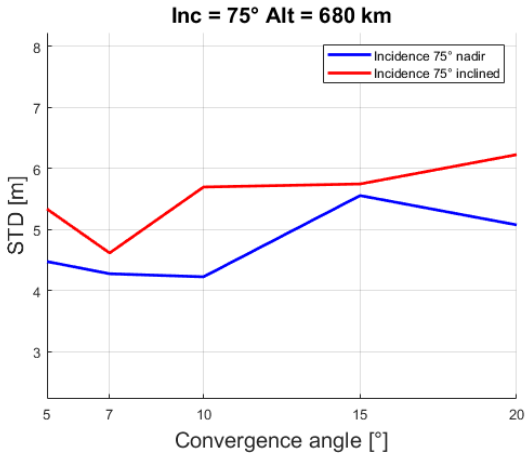
Inc = 75° Alt = 680 km
Incidence 75° nadir
Incidence 75° inclined
STD [m]
Convergence angle [°]

(g)

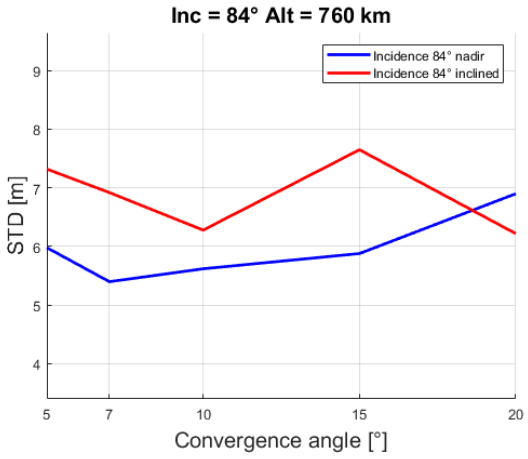
Inc = 84° Alt = 760 km
Incidence 84° nadir
Incidence 84° inclined
STD [m]
Convergence angle [°]

(h)

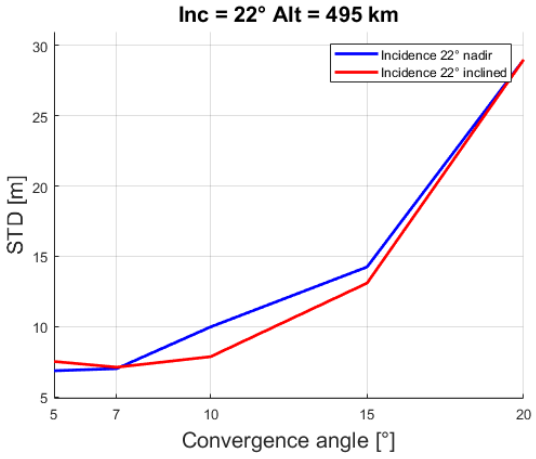
Inc = 22° Alt = 495 km
Incidence 22° nadir
Incidence 22° inclined
STD [m]
Convergence angle [°]

(i)

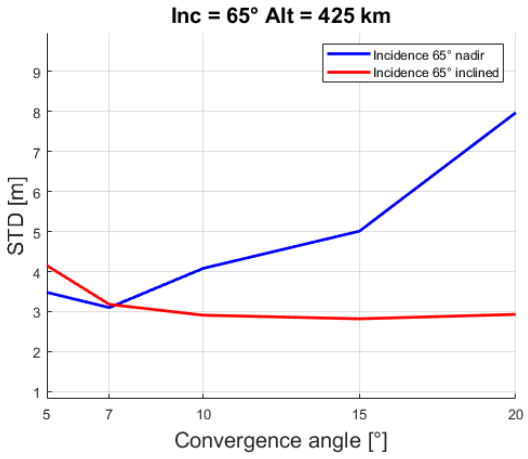
Inc = 65° Alt = 425 km
Incidence 65° nadir
Incidence 65° inclined
STD [m]
Convergence angle [°]

(j)

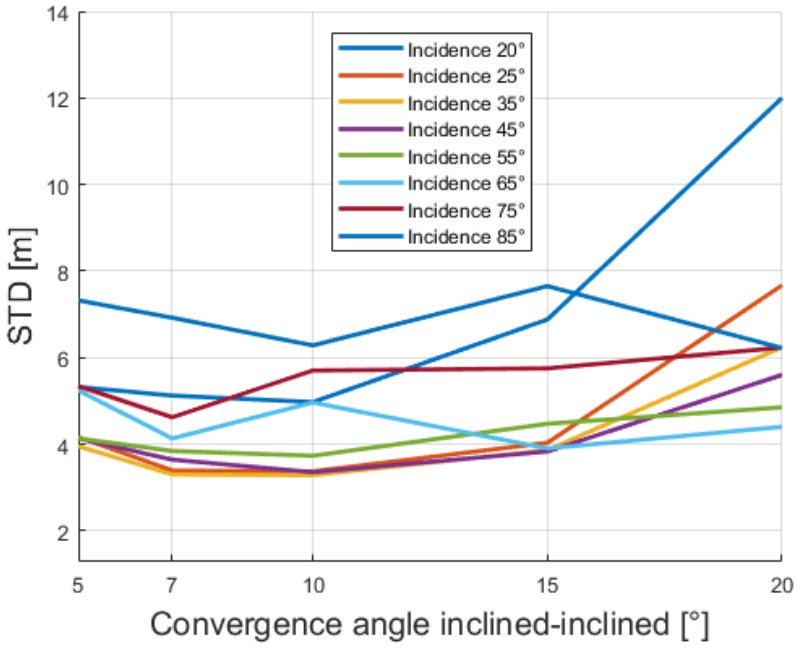
Incidence 20°
Incidence 25°
Incidence 35°
Incidence 45°
Incidence 55°
Incidence 65°
Incidence 75°
Incidence 85°
STD [m]
Convergence angle inclined-inclined [°]

(k)

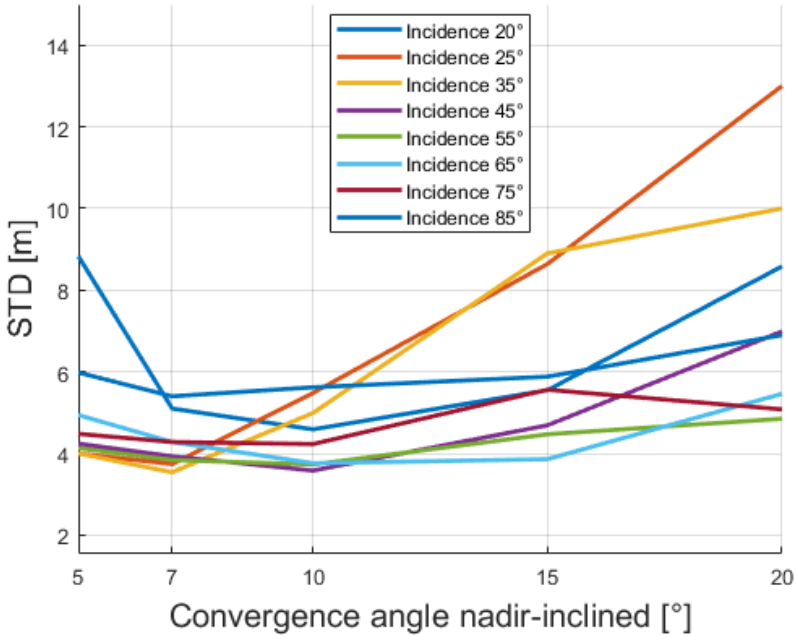

(l)

Fig 81 DTM comparison

The set of images from (a) to (h) was simulated along the same orbit near the Aphelion: in this way the value of the incidence angle is equal to latitude where the image was taken, such as images with 20° of incidence angle were taken at 20° of latitude, images with 25° of incidence angle were taken at 25° of latitude and so on. The graphs of the position (i) and (j) instead correspond to position on different orbits at different TA, nominally the position described in Fig 79. In this case, even if the position on the planet is the same, the illumination conditions are different.

The last two graphs (k) and (l) compare the different situations, where in (k) the stereo pair is obtained from two images with inclined perspectives and in (l) from one image nadir and one inclined.

6.2 Limitations in the simulation

Rendered images prove to be an efficient solution to simulate acquisition planning, stereo pairs and DTMs. On the other hand, it is important to remind that these images are synthetic and have clear differences if compared to real images.

SurRender is capable of simulating the albedo by means of a customized BRDF function, using in particular the Hapke model.
On the other hand, the material of the target rendered with the simulation is homogeneous, so the albedo is constant in every point, while in the real situation it would change in dependence of the material present on the surface. Noises and other errors related to the sensor (e.g. dark current, operative temperature, pixel non-uniformity…) cannot be simulated as well. In addition, the targets simulated are portions of the surface of the Moon or Mars, so they are not strictly representative for Mercury.
Thus the simulation can only accurately reproduce the geometry of the acquisition, meaning the relative position of the camera, of the spacecraft and of the illumination source.
For these reasons, the results in terms of accuracy in the reproduction of the DTM must not be taken as representative for the real future scientific output.
On the other hand, the results of the different simulations are consistent as the procedure, the assumptions and the simplifications are always maintained through all the process. As a result, a coherent acquisition planning can be foreseen.
In conclusion, with this simulation is it possible to compare the quality of the results under the different acquisition conditions. Thus, if for example a DTM has a better quality with a specific illumination condition, it can be assumed that the real DTM will still have a better quality under that specific illumination condition.

6.3 Error budget

This section describes the principal errors that influence the pointing performances of SIMBIO-SYS. An error is always present for every acquisition, and influences both the image acquisition and the consequent DTM creation. Due to the lack of available information, some of the contributions are only briefly described without entering in the details of the procedures used for the evaluation.
The major error contributions are the following:

- Satellite position error
- Satellite attitude error
- Camera attitude error
- Image correlation error

The errors described in this section are not simulated to obtain the results presented so far: in this way, the results present the ideal case. On the other hand, when the real images will be acquired, every data will be affected by an error which magnitude depends on timing of the acquisition.

6.3.1 Position of the spacecraft respect to Mercury

The position of the spacecraft is defined respect to an inertial frame centered in Mercury and the satellite error position is due to the shift of the center of mass of the spacecraft respect to the expected position [52]. The position of MPO is tracked with the MORE radio-science experiment [53]. The knowledge in the position of the spacecraft is estimated within 10 m. Defined the radial component in the direction perpendicular to the surface, the radial error can be neglected while compared to the altitude of the spacecraft. Errors in the knowledge of the position of the spacecraft in the along-track and cross-track directions correspond to the same displacement on ground in the along-track and cross-track directions, independently to the spacecraft's altitude. Thus, every point of an image fell inside a circle of un certainty with ray of 10 meters.

6.3.2 Orientation of the spacecraft

The orientation of the spacecraft measures the angular separation achievable with the attitude control system between the desired configuration of the spacecraft and the actual one.
The orientation is measured with star trackers onboard MPO, and the misaligned between the spacecraft and the celestial reference frame is of the order of 2.5 arcsec.
The attitude control of MPO is achieved with a combination of reaction wheels and thrusters.

6.3.3 Attitude of the camera and thermo-elastic effects

There are different parameters to define the measurement of the pointing error of a generic instrument. The two most important terms are:
1) AME (Absolute Measurement Error): difference between the actual parameter (attitude, geolocation, etc.) and the known (measured or estimated) parameter in a specified reference frame.

2) APE (Absolute Performance Error): difference between the target (commanded) parameter (attitude, geolocation, etc.) and the actual parameter in a specified reference frame.

Fig 82 can be useful to clarify the two terms.

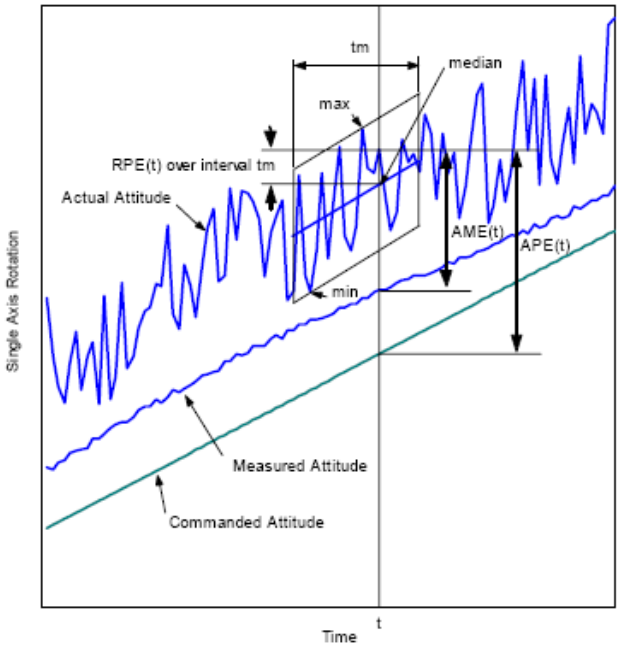

Fig 82 AME and APE

For what concerns the pointing of the camera, only AME is taken into account.
Normal contributions to the AME budget are the following:

1) Ground to orbit effects
2) Attitude estimation performance
3) Thermo-elastic effects
4) Residual calibration effects

The ground to orbit effects are caused by the change of the parameters of the camera (focal length, position of the lenses, distortions…) due to the solicitations occurred during the launch of the spacecraft.
The attitude determination performance depends on the knowledge of the position of the spacecraft. In this term two contributions are present: the knowledge of the position of the spacecraft respect to the target and the instantaneous attitude of the spacecraft respect to an absolute frame that describes its orientation.

The thermo-elastic effects are present because the camera is facing the surface of Mercury that has a high temperature (up to 700 K in the dayside) that can deform the optics. As the altitude and position of the spacecraft varies in time, this contribution is not constant but changes as well.

The residual calibration effects represent the ground to orbit effects after that an in-flight calibration of the instrument is performed.

The boresight of a camera indicates the direction that the instrument is pointing, and the attitude error represents the misalignment of the camera with respect to the expected nadir pointing.

This term is actually a sum of different terms: the direction of the camera itself, the relative position of the camera respect to the spacecraft and the thermo-elastic contributions that can change both of the previous parameters described. As previously mentioned, the thermo-elastic effects depend on the position of the spacecraft so it can be useful to quantify this value for different cases.

In the document [52] the pointing error of the boresight of HRIC and STC is defined. These data are simulated after performing multiple in-flight calibrations with the purpose of decreasing the pointing error, resulting in a very accurate precision.

The next tables summarize the best and worst-case scenarios achievable for HRIC and STC. The positions are calculated with respect to the true anomaly of Mercury. The AME nominal requirement is 5'' for HRIC and 10'' for STC.

Configuration	Perihelion		45°		Spring/ Autumn	135°		Aphelion	
	Hot	Cold	Hot	Cold		Hot	Cold	Hot	Cold
Best-case	4.7''	2.1''	2.6''	2.1''	2.1''	2.7''	2.1''	4.1''	2.1''
Worst-case	8''	5.5''	6''	5.5''	5.5''	6.1''	5.5''	7.4''	5.5''

Tab 21 Total AME for HRIC

Configuration	Perihelion		45°		Spring/ Autumn	135°		Aphelion	
	Hot	Cold	Hot	Cold		Hot	Cold	Hot	Cold
Best-case	5.2''	2.5''	3''	2.5''	2.5''	3.2''	2.5''	4.6''	2.5''
Worst-case	11.9''	9.3''	9.8''	9.3''	9.3''	9.9''	9.3''	11.2''	9.3''

Tab 22 Total AME for STC

No thermal model for the prediction of the deformation is used in this calculation. Clearly, adding a thermal model in the simulation of the workflow for the calculation of the camera

pointing would increase the precision of the result. A study [54] calculated the internal deformation of HRIC due to thermo-elastic distortions, concluding that the pointing error is small and can be ignored. On the other hand, no predictions about the deformation of the focal plane were evaluated, so further studies must be conducted in order to fully evaluate the impacts of the thermo-elastic distortions.
Not all the orbital positions are suitable for acquiring images and the positions with the cold case are not usable because the planet is not illuminated by the Sun, resulting that only the hot case must be considered.
It is clear that the requirement of AME of 5'' for HRIC and 10'' for STC are only achieved for the best-case scenario, while in the worst-case the requirements are never achieved for HRIC and only partially for STC.

6.3.4 Image correlation error

This term of error is not related to the pointing of the camera but is related to the elaboration of the images. It can be caused for example by distortion effects inside the lenses or different characteristic in the images to match, as the illumination condition, resolution, shape of the features.
Different studies [44] [55] prove that low and high incidence angles should be avoided while taking images because of the absence or dimensions of shadows. At the same time, great differences in the illumination conditions of two images to match should be avoided as well, as they may produce difficulties in the recognition of the same feature.
The image correlation error can be assumed of a value of 1 pixel, and the displacement on ground depends on the altitude of the spacecraft. In particular, in the Periherm the displacement corresponds to an error of 6 meters, in the Apoherm to a displacement of 19 meters.
In any case, the image correlation error has a lesser impact in the error budget than the pointing error, as the its worst-case scenario is comparable to the best case scenario of the pointing.

6.3.5 Error budget example

In this section it is given an example of the pointing error of the camera on ground. All the previous errors are taken in account and are calculated in dependence of the altitude of the spacecraft.

From a conservative point of view let us consider the worst-case scenarios of HRIC in hot case at Perihelion and the hot case at Aphelion.

The contribution to the hot case at Perihelion are:

- 8'' of pointing = 18,6 m at an altitude of 480 km
- 10 m of position of the spacecraft
- 1 pixel = 6 m at an altitude of 480 km

All the errors are independent from each other so the total root mean square of the error is calculated as the following:

$$\sqrt{18.6^2 + 10^2 + 6^2} = 22\ m \tag{21}$$

The contribution to the hot case at Aphelion are:

- 5.5'' of pointing = 40 m at an altitude of 1500 km
- 10 m of position of the spacecraft
- 1 pixel = 18,7 m at an altitude of 1500 km

All the errors are independent from each other so the total root mean square is:

$$\sqrt{40^2 + 10^2 + 18.7^2} = 45\ m \tag{22}$$

6.3.6 Influence of the thermo-elastic distortions on the DTM creation

The previous section describes the effects of the thermo-elastic distortions on the pointing on ground. Here, thermo-elastic effects are simulated in the procedure for the creation of DTMs.

Thermo-elastic deformations can basically change the camera geometry in two different ways: changing the focal length and changing the direction of the boresight. This two effects are simulated inserting a coefficient error in the projection matrix associated to every image utilized to produce a DTM. The focal length's change is simulated varying the focal length in the intrinsic parameters and the pointing error with a rotation applied on the extrinsic parameters.

The effect of focal length's change is easy to identify: the DTM is shifted along the pointing direction and consequently "zoomed" or "de-zoomed", thus changing its position and dimension but not affecting the shape of the features.

The effect of the change of the boresight direction is more difficult to grasp: while the DTM maintains its correct position and dimension, the features reconstruction appears to be less

precise, increasing the difference with the reference target. It is not clear if the difference is provoked by just a shift of the DTM along the planetary surface (so that the features do not overlap precisely with the corresponding features on the reference target) or by an imprecise features reconstruction.
While simulated together, the two phenomena coexist.

6.4 Libration

One of the major objective of the BepiColombo mission is to determine the interior structure of Mercury. Its characterization will increase our knowledge in the formation and evolution of the terrestrial worlds. Experiments conducted by the previous mission Mariner 10 and MESSENGER proved that Mercury has a feeble magnetic field, probably caused by the presence of a liquid core. This discovery is quite puzzling because the small size of Mercury should have caused a complete solidification of the internal core.
The rotation experiment of BepiColombo is designed to acquire information about the interior of Mercury and its rotational state. From pairs of images of identical areas of the surface acquired at different epochs it is possible to calculate a rotation variation respect to a uniform rotational state. This phenomenon is due to librations, an oscillation of the surface of a planet that is shifting on the liquid interior, caused by gravitational attractions from other celestial bodies [55] [56] [57] [58].
The celestial bodies, which are not rigid, deform under the influence of massive bodies. The deformations are related with the distribution of masses and different moments of inertia.
Mercury has an equatorial asymmetry and the Sun exerts a torque on it, causing a periodic variation of the nominal planet rotation with a period of 88 days called annual forced libration. Another long term libration with period of 12 years is present, but it is not possible to characterize it with the mission BepiColombo that has a nominal duration of only one year.
The amplitude of the libration is linked to the state of the planet's core. In fact, the presence of a liquid core increases the amplitude of the libration of a factor two respect to the case of a complete solid core because the liquid does not participate in the libration and so the moment of inertia of the planet is only due to the mantle, halving its magnitude. The knowledge of the ratio of the moments of inertia between the mantle and the whole body allows the understanding of the internal structure of Mercury and the dynamics of the fluid core.

The tide that moves the surface upon the liquid core does not act on the orbiting spacecraft, that remains in its orbit without influences and can measure the amplitude of the librations without being affected by them.
The estimation of the libration amplitude is a challenging task: a high precision in the observation of landmarks on the surface is required, along with the difficulty to plan an efficient observation strategy because of the combination of Mercury's 3:2 spin-orbit resonance and the absence of drift of the MPO polar orbit plane.

6.4.1 The libration experiment

The basic idea of the experiment is to take images of the same landmarks identified on the surface at different True Anomalies of Mercury. If the camera observes a point in the surface at least twice, two pictures with the same landmark can be superimposed and a displacement between them is calculated. From this displacement, along with information of the attitude and tracking of the spacecraft, it is possible to evaluate the libration of the surface and consequently the rotational state of Mercury, composed by a pure rotation and a libration motion. To give an example, a displacement of 10 arcsec corresponds to a shift of 118 m at the equator where the radius is 2440 km. The amplitude of the libration is expected to be of the order of 35 arcsec, equivalent to a 400 m shift at the equator so the images obtained with HRIC are surely able to recognize the shifts of the landmarks on the surface.
The image resolution is inversely proportional to the altitude so the libration is best observed at the equator in the Periherm phase, and the landmark images should be taken there.
One of the most challenging aspect of the experiment is the planning of the images acquisition. In fact, because of the 3:2 spin-orbit resonance, the same area of the surface is revisited again only after a precise interval of time (few months). It is important not to miss any of the acquisition opportunity, otherwise the whole experiment could be compromised for the absence of data.
Some studies [58] consider a camera offset in order to increase the number of observations, augmenting the estimated libration precision because of more favorable observations. As previously explained, off pointing maneuvers have to be carefully planned but are necessary for the stereo acquisition with HRIC. Thus, the same images can be used as well for the libration experiment.

The use of DTM instead of simple images for the libration experiment adds information about the altitude of the landmarks, increasing the knowledge precision of their position.

6.5 Co-registration of SIMBIO-SYS and BELA

BELA is the laser altimeter onboard MPO and will work in synergy with SIMBIO-SYS to create DTMs of the Hermean surface [59]. The laser produces a beam with a spot of 20-50 m on the surface that is reflected back to the detector: from the time of flight and the intensity and width of the pulse it is possible to reconstruct the shape of the surface. Samples will be acquired with a spatial resolution of 250 m along-track and 25 km cross-track at the equator. Acquisitions during successive orbits over one year of mission will decrease the cross-track resolution up to 6 km. The instrument will provide information about the surface albedo and roughness.
Due to the high temperature of the surface of Mercury, thermal distortions can deform the optical bench and misalign the pointing of BELA. The seasonal changes of the alignment of BELA must be corrected through calibrations. BELA will be calibrated with the correlation with SIMBIO-SYS data. The idea is to use science data of both instruments: the camera and the laser altimeter both observe the same targets so that co-registration between images/DTMs and laser profiles can be established.
Only simultaneous observations of the two instruments should be taken into account for calibration so that the spacecraft orientation can be considered constant.
The work presented in [60] describes the procedure for the co-registration for laser profiles and DTMs, where the difference of the laser profile h_{LA} and DTM heights h_{DTM} must be minimized in the following formula:

$$\sum [h_{DTM}(\lambda + \Delta\lambda, \phi + \Delta\phi) - (h_{LA} + \Delta h)]^2 \tag{23}$$

The co-registration is parameterized by three parameters: the along-track shift $\Delta\lambda$, the cross-track shift $\Delta\phi$ and the radial offset Δh.
Two techniques can be used to calibrate BELA: in the first the co-registration is obtained with the laser profile and an image, in the second with the laser profile and a DTM.
For the first technique an auxiliary DTM is still necessary to convert the laser profile heights of BELA in gray scale values. Once this effect is achieved, the BELA gray values can be co-registered with the gray values of an image of the same portion of the surface. The DTM should

have a resolution equal to the resolution of the image used for the calibration. The advantage of this method is that the auxiliary DTM can be obtained in a position or time unrelated with the actual BELA acquisition.
In the second technique a DTM and a BELA acquisition of the same area must be taken at the same time. Then, the laser profile is co-registered with the DTM.
Results [60] prove that co-registration to an image using an auxiliary DTM achieves better performance and the error is almost independent from the distance from the surface and the solar incidence angle. In principle, the calibration of BELA can be achieved with both STC and HRIC images. However, the resolution of STC images is proven inadequate, as the calibration error has a value of 50-150 arcsec compared to the 3-5 arcsec using HRIC images. Thus, an auxiliary DTM obtained with HRIC images is necessary.

6.6 Cross-calibration

Satellite optical instruments are calibrated on-ground prelaunch. Speaking of optical instruments, the goal of the calibration is to convert the image Digital Numbers (DN) specific of every instrument to physical units. Radiometric calibration is the process that quantitatively define the system response to a known controlled input, linking what the instrument measures (the digital numbers) and what one wants to measure.
Unfortunately, on-ground calibration are not sufficient because the severe stress of the launch and the harsh space environment can damage the instruments changing their operative performances. Thus, continuous in-flight calibrations are necessary for the production of coherent radiometric data [61].
In-flight calibrations can be divided in three categories: onboard calibrations, vicarious calibrations and cross-calibrations.
Onboard calibrations are normally performed using an internal light source.
Vicarious calibrations are accomplished by comparing radiometric data acquired on orbit and radiometric data acquired on ground of the same test target.
Cross-calibrations are achieved from the comparison of radiometric data acquired from different satellites/instruments.
Different calibration phases and typologies are foreseen for SIMBIO-SYS.
The first phase is performed during the commissioning, just after the launch, with the intention of evaluating the eventual changes occurred during the launch.

A second phase, principally aimed to geometric correction, is performed by pointing at the starts to calculate the boresight of the instrument respect to the spacecraft attitude. This procedure will be repeated several times during the whole mission duration. The principle of this calibration is to detect a known star and derive the boresight of the camera by triangulate its position. The exposure time is chosen as a trade-off between improving the SNR (high exposure time) and FOV immovability (low exposure time), affected by spacecraft pointing stability and jittering and thermo-elastic distortions.

A third phase is performed by pointing at the surface of the planet for the sake of calculating the radiometric response of the camera.

Cross-calibration, or intercalibration, of satellite instruments is an effective way to scale one instrument respect to another. This option is valid only if the reference instrument is stable and calibrated. The basic idea is that two instruments should make identical measurements while viewing the same target under the same conditions. Since these conditions never occur in reality, the process of cross-calibration aims to identify, correct and possibly eliminate the causes of a relative bias between different instruments.

A test target for in-flight radiometric calibration must present some general favorable characteristics:

1) High reflectance in order to reduce the atmospheric scattering.
2) Elevation of at least 1 km in order to reduce the amount of atmospheric aerosols.
3) High-spatial uniformity in the morphological characteristics and high-spectral homogeneity.
4) Seasonal changes should be minimal.
5) Flat surface in order to reduce the illumination changes and shadow problems.

In-flight calibration in celestial bodies other than the Earth is facilitated due to the lack of the atmosphere, eliminating the scattering and aerosols problems. Moreover, if the target is not geologically active as Mercury, seasonal changes between different acquisitions are not present. Thus, the ideal characteristics for targets for radiometric calibration are reduced to flatness and spatial uniformity.

For Earth observation satellites, the cross-calibration is made by comparing data of the same target acquired from different satellites, where one is considered as a standard reference. For the mission BepiColombo this is clearly impossible to achieve, as only the previous mission MESSENGER provided some radiometric data of Mercury. On the other hand, a cross-calibration strategy is possible between the different channels of SIMBIO-SYS, in particular

HRIC and STC. The idea is to compare the data of the two channels and average them in some way, rather than considering one as reference as it is normally done on the Earth.

The two channels have to acquire images of the same target and the different data have to be compared. As HRIC is nadir pointing and STC's boresight is inclined, the target should be as smooth as possible in order to avoid the presence of different shadows between the two acquisitions.

A mosaic of HRIC images (details are found in section 4.6 Mosaic) can facilitate the comparison of the data of the two channels. In section 4.6.1 Illumination changes in the mosaics, information about the illumination conditions inside the mosaic are given. Inside mosaics with the size of STC images with cross-track acquisitions in successive orbits the illumination conditions remain mostly constant. Thus, smooth plains at latitudes higher than 60° (-60°) should provide good targets for cross-calibration of the HRIC and STC channels.

From the cross-calibration between the two channels is possible to retrieve information about the boresight pointing and the absolute radiometric response.

The boresight pointing can be verified by comparing images of the same area obtained with different channels. In the same way, the absolute radiometric response can be verified from the comparison of different radiometric response of different images of the same area obtained from the different channels.

The different channels of SIMBIO-SYS share the same optical bench, so a misalignment of the optical bench respect to the spacecraft due to thermo-elastic distortions will affect in the same way the pointing's direction of the different boresights. Performing a geometric cross-calibration pointing to the stars allows to evaluate the relative direction of the boresights of the channels neglecting the displacement between the optical bench and the spacecraft. Thus, only the internal thermo-elastic deformations of every channel are considered. A study [54] proves that the internal thermo-elastic deformations of HRIC are negligible, so that the boresight can be assumed pointing always in the same fixed direction.

In conclusion, the data from the different SIMBIO-SYS channels can be integrated together in order to improve the scientific output in different and innovative ways, proving the flexibility and efficiency of the design of the camera.

6.7 Super resolution and tri-stereo

Super resolution is a computational technique aimed to reconstruct a high resolution image from one or more low resolution images [62]. The approach can be divided in two main categories: single-image super resolution and multi-image super resolution.

The single-image technique utilizes deep-learning algorithms that exploit spatial correlation to improve the resolution of the image. The algorithms are trained to recognize specific scenarios and features and then this information is used to improve the quality of similar structures and increase the resolution of images.

The multi-image technique utilizes more images of the same scene to recover complementary information and reconstruct high spatial-frequency details. Multi-image techniques prove to be more effective and bring out more details, with the disadvantages of a higher computational cost and the need of an extensive data set.

Super resolution can be performed either post processing or onboard of satellites equipped with a graphic processing unit.

Giving the details about the different procedures and algorithms of the different super resolution techniques is behind the purpose of this work. Here it is just important to highlight the possibility of using these techniques in order to improve the resolution of the images acquired with SIMBIO-SYS and consequently increase also the precision of the DTMs obtained.

Different studies have been performed using satellites images, with both single-image and multi-image techniques. Tao [63] used a single-image technique to improve the quality of CASSIS image of a factor of about 3. Other interesting works were conducted with the multi-image techniques [64] [65]. Using a set of multi angle images of the same target, the resolution was enhanced by a factor of 2-5. The technique uses sub-pixel information derived from slight translational shifts and large view angles to improve the quality of the input images. The dataset was composed by 9 images.

Studies were conducted either on Earth and on Mars with promising results.

The same super resolution techniques can be used for the image acquired with SIMBIO-SYS.

Single-image techniques require only one image so they can be utilized whenever it is necessary. Multi-image techniques require a set of images so their acquisition must be carefully planned. Due to the 3:2 spin-orbit resonance of Mercury, MPO revisits the same target after two Mercury year. A Mercury year lasts around 88 Earth days, so a re-visitation condition occurs around every 6 months. The mission BepiColombo is scheduled to last for one year,

with a possible extension of another year. In case of extension, a target can be visited from 4 to 6 times in dependence of its position on the planet. The dataset of images is smaller than the one used in the previous work, but could be sufficient to enhance at least a little the quality of the images. Further investigations are necessary to clear this aspect.
Super resolution can be used with both HRIC and STC images. Even if the 3:2 spin-orbit resonance is present, it is difficult that two identical acquisition conditions occur, e.g. MPO repasses in the exact same coordinates, and the boresight can point toward the surface with some kilometers of discrepancy. For this reason, the acquisition of "identical" HRIC images (meaning in this case different images that cover the exact area of the surface) can result unfeasible in practice, because of the narrow FOV of the camera. With STC the acquisition results easier thanks to the larger FOV, enabling at least a big overlapping between different images. Moreover, STC is composed by two channels, doubling the number of images acquired for every target and providing a different view angle. In addition, if a HRIC mosaic is performed, a third image from a different perspective is present for every target. These characteristics probably make STC images more suited for the application of super resolution techniques.
One limitation in the set of images is the changing of orbit of MPO during the mission. The topic was covered in section 5.2 MPO orbit changeconcluding that the pixel on ground dimension changes in time.
In conclusion, super resolution techniques are new but promising methods to increase the quality of images from satellites. This section is just a brief overview of the topic and specific analysis must be performed in order to understand if super resolution can be efficiently used for the mission BepiColombo.

While normally the tridimensional reconstruction of a planetary surface is achieved by triangulating a stereo pair, it is also possible to use more than two images: in this case the procedure is referred as multi-image reconstruction. Tri-stereo techniques for example utilizes a set of three images of the same target, two acquired with an inclination and one from a nadir perspective [66] [67] [68]. This technique is particularly suited for creating DTMs of urban areas with high buildings, where the area between them is occluded for inclined images acquired from satellites while instead is visible from a nadir point of view.
For the mission BepiColombo this technique can be used as well, where the two inclined images are provided by the two channels STC and the nadir by a HRIC mosaic.

While tri-stereo reconstruction proves to be reliable for urban areas, its efficiency in the natural landscapes is more questionable. Either way, the tri-stereo technique is a new and innovative method and up to date few satellites are equipped with tri-stereo sensors.

In conclusion, tri-stereo can be utilized for the DTM reconstruction with SIMBIO-SYS, especially if in the future more studies will be conducted on the topic.

Conclusions

Satellite images and Digital Terrain Models are the most useful tools for the study of surfaces of celestial bodies. The increasing interest in the Solar System exploration led to the development of new strategies and approaches in the sector of photogrammetry from satellites images.

The work presented in this thesis can be of great help for the acquisition planning of SIMBIO-SYS on the ESA mission BepiColombo to Mercury.

Different aspects are covered, in particular:

- BepiColombo mission and the instrument SIMBIO-SYS are described in detail.
- A mission planning for SIMBIO-SYS is presented: it is analyzed the changes of illumination conditions, on-ground resolution, data volume and acquisition scenarios during different phases of the mission.
- A complete workflow for the creation of DTMs from synthetic images of planetary surfaces is presented. The procedure makes use of customized MATLAB algorithms exploiting the SPICE kernels, a ray tracing software for rendering synthetic images, a software for the tridimensional reconstruction and a software for the visualization of the products. The quality of the DTMs is evaluated in dependence of acquisition conditions of the stereo pair, in terms of illumination and convergence angle.
- Close attention is given to the production of DTMs from satellite images (stereo couples), with a particular attention on the possibility to use the high resolution channel HRIC to obtain high resolution DTMs. As HRIC is nadir-pointing, a rotation of the spacecraft is foreseen for retrieving the necessary data. An analysis of best acquisition conditions for a stereo couple is performed. The quality of the HRIC DTMs is around ten times better than the quality of the normal DTMs obtained from STC images.
- An image acquisition strategy for HIRC is presented, with special consideration to the polar regions of the planet. In addition, a combination of STC and mosaicked HRIC images for the production of stereo pairs for DTMs is evaluated. This strategy proves to be more effective in the polar regions than the normal stereo couples with STC images.
- A strategy to produce extended mosaics from HRIC images is exposed. A dedicated mosaicking algorithm is coded in MATLAB for the purpose.

- Some specific usages of DTMs are presented, as for example for the libration experiment or for the BELA calibration. In addition, the possibility to integrate the data retrieved by the different channels of SIMBIO-SYS is explained, pointing up the strength of the instrument design.
- An error budget is performed, taking into account the error in the knowledge of the position of the spacecraft and the thermo-elastic distortions of the channels of SIMBIO-SYS.

The research conducted proves that SIMBIO-SYS has great potential for the exploration and the tridimensional reconstruction of the surface of Mercury. In particular, the possibility to integrate the information from the different channels of the suite can greatly improve the quality of the scientific data acquired.

A careful planning for the acquisition of images with SIMBIO-SYS is necessary to optimize the data volume and the scientific output. In particular, great attention must be posed when planning to mosaic images of HRIC, as revisitation time and illumination conditions change during the mission.

Bibliography

[1] S. C. Solomon, R. L. McNutt, R. E. Gold, and D. L. Domingue, *MESSENGER mission overview*, vol. 131, no. 1–4. 2007.

[2] J. Benkhoff *et al.*, "BepiColombo-Comprehensive exploration of Mercury: Mission overview and science goals," *Planet. Space Sci.*, vol. 58, no. 1–2, pp. 2–20, 2010, doi: 10.1016/j.pss.2009.09.020.

[3] D. T. Blewett *et al.*, "Mercury's hollows: Constraints on formation and composition from analysis of geological setting and spectral reflectance," *J. Geophys. Res. E Planets*, vol. 118, no. 5, pp. 1013–1032, 2013, doi: 10.1029/2012JE004174.

[4] A. Milillo *et al.*, "Investigating Mercury's Environment with the Two-Spacecraft BepiColombo Mission," *Space Sci. Rev.*, vol. 216, no. 5, 2020, doi: 10.1007/s11214-020-00712-8.

[5] R. Jehn, "BepiColombo Mercury cornerstone consolidated report on mission analysis," *Bc-Esc-Rp-05500*, no. 525, 2015.

[6] M. Casasco, "The BepiColombo Attitude and Orbit Control System," no. June 2014, 2014.

[7] G. Cremonese *et al.*, "SIMBIO-SYS: Scientific Cameras and Spectrometer for the BepiColombo Mission," *Space Sci. Rev.*, vol. 216, no. 5, 2020, doi: 10.1007/s11214-020-00704-8.

[8] E. Martellato *et al.*, "Preliminary results of the optical calibration for the stereo camera STC onboard the Bepicolombo mission," vol. 10563, no. October, p. 64, 2017, doi: 10.1117/12.2304124.

[9] M. Zusi *et al.*, "Radiometric Model and Operation-Define-Tool for HRIC SIMBIO-SYS on the BepiColombo mission to Mercury," *Mem. della Soc. Astron. Ital. Suppl.*, vol. 12, p. 72, 2008, [Online]. Available: http://adsabs.harvard.edu/cgi-bin/nph-data_query?bibcode=2008MSAIS..12...72Z&link_type=ABSTRACT%5Cnpapers2://publication/uuid/68CE055C-A771-45C1-8ED3-D0769E39C699.

[10] G. Filacchione *et al.*, "The pre-launch characterization of SIMBIO-SYS/VIHI imaging spectrometer for the BepiColombo mission to Mercury. I. Linearity, radiometry, and geometry calibrations," *Rev. Sci. Instrum.*, vol. 88, no. 9, 2017, doi: 10.1063/1.4989968.

[11] X. Long Dai and J. Lu, "Object-based approach to automated image matching," *Int. Geosci. Remote Sens. Symp.*, vol. 2, pp. 1189–1191, 1999.

[12] K. Mikolajczyk *et al.*, "A comparison of affine region detectors," *Int. J. Comput. Vis.*, vol. 65, no. 1–2, pp. 43–72, 2005, doi: 10.1007/s11263-005-3848-x.

[13] D. G. Low, "Distinctive image features from scale-invariant keypoints," *Int. J. Comput. Vis.*, pp. 91–110, 2004, [Online]. Available: https://www.cs.ubc.ca/~lowe/papers/ijcv04.pdf.

[14] H. Bay, T. Tuytelaars, and L. Van Gool, "LNCS 3951 - SURF: Speeded Up Robust Features," *Comput. Vision–ECCV 2006*, pp. 404–417, 2006, [Online]. Available: http://link.springer.com/chapter/10.1007/11744023_32.

[15] J. P. (Industrial L. & M. Lewis, "Fast Normalized Cross-Correlation Template Matching by Cross-," *Vis. Interface*, vol. 1995, no. 1, pp. 1–7, 1995.

[16] A. W. Gruen, "Adaptive least squares correlation: a powerful image matching technique," *South African J. Photogramm. Remote Sens. Cartogr.*, vol. 14, no. 3, pp.

175–187, 1985, [Online]. Available: http://citeseerx.ist.psu.edu/viewdoc/summary;jsessionid=8478C7133B070BA354E5DED2EFF60262?doi=10.1.1.93.6891%5Cnhttp://www.idb.arch.ethz.ch/files/alsm_awgruen.pdf.

[17] C. A. Rokhmana, M. E. Tjahjadi, and F. D. Agustina, "Cadastral Surveys with Non-metric Camera Using Uav: A Feasibility Study," *KnE Eng.*, no. December, 2019, doi: 10.18502/keg.v4i3.5856.

[18] E. Simioni *et al.*, "3DPD: A photogrammetric pipeline for a PUSH frame stereo cameras," *Planet. Space Sci.*, vol. 198, no. April 2020, 2021, doi: 10.1016/j.pss.2021.105165.

[19] P. L. Guth *et al.*, "Digital elevation models: Terminology and definitions," *Remote Sens.*, vol. 13, no. 18, 2021, doi: 10.3390/rs13183581.

[20] B. Kloc, A. Mazur, and M. Szumiło, "Comparison of Free and Commercial Software in the Processing of Data Obtained from Non-Metric Cameras," *J. Ecol. Eng.*, vol. 22, no. 2, pp. 213–225, 2021, doi: 10.12911/22998993/131074.

[21] M. Lehoczky and Z. Abdurakhmonov, "Present software of photogrammetric processing of digital images," *E3S Web Conf.*, vol. 227, 2021, doi: 10.1051/e3sconf/202122704001.

[22] M. E. Brecher, "Technical Manual," *Am. Assoc. Blood Banks*, 2005.

[23] R. A. Beyer and M. Lundy, "The Ames Stereo Pipeline :," *Development*, 2010.

[24] S. Breast, L. Access, S. Breast, L. Access, S. B. Access, and S. Breast, "User Manual ● 사용설명서 ●," *Screen*, pp. 1–24.

[25] D. T. M. P. Team, "DTM Production Team SOCET SET Instruction Manual," 2014.

[26] H. Hu and B. Wu, "PLANETARY3D: A PHOTOGRAMMETRIC TOOL for 3D TOPOGRAPHIC MAPPING of PLANETARY BODIES," *ISPRS Ann. Photogramm. Remote Sens. Spat. Inf. Sci.*, vol. 4, no. 2/W5, pp. 519–526, 2019, doi: 10.5194/isprs-annals-IV-2-W5-519-2019.

[27] C. H. Acton, "Ancillary data services of NASA's navigation and Ancillary Information Facility," *Planet. Space Sci.*, vol. 44, no. 1 SPEC. ISS., pp. 65–70, 1996, doi: 10.1016/0032-0633(95)00107-7.

[28] M. Park and C. Acton, "COSMOGRAPHIA- - - SPICE USER ' S GUIDE Prepared by JPL Summer Intern Students Revised by," 2014.

[29] M. S. Robinson *et al.*, "Lunar reconnaissance orbiter camera (LROC) instrument overview," *Space Sci. Rev.*, vol. 150, no. 1–4, pp. 81–124, 2010, doi: 10.1007/s11214-010-9634-2.

[30] R. Vondrak, J. Keller, G. Chin, and J. Garvin, "Lunar reconnaissance orbiter (LRO): Observations for lunar exploration and science," *Space Sci. Rev.*, vol. 150, no. 1–4, pp. 7–22, 2010, doi: 10.1007/s11214-010-9631-5.

[31] S. G. Pugacheva and V. V. Shevchenko, "Photometric relief of the previously uninvestigated surface of mercury," *Sol. Syst. Res.*, vol. 48, no. 1, pp. 1–10, 2014, doi: 10.1134/S0038094613060075.

[32] P. Sciences, "Bidirectional Reflectance Spectroscopy 2 . Experiments and Observations with the Grum and Neither of these reflectance Kodak Dots : after by comparison of thin of powder," *October*, vol. 86, pp. 3055–3060, 1981.

[33] D. L. Domingue, B. W. Denevi, S. L. Murchie, and C. D. Hash, "Application of multiple photometric models to disk-resolved measurements of Mercury's surface: Insights into Mercury's regolith characteristics," *Icarus*, vol. 268, pp. 172–203, 2016, doi: 10.1016/j.icarus.2015.11.040.

[34] M. Kato, S. Sasaki, and Y. Takizawa, "The Kaguya mission overview," *Space Sci. Rev.*, vol. 154, no. 1–4, pp. 3–19, 2010, doi: 10.1007/s11214-010-9678-3.

[35] G. Neukum and R. Jaumann, "HRSC: The high resolution stereo camera of Mars

Express, in: Mars Express: The Scientific Payload," *Mars Express Sci. payload. Ed. by Andrew Wilson*, pp. 1–19, 2004, [Online]. Available: http://adsabs.harvard.edu/abs/2004ESASP1240...17N.
[36] R. Schmidt, J. D. Credland, A. Chicarro, and P. Moulinier, "ESA's Mars Express mission - Europe on its way to Mars," *Esa Bull. Sp. Agency*, no. 98, pp. 56–66, 1999.
[37] R. Brochard *et al.*, "Scientific image rendering for space scenes with the surrender software," *arXiv*, no. October, 2018.
[38] C. Re, S. Tulyakov, E. Simioni, T. Mudric, G. Cremonese, and N. Thomas, "Performance evaluation of 3dpd, the photogrammetric pipeline for the cassis stereo images," *Int. Arch. Photogramm. Remote Sens. Spat. Inf. Sci. - ISPRS Arch.*, vol. 42, no. 2/W13, pp. 1443–1449, 2019, doi: 10.5194/isprs-archives-XLII-2-W13-1443-2019.
[39] N. Thomas *et al.*, "The Colour and Stereo Surface Imaging System (CaSSIS) for the ExoMars Trace Gas Orbiter," *Space Sci. Rev.*, vol. 212, no. 3–4, pp. 1897–1944, 2017, doi: 10.1007/s11214-017-0421-1.
[40] J. Vago *et al.*, "ESA ExoMars program: The next step in exploring Mars," *Sol. Syst. Res.*, vol. 49, no. 7, pp. 518–528, 2015, doi: 10.1134/S0038094615070199.
[41] M. A. Fischler and R. C. Bolles, "Random sample consensus: A Paradigm for Model Fitting with Applications to Image Analysis and Automated Cartography," *Commun. ACM*, vol. 24, no. 6, pp. 381–395, 1981, doi: 10.1145/358669.358692.
[42] P. Cignoni, C. Montani, R. Perego, and R. Scopigno, "Parallel 3D Delaunay Triangulation," *Comput. Graph. Forum*, vol. 12, no. 3, pp. 129–142, 1993, doi: 10.1111/1467-8659.1230129.
[43] G. G. Michael *et al.*, "Systematic processing of Mars Express HRSC panchromatic and colour image mosaics: Image equalisation using an external brightness reference," *Planet. Space Sci.*, vol. 121, pp. 18–26, 2016, doi: 10.1016/j.pss.2015.12.002.
[44] C. Re *et al.*, "Effects of image compression and illumination on digital terrain models for the stereo camera of the BepiColombo mission," *Planet. Space Sci.*, vol. 136, no. May, pp. 1–14, 2017, doi: 10.1016/j.pss.2016.10.018.
[45] I. Polyansky *et al.*, "Stereo topographic mapping concept for the upcoming Luna-Resurs-1 orbiter mission," *Planet. Space Sci.*, vol. 162, no. September 2017, pp. 216–232, 2018, doi: 10.1016/j.pss.2017.09.013.
[46] R. L. Kirk *et al.*, "Evaluating Stereo Digital Terrain Model Quality at Mars Rover Landing Sites with HRSC , CTX , and HiRISE Images," pp. 1–41, 2021.
[47] D. J. Lawrence *et al.*, "Evidence for Water Ice Near Mercury ' s," vol. 339, no. January, pp. 292–297, 2013.
[48] R. L. Kirk, "Futher adventures in Mars DTM quality: smoothing errors, sharpening details," *ISPRS Ann. Photogramm. Remote Sens. Spat. Inf. Sci.*, 2021.
[49] M. Massironi *et al.*, "Simulations using terrestrial geological analogues to assess interpretability of potential geological features of the Hermean surface restituted by the STereo imaging Camera of the SIMBIOSYS package (BepiColombo mission)," *Planet. Space Sci.*, vol. 56, no. 8, pp. 1079–1092, 2008, doi: 10.1016/j.pss.2008.02.005.
[50] D. Girardeau-Montaut, "CloudCompare version 2.6.1. user manual," p. 181, 2015, [Online]. Available: http://www.danielgm.net/cc/.
[51] R. L. Kirk *et al.*, "High-resolution topomapping of candidate MER landing sites with Mars Orbiter Camera narrow-angle images," *J. Geophys. Res. E Planets*, vol. 108, no. 12, 2003, doi: 10.1029/2003je002131.
[52] M. Casasco, "BepiColombo pointing and micro-vibration performance," pp. 1–50, 2018.
[53] A. Milani, A. Rossi, D. Vokrouhlický, D. Villani, and C. Bonanno, "Gravity field and rotation state of Mercury from the BepiColombo Radio Science Experiments," *Planet. Space Sci.*, vol. 49, no. 14–15, pp. 1579–1596, 2001, doi: 10.1016/S0032-

0633(01)00095-2.
[54] D. Dipasquale, S. Debei, G. Cremonese, F. Capaccioni, and P. Palumbo, “Optical performance evaluation of the high spatial resolution imaging camera of BepiColombo space mission,” *Opt. Laser Technol.*, vol. 141, no. March, p. 107172, 2021, doi: 10.1016/j.optlastec.2021.107172.
[55] G. Pfyffer, T. Van Hoolst, and V. Dehant, “Librations and obliquity of Mercury from the BepiColombo radio-science and camera experiments,” *Planet. Space Sci.*, vol. 59, no. 9, pp. 848–861, 2011, doi: 10.1016/j.pss.2011.03.017.
[56] J. L. Margot, S. J. Peale, R. F. Jurgens, M. A. Slade, and I. V. Holin, “Large longitude libration of mercury reveals a molten core,” *Science (80-.).*, vol. 316, no. 5825, pp. 710–714, 2007, doi: 10.1126/science.1140514.
[57] R. Jehn, C. Corral, and G. Giampieri, “Estimating Mercury’s 88-day libration amplitude from orbit,” *Planet. Space Sci.*, vol. 52, no. 8, pp. 727–732, 2004, doi: 10.1016/j.pss.2003.12.012.
[58] N. Sánchez Ortiz, M. Belló Mora, and R. Jehn, “BepiColombo mission: Estimation of Mercury gravity field and rotation parameters,” *Acta Astronaut.*, vol. 58, no. 4, pp. 236–242, 2006, doi: 10.1016/j.actaastro.2005.09.008.
[59] A. Stark, G. Steinbrügge, and P. Gläser, “BELA to SIMBIO-SYS Calibration Report Prepared by : Author,” 2016.
[60] “BELA to HRIC images calibration campaign BELA to HRIC DTM calibration campaign.”
[61] G. Chander, T. J. Hewison, N. Fox, X. Wu, X. Xiong, and W. J. Blackwell, “Overview of intercalibration of satellite instruments,” *IEEE Trans. Geosci. Remote Sens.*, vol. 51, no. 3, pp. 1056–1080, 2013, doi: 10.1109/TGRS.2012.2228654.
[62] A. Bordone Molini, D. Valsesia, G. Fracastoro, and E. Magli, “DeepSUM: Deep Neural Network for Super-Resolution of Unregistered Multitemporal Images,” *IEEE Trans. Geosci. Remote Sens.*, vol. 58, no. 5, pp. 3644–3656, 2020, doi: 10.1109/TGRS.2019.2959248.
[63] Y. Tao and J. P. Muller, “A novel method for surface exploration: Super-resolution restoration of Mars repeat-pass orbital imagery,” *Planet. Space Sci.*, vol. 121, pp. 103–114, 2016, doi: 10.1016/j.pss.2015.11.010.
[64] Y. Tao and J. P. Muller, “Quantitative assessment of a novel super-resolution restoration technique using hirise with navcam images: How much resolution enhancement is possible from repeat-pass observations,” *Int. Arch. Photogramm. Remote Sens. Spat. Inf. Sci. - ISPRS Arch.*, vol. 41, no. July, pp. 503–509, 2016, doi: 10.5194/isprsarchives-XLI-B4-503-2016.
[65] Y. Tao and J. P. Muller, “Super-resolution restoration of MISR images using the UCL MAGiGAN system,” *Remote Sens.*, vol. 11, no. 1, 2019, doi: 10.3390/rs11010052.
[66] J. Jeong, C. Yang, and T. Kim, “Geo-positioning accuracy using multiple-satellite images: IKONOS, QuickBird, and KOMPSAT-2 stereo images,” *Remote Sens.*, vol. 7, no. 4, pp. 4549–4564, 2015, doi: 10.3390/rs70404549.
[67] R. Li, X. Niu, C. Liu, B. Wu, and S. Deshpande, “Impact of imaging geometry on 3D geopositioning accuracy of stereo ikonos imagery,” *Photogramm. Eng. Remote Sensing*, vol. 75, no. 9, pp. 1119–1125, 2009, doi: 10.14358/PERS.75.9.1119.
[68] L. Piermattei *et al.*, “Impact of the acquisition geometry of very high-resolution Pléiades imagery on the accuracy of canopy height models over forested alpine regions,” *Remote Sens.*, vol. 10, no. 10, 2018, doi: 10.3390/rs10101542.